THE SYNTHESIS OF PHOTOSENSITIZERS FOR THE PHOTODYNAMIC INACTIVATION OF *ESCHERICHIA COLI*

by

Alexandra Nicole Hurst

A thesis submitted to the faculty of
The University of North Carolina at Charlotte
in partial fulfillment of the requirements
for the degree of Master of Science in
Chemistry

Charlotte

2017

Approved by:

_____
Juan Vivero-Escoto

_____
Jerry Troutman

_____
Michael Walter

_____
Ian Marriott

ABSTRACT

ALEXANDRA NICOLE HURST. The synthesis of photosensitizers for the photodynamic inactivation of *Escherichia coli*. (Under the direction of DR. JUAN VIVERO-ESCOTO)

The development of antibiotic resistance is a natural phenomenon that occurs when bacteria cells exchange resistant traits amongst each other or when mutations occur during replication. This causes bacteria to be able to withstand attack by antibiotic drugs so that standard treatments which have been successful for decades become ineffective in treating common infections. To combat antibiotic resistance an alternate treatment method, photodynamic inactivation (PDI) of bacteria, is currently being explored, and have been shown to be successful with less potential for development of resistance. PDI utilizes light, oxygen, and a photosensitizer to effectively kill bacteria. However, PDI has been shown to be less effective towards killing Gram-negative bacteria because Gram-negative bacteria cells have two cell membranes which makes them impermeable by the photosensitizer compounds. The PS have been changed with positively-charged groups to improve the electrostatic interaction with the negatively-charged outer membrane of the bacteria. In the present project, a series of PS which have positively-charged groups, trimethylammonium, were synthesized and characterized. Dark and light cytotoxicity studies were investigated to examine the charge effect of the cationic PS in the photodynamic inactivation against *E. coli*, a model for Gram-negative bacteria. Additionally, the mechanism of interaction between the cationic porphyrin and *E. coli* cells was shown using confocal fluorescence microscopy.

DEDICATION

I would like to dedicate the work of this project to my family.

ACKNOWLEDGEMENTS

I would firstly like to thank Dr. Juan L. Vivero-Escoto for his supervision and encouragement during my MS Thesis. I would also like to thank the following people who have contributed to this project: Dr. Jerry Troutman and Beth Scarbrough for their support with the bacterial assays; Dr. Richard Chi and Shreya Goya for their help with fluorescence microscopy images; Dr. Michael Walter and Dawn Marin for their guidance and advice with the singlet oxygen quantum yield experiments.

TABLE OF CONTENTS

LIST OF TABLES

LIST OF FIGURES

LIST OF SCHEMES

LIST OF ABBREVIATIONS

A^+TPP	5-(4'-*N*,*N*,*N*-ammoniumphenyl)-10,15,20-triphenylporphyriniodide
ANOVA	Analysis of variance
$CDCl_3$	Deuterated chloroform
CFU	Colony-forming unit
DMA	9,10-dimethylanthracene
DMF	*N*,*N*-Dimethylformamide
DMSO	Dimethyl sulfoxide
DMSO-d_6	Deuterated dimethyl sulfoxide
DP	Deuteroporphyrin
DPBF	1,3-diphenylbenzofuran
EDTA	Ethylenediaminetetraacetic acid
ESI-MS	Electrospray ionization mass spectroscopy
FTIR	Fourier transform infrared spectroscopy
^1H NMR	Proton nuclear magnetic resonance
IC50	Inhibitory concentration at 50
ISC	Intersystem crossing
LB	Luria-Bertani
LPS	Lipopolysaccharides
MALDI-TOF	Matrix-assisted laser desorption ionization-time of flight
MDR	Multidrug resistant bacteria
MIC	Minimum inhibitory concentration

NIR	Near-infrared radiation
$^1O_2$	Singlet oxygen
PBS	Phosphate buffer solution
PDI	Photodynamic inactivation
PMBN	Polymyxin B nonapeptide
PS	Photosensitizer
ROS	Reactive oxygen species
SDS	Sodium dodecyl sulphate
TA_2PP	C*is*-5,10-bis(4'-aminophenyl)-15,20-diphenylporphyrin and *trans*-5,15-bis(4'-aminophenyl)-10,20-diphenylporphyrin
TA_3PP	5,10,15-tris(4'-aminophenyl)-20-phenylporphyrin
$TA^{+2}PP$	*Cis*-5,10-bis(4'-*N*,*N*,*N*-trimethylammoniumphenyl)-15,20-diphenylporphyrin iodide and *trans*-5,15-bis(4'-*N*,*N*,*N*-trimethylammoniumphenyl)-10,20-diphenylporphyrin iodide
$TA^{+3}PP$	5,10,15-tris(4'-*N*,*N*,*N*-trimethylammoniumphenyl)-20-phenylporphyrin iodide
$TA^{+4}PP$	5,10,15,20-tetrakis(4'-*N*,*N*,*N*-trimethylammoniumphenyl)phenylporphyrin iodide
TN_2PP	C*is*-5,10-bis(4'-nitrophenyl)-15,20-diphenylporphyrin and *trans*-5,15-bis(4'-nitrophenyl)-10,20-diphenylporphyrin
TN_3PP	5,10,15-tris(4'-nitrophenyl)-20-phenylporphyrin
TPP	Tetraphenylporphyrin
TPy^+P	5,10,15,20-tetrakis(*N*-methylpyridinium)porphyrin
UV	Ultraviolet
VIS	Visible

CHAPTER 1: INTRODUCTION

1.1 Bacteria

Bacteria are found throughout Earth's ecosystems and serve vital roles in the survival of plants and animals. Bacteria vary in size and come in three basic shapes: spherical (coccus), rod-like (bacillus), and curved (spirilla). The general structure of most bacteria cells contain flagellum (aid in cellular locomotion), cell membrane (surrounds the cytoplasm and regulates the flow of molecules in and out of the cell), cell wall (surrounds the plasma membrane and protects the bacterial cell from changes in water pressure), cytoplasm (a gel-like substance composed mainly of water), ribosomes (responsible for protein production), and nucleoid (contains the single DNA molecule) (Figure 1).[1]

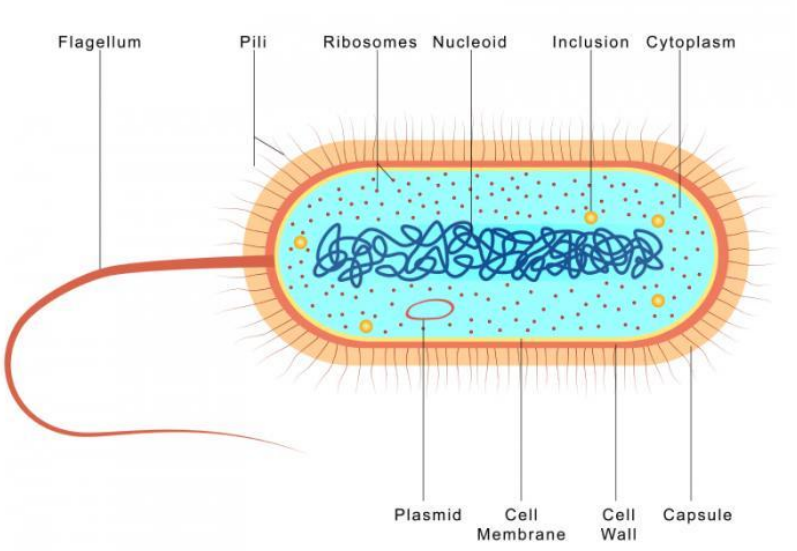

Figure 1. A diagram of a bacterial cell.[2]

Bacteria are categorized as Gram-positive or Gram-negative depending on their response to Gram staining. Gram staining was developed by Danish scientist Hans

Christian Gram, and it differentiates bacteria based on the presence of peptidoglycan, a component of the cell wall. Gram-positive bacteria have a thick mesh-like cell wall made up of peptidoglycan (50 – 70% of cell wall) that allows the bacteria to be easily stained purple by crystal violet. Gram-negative bacteria have a thinner layer of peptidoglycan (approximately 10% of cell wall) and is insusceptible to retain the purple stain during washing. Instead, the bacteria retain the counter dye, safranin, and is stained pink (Figure 2).[3]

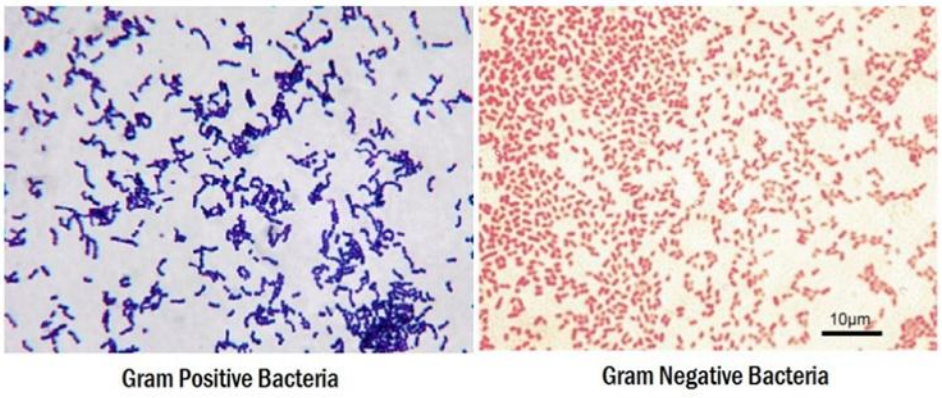

Figure 2. Gram staining of Gram-positive and Gram-negative bacteria.[3]

1.1.1 Gram-positive bacteria

The cell wall of Gram-positive bacteria is between 15 to 50 nm thick and surrounds the cell membrane. The cell wall is made up of approximately 50% peptidoglycan. The cell wall also contains negatively-charged acidic polysaccharides called teichoic acids, and displays a high degree of porosity allowing the entry of macromolecules with molecular weights ranging from 30 KDa to 60 KDa to diffuse to the inner plasma membrane (Figure 3).[4–6]

1.1.2 Gram-negative bacteria

Unlike Gram-positive bacteria, the cell wall of Gram-negative bacteria is surrounded by an inner and outer membrane (Figure 3). The outer membrane is 10 to 15 nm thick, and is made up of an inner phospholipid layer and an outer layer comprising lipopolysaccharide (LPS) molecules.[4–6] The LPS molecules have a strong affinity for divalent cations, Ca^{2+} and Mg^{2+}, which give thermodynamic stability by cross-linking neighboring LPS molecules. The outer membrane acts as a permeability barrier preventing the movement of molecules across the membrane. Embedded in the outer membrane are proteins called porins that facilitate transport across the membrane.[7]

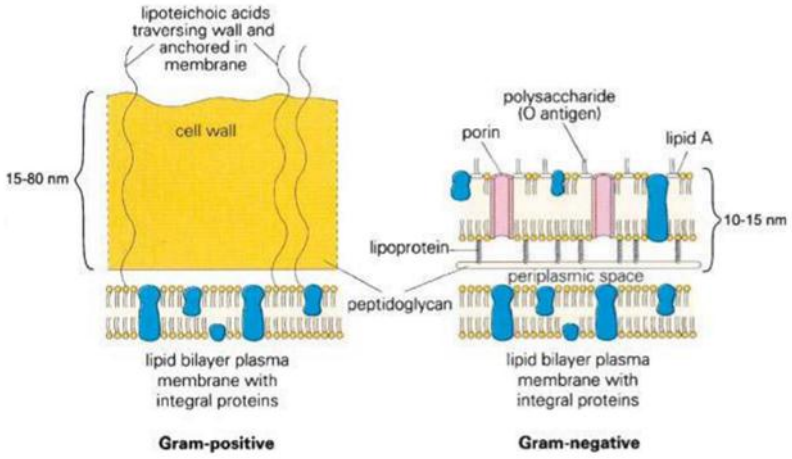

Figure 3. Schematic representation of the cell wall of Gram-positive (left) and Gram-negative (right) bacteria.[4]

1.2 Antibiotics

Although some bacteria can be beneficial to humans, other bacteria can cause infectious diseases. To combat infectious pathogens, more than 20 antibiotics were discovered in the 20th century. Antibiotics are compounds produced by fungi and bacteria to kill or inhibit competing microbes. The discovery of antibiotics played vital roles in achieving major advancements in medicine and surgery and extended expected

lifespans.[8,9] Antibiotics can either be natural products (β-lactams, cephalosporins, carbapenems, and aminoglycosides) or synthetic chemicals (sulfonamides, quinolones, and oxazolidinones).[10–14] Most of the antibiotics have been natural products or semisynthetic products.[10,12]

Different antibiotics have different mechanisms of action such as inhibition or regulation of enzymes involved in cell wall synthesis, protein synthesis or nucleic acid synthesis and repair, or disruption of cell membrane function.[12] The first natural antibiotic discovered by Alexander Fleming in 1929, penicillin, worked by inhibiting the formation of peptidoglycan in the bacterial cell wall of Gram-positive bacteria by binding to the enzyme DD-transpeptidase. Without formation of a peptidoglycan cross-linked cell wall, the cell wall loses its integrity and degrades in harsh environments.[5,12,13] The activity of an antibiotic is described by the lowest concentration that completely inhibits visible growth of the organism (minimum-inhibitory concentration, MIC) or the concentration where the response is reduced by half (IC_{50}).

1.3 Antibiotic resistance

Since the discovery of antibiotics, treatment of bacterial infections has become increasingly difficult due to antibiotic resistance. This natural phenomenon occurs because of evolution via natural selection. Overtime, bacteria have developed resistant genes caused by genetic mutations to protect themselves against competing fungi and other bacteria.[15] Additionally, bacteria and fungi, which produce the natural products used for antibiotics, develop autoimmunity mechanisms to provide self-protection from the lethal chemical weapons they were producing.[12]

Some mutations enable the bacteria to produce enzymes that inactivate antibiotics. While other resistant genes change the biomolecular target that antibiotics attack. Moreover, some mutations close the entry ports that allow antibiotics to enter the bacterial cell or manufacture pumping mechanisms that expel antibiotics so they never reach their target.[12]

Once a resistant gene is developed, the resistant gene can spread through bacterial populations vertically and horizontally as shown in Figure 4. Vertical transfer occurs when new generations inherit antibiotic resistant genes.[12,16] The large number of bacterial cells in a population and short generation times facilitate the development of vertical gene transfer. If one of the bacteria contains a resistant gene, in the presence of a given antibiotic, then the resistant bacterium will grow and take over the culture.[9,12,17–19]

Horizontal gene transfer occurs when bacteria share or exchange genetic material with other bacteria through conjugation, transduction, and transformation. During conjugation, a bacterium transfers a plasmid carrying resistant genes to another bacterium through a mating bridge that joins the two bacteria. In transduction, resistant genes are transferred via bacteriophages. During transformation, a bacterium acquires resistant genes from other bacteria that have released their DNA into the environment after cell lysis. Horizontal gene transfer can occur between different bacterial species. Additionally, bacteria can collect multiple resistant traits and become resistant to many different classes of antibiotics leading to multidrug-resistant (MDR) bacteria.[8,10,12,16–19]

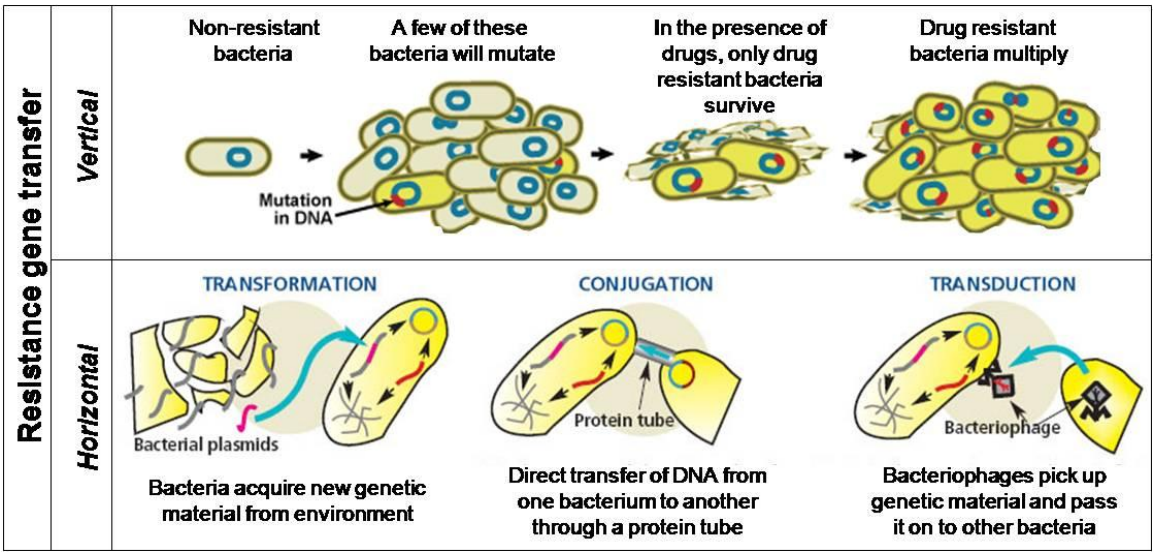

Figure 4. Illustration of resistance gene transfer.

Although antibiotic resistance is a natural phenomenon, the irresponsible overuse of antibiotics, inappropriate prescribing and extensive agriculture use has led to the rapid spread of antibiotic resistance. As shown in Figure 5, once a new antibiotic is introduced into clinical use, resistance can appear as quickly as a few months or years. The more widely used the antibiotic, the more probable the resistance.[12]

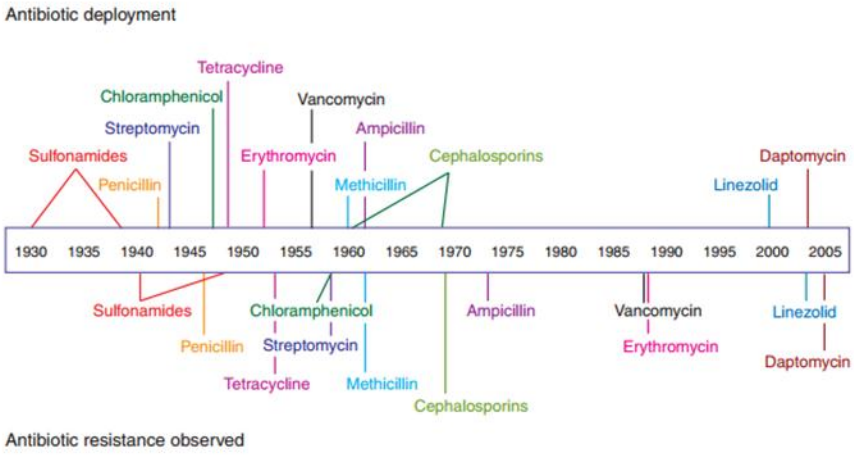

Figure 5. Timeline of antibiotic deployment and the evolution of antibiotic resistance.[20]

In addition to the appearance of antibiotic resistant genes, there has been a decline in antibiotic development. Since the discovery of antibiotics, only four new classes of

antibiotics have been marketed and none of these new classes are novel: daptomycin (approved 2003) was discovered in 1980s; linezolid (approved 2000) derives from a synthetic lead discovered in the 1970s; pleuromutilin (approved 2007) have been widely used for about 30 years in veterinary medicine; and fidaxomicin (approved 2011) was first reported in the 1970s.[14]

1.4 Photodynamic inactivation

The development and rapid spread of antibiotic resistance has limited the lifespan of antibiotics and created a constant need of new antibiotics. Therefore, alternative treatment methods are needed to prevent the development of new resistant traits and slow down the spread of current resistant genes. Photodynamic inactivation (PDI) of microbes is a non-antibiotic approach that uses light, a photosensitizing molecule(PS), and molecular oxygen to generate singlet oxygen ($^1O_2$) and reactive oxygen species (ROS). The photogenerated species oxidize biomolecules causing cellular damage and cell death.[4,6,21–30]

The mechanism to produce $^1O_2$ and ROS is illustrated in the Jablonski diagram (Figure 6). After irradiation from a light source, the PS is excited from the ground state to an excited singlet state. The excited singlet state of the PS can lose energy by fluorescence emission returning to the singlet ground state or by an intersystem crossing (ISC) process. During ISC process, the electron changes spin multiplicity from an excited singlet state to an excited triplet state. In this state, the return to ground state can occur radiatively by phosphorescence emission (P) or non-radiatively by spin exchange with

another triplet state molecule such as molecular oxygen through type II mechanism or electron transfer with substrates through type I mechanism.[4,21,23,30]

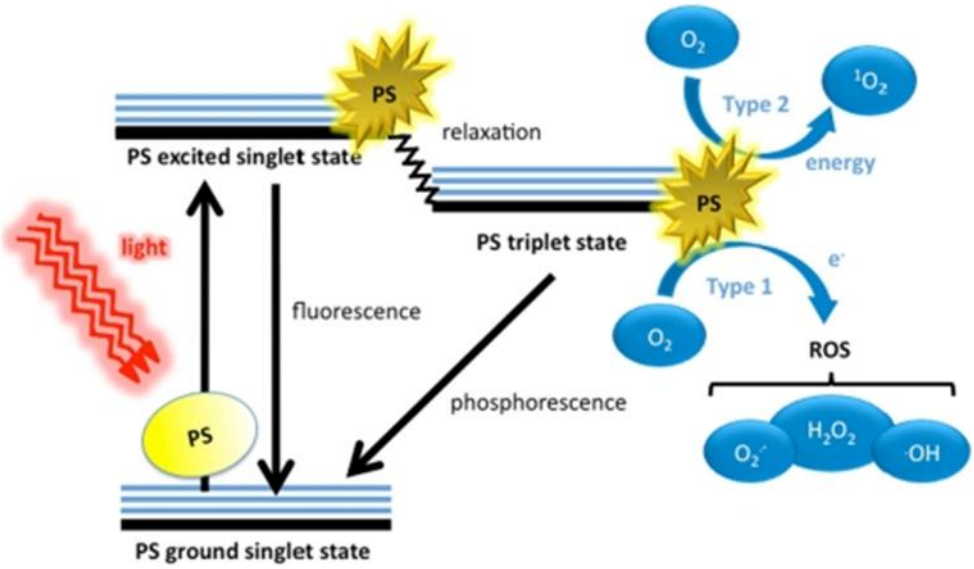

Figure 6. Jablonski diagram of photodynamic inactivation mechanism.[31]

In Type I mechanism, the excited PS reacts with substrates via electron transfer or hydrogen abstraction to yield free radicals such as superoxide radical anion ($O_2^{\cdot-}$), hydrogen peroxide (H_2O_2), and hydroxyl radicals (·OH). ROS readily react with polyunsaturated fatty acids of the fatty acid membrane, starting a self-propagating chain reaction resulting in considerable damage.

In type II mechanism, the excited PS transfers energy to ground state molecular oxygen, returning the PS to its ground state and yielding highly reactive $^1O_2$. As shown in Table 1, ROS and $^1O_2$ can react with more than one biomolecule target, including lipids, proteins and DNA bases.[30]

Table 1. Photocytotoxic pathways in microbial cells.[23]

Site of Action	Action	Result	Consequence	Cytotoxic Event
Water	Hydrogen abstraction	Formation of hydroxyl radical (HO·)	Formation of hydrogen peroxide and superoxide	Further oxidative stress
Cell Wall; membrane unsaturated lipids; sterols	Peroxidation	Peroxidation	Hydroperoxide formation	Increase ion permeability (Na^+/K^+ leakage)
Peptide	Hydrogen abstraction	Peptide cross-linking	Enzyme inactivation	Loss of repair facility; lysis
Cytoplasmic enzymes	Oxidation or cross-linking			Inhibition of ribosome assembly
Nucleic acid residues (guanosine)	Oxidation of base or sugar	8-hydroxy Guanosine	Nucleotide degradation	Base substitution; strand cleavage; mutation; inhibition of replication

Although bacteria do not currently have any reported development of resistance against PDI, bacteria have several mechanisms to elude oxidative stress from the environment. The protective system consists of antioxidant enzymes such as superoxide dismutase, catalase, and peroxidases to deactivate ROS. However, this protective system does not provide protection against $^1O_2$ which is able to inactivate antioxidant enzymes. As a result, compared to type I, type II mechanism is accepted as the major pathway in oxidative cell damage.[25,32,33] Maisch *et al.* demonstrated photoinactivation of *S. aureus* and *E. coli* strains mediated predominantly by $^1O_2$. They showed that the PDI effect was not changed when mannitol, a quencher of superoxide anion and hydroxyl radical, was used. However, the PDI affect was inhibited when 1,4-diazabicyclo-(2,2,2)octane (DABCO) or sodium azide was used as type II, $^1O_2$, scavengers.[34]

It has been suggested that PDI potentially eliminates the development of new resistant genes because the photogenerated ROS and $^1O_2$ target a large variety of biomolecules and internalization of the PS is not required to effectively kill microbes.[23] Therefore, PDI is an effective alternate treatment to antibiotics. However, the efficacy of PDI depends on the type of PS employed and the chemical structure of the PS. PS which are nontoxic to mammalian cells and efficient at ISC to generate ROS and $^1O_2$ are ideal PS in PDI. One of the most studied groups of PS consists of porphyrin derivatives.

1.5 Porphyrins

Porphyrins are involved in vital functions such as photosynthesis, biological oxidation and reduction, and the transport of oxygen by hemoglobin.[35] Porphyrins are aromatic tetrapyrrolic macrocycles containing 22 total π electrons. The conjugated portion of the porphyrin molecule consists of 18 π electrons, following Hückel's rule of 4n+2 π electron, where n = 4. Porphyrins have a planar ring system which allows maximum overlap of the p orbitals. The basic structure of porphyrins consists of four pyrrole units linked by four methene bridges as shown in Figure (7).[36]

The porphyrin core is numbered from 1 to 20 where the 5, 10, 15 and 20 positions are known as the *meso* positions and the 2, 3, 7, 8, 12, 13, 17 and 18 positions are the β-positions. *Meso*-porphyrins are substituted at the methanic hydrogens by alkyl or aryl groups, such as phenyls, as in 5,10,15,20-meso-tetrakisphenylporphyrin (TPP). Peripheral substituents can be attached at the ortho (2'), meta (3') or para (4') positions.[36]

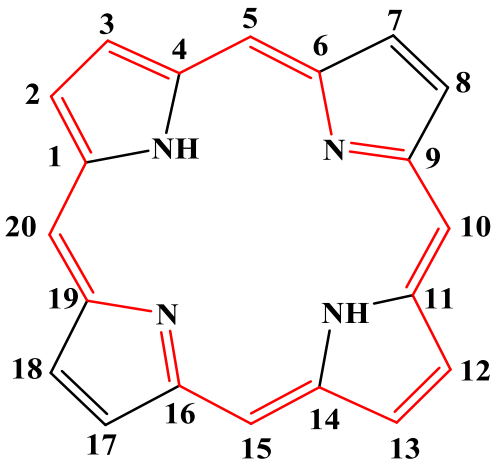

Figure 7. The porphyrin core.

1.5.1 Photophysical properties

Porphyrins are intensely colored and absorb light in the visible part of the spectrum (wavelengths 400 – 700 nm). The absorbance spectrum of free-base porphyrins has one intense band, called the Soret band (B), in the near-ultraviolet region between 390 nm to 425 nm, and four low-intensity absorption Q bands at higher wavelengths in the visible region from 480 to 650 nm. Free-base porphyrins also exhibit two fluorescence peaks from 600 to 730 nm.[37] The efficiency of fluorescence is determined by the fluorescence quantum yield. The fluorescence quantum yield is the number of photons emitted by the sample per absorbed photon and can be determined using the comparative method to a known standard using Eq (1)

$$\Phi_{F,\ Sample} = \Phi_{F,\ Reference} \times \frac{m_{Sample}}{m_{Reference}} \times \frac{n^2_{Sample}}{n^2_{Reference}} \qquad (1)$$

where $\Phi_{F,\ Reference}$ represents the fluorescence quantum yield of the reference fluorophore, m represents the slope of the line when the area of the emission peak is plotted against

the absorption of the fluorophore at the excitation wavelength for the sample and reference, n is the refractive index of the solvent.[38]

Porphyrin derivatives are common PS in PDI because porphyrins readily undergo ISC to the triplet excited state where energy is transferred to oxygen to afford $^1O_2$. Singlet oxygen plays a vital role in the inactivation of microorganisms using PDI.[23] Molecular oxygen has two excited singlet states, $^1\Delta_g$ and $^1\Sigma^+_g$, 22.5 kcal/mol and 31.5 kcal/mol above the triple state ground state ($^3\Sigma^-_g$), respectively. The two excited singlet states differ only by the structure of the π-antibonding orbitals as shown in Figure 8. The $^1O_2$ in PDI is notated as the first excited state of oxygen ($^1\Delta_g$) and not the second excited state ($^1\Sigma^+_g$) because the transition from $^1\Delta_g$ to triplet ground state is spin forbidden, causing $^1\Delta_g$ to be a long-lived species. However, the transition from $^1\Sigma^+_g$, to $^1\Delta_g$ is a spin-allowed transition causing the second excited state of oxygen to be short-lived.[30]

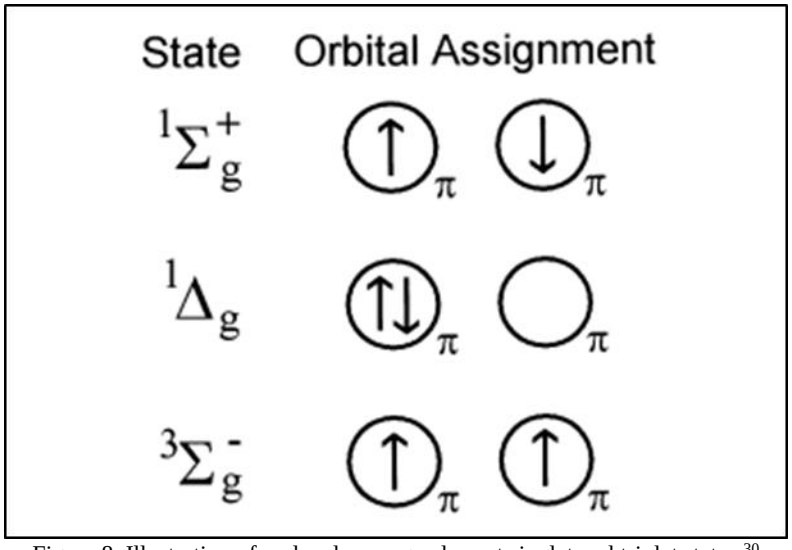

Figure 8. Illustration of molecular oxygen lowest singlet and triplet states.[30]

The efficiency of a PS to use light energy to convert oxygen to $^1O_2$ is determined by its quantum yield. Singlet oxygen quantum yield (Φ_Δ) is defined as the number of

singlet oxygen molecules generated per number of photon absorbed by the PS.[30,39] The absorption of a single photon has the capacity to regenerate only one molecule of $^1O_2$. Therefore, Φ_Δ is an integer with a value between zero and one. A Φ_Δ of one would mean every photon which undergoes ISC generates an $^1O_2$ molecule.[40]

There are several methods used to measure the Φ_Δ. For example, direct detection methods such as time-resolved near infrared (NIR) luminescence,[38–40] and indirect methods which monitor the activity of a secondary compound.[38,39,41,42] Although NIR luminescence technique is a direct method to monitor the emission of $^1O_2$, the lifetimes of $^1O_2$ in different solvents such as DMF, DMSO or water are short compared to halogenated solvents leading to weak emission intensities.[42] To avoid inaccurate measurements, $^1O_2$ generation may also be monitored indirectly.

The reaction between an acceptor or quencher compound with $^1O_2$ is a common indirect detection method. The production of $^1O_2$ is measured via monitoring the disappearance of the $^1O_2$ quencher or the appearance of the reaction's product. The most common $^1O_2$ acceptor found in literature is 1,3-diphenylbenzofuran (DPBF). DPBF reacts irreversibly and quickly with $^1O_2$ in a 1:1 stoichiometry without any side reactions. DPBF undergoes a 1,4-cycloaddition reaction with singlet oxygen forming endoperoxides, which are decomposed to yield 1,2-dibenzoylbenzene (DBB) as shown in Scheme 1. DPBF has a strong absorbance at 415 nm while DBB has no absorption in this range; therefore, the reaction between DPBF and $^1O_2$ can be monitored by the decrease in the intensity of the absorption band of DPBF.[38,41,42]

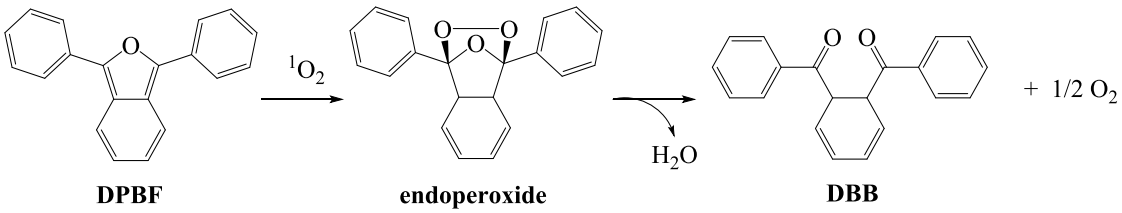

Scheme 1. Photooxidation reaction between DPBF and singlet oxygen to yield DBB and molecular oxygen.[41]

However, using DPBF to monitor $^1O_2$ generation of porphyrins is challenging because the absorbance maxima of porphyrins also appear around 415 nm causing overlap and instrument saturation at high concentrations of PS and DPBF. Additionally, DPBF photobleaches quickly. To avoid the challenges of DPBF, 9,10-dimethylanathracene (DMA) is an alternative $^1O_2$ acceptor that also undergoes a 1,4-cycloaddition reaction with $^1O_2$ (Scheme 2) and displays three absorbance bands below the Soret band of porphyrins (Figure 9), making DMA more suitable for the indirect detection of $^1O_2$ quantum yield in porphyrin systems.[43]

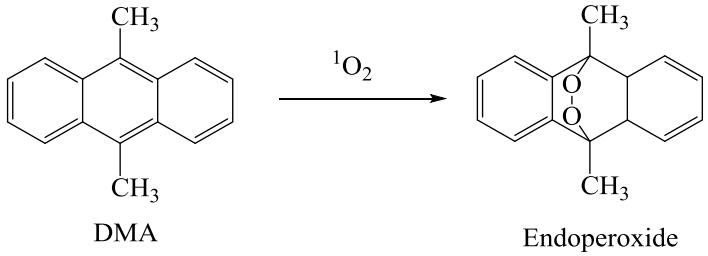

Scheme 2. DMA reaction with $^1O_2$ forming an endoperoxide.[43]

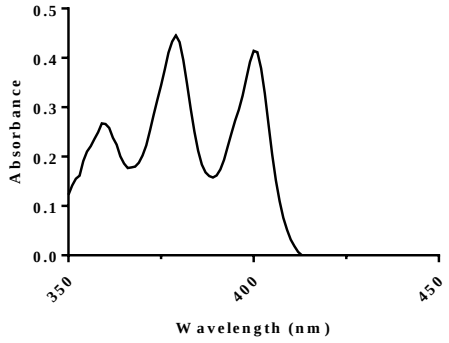

Figure 9. DMA absorption spectrum.

The reaction of DMA and $^1O_2$ is monitored at the absorbance maxima of DMA (380 nm). The $^1O_2$ quantum yield is calculated using the comparative method, as shown in Eq (2),

$$\Phi_{\Delta,S} = \Phi_{\Delta,R} \times \frac{m_S}{m_R} \times \frac{1 - 10^{-Abs_R}}{1 - 10^{-Abs_S}} \quad (2)$$

where m_S and m_R are the slopes of Stern-Volmer plots ($Ln(A_0/A)$ versus irradiation time) of photodegradation of DMA by the sample and reference, respectively. Abs_R and Abs_S represent the absorbance of the PS at the irradiation wavelength for the reference and sample, respectively.

1.6 Current methods to optimize PDI

$^1O_2$ is a highly reactive species, leading to a short lifetime in water (~ 3.5 μs).[44,45] Additionally, the diffusion distance of $^1O_2$ in cellular membranes is only 0.4 μm.[46] Therefore, the efficacy of PDI is heavily dependent on the PS localization. PS that interact sufficiently with bacterial cell membranes have the advantage of positioning $^1O_2$ near abundant biomolecules.[28]

Gram-positive bacteria have shown to be more susceptible to PDI than Gram-negative bacteria.[28] The difference in susceptibility can be explained by the structural differences between Gram-positive and Gram-negative bacteria. The membrane barrier of Gram-positive bacteria consists of a porous cell wall. On the other hand, Gram-negative bacteria is composed of a complex outer membrane comprised of many constituents. The complexity of the outer membrane creates an impermeable barrier to molecules.[4–7]

Research of PDI has shown that neutral and anionic PS can photodynamically inactivate Gram-positive bacteria.[21,27,28,33,47] However, neutral and anionic PS are not able

to inactivate Gram-negative bacteria.[48] LPS molecules are the main components of the outer membrane of Gram-negative bacteria and are mostly responsible for the cell impermeability character.[49] Therefore, two main approaches have been used to increase the permeability of gram-negative bacterial cells by altering the stability of LPS molecules. One method is the pre-treatment of bacterial cells with ethylene diamine tetraacetic acid (EDTA). A second method is the use of polycation membrane-disorganizing agents such as polymyxin B nonapeptide (PMBN).[28,48]

It was demonstrated that pre-treatment of Gram-negative wild-type cells with EDTA caused cells to lose up to 50% of their LPS molecules and become sensitive to hydrophobic molecules.[28,50] EDTA molecules chelate divalent cations (e.g. Mg^{+2}) that provide stability to LPS molecules. Chelation of the divalent cations cause electrostatic repulsion between LPS molecules, and consequently, LPS molecules are released from the outer leaflet.[28,50] Unlike EDTA, PMBN does not cause the release of LPS molecules. Instead PMBN expands the outer leaflet of the outer membrane by displacing divalent cations. Nitzan *et al.* demonstrated the photosensitization of *E. coli* and *P. aeruginosa* cells by deuteroporphyrin (DP) (Figure 10) in the presence of PMBN.[48]

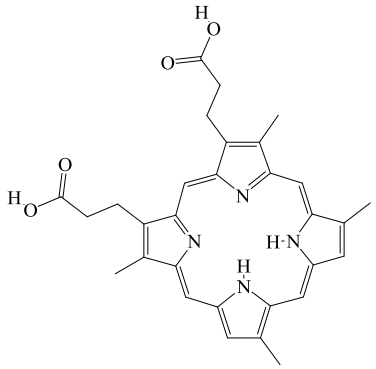

Deuteroporphyrin

Figure 10. Deuteroporphyrin tested against *E. coli* and *P. aeruginosa*.[48]

1.6.1 Cationic Porphyrins

Several studies have used PS molecules with intrinsic positive charges to increase the sensitivity of Gram-negative bacteria.[7,21,28,50–52] Cationic PS have a greater affinity for negatively-charged constituents of LPS molecules than the divalent cations. The competitive binding displaces the divalent cations like the mechanism of interaction of PMBN. The enhanced interaction between the PS and the bacterial cells decrease the distance between $^1O_2$ and PDI targets.

Caminos *et al* investigated the photodynamic activity of a series of cationic porphyrin derivatives with different patterns of substitution to inactivate *E. coli* (Figure 11).[54] The activity of the cationic porphyrins was compared with a tetraanionic porphyrin, 5,10,15,20-tetra(4-sulfonatophenyl)porphyrin sodium. The authors investigated the amount of cationic porphyrin bound to *E. coli* and the photodynamic inactivation effect against *E. coli*. It was found that the tricationic porphyrin (A_3B^{3+}) was highly bound to *E. coli* cells after 5, 10, and 30 min incubation times and 3 washing steps in comparison with the other cationic porphyrins. Additionally, i*n vitro* studies ([PS] = 1 μM; incubation = 30 min; light intensity = 54 mW cm^{-2}) showed that the tri-cationic porphyrin produced the highest photoinactivation, ~3.6 log reduction of *E. coli* cells. In comparison, the photoinactivation of cells by the di-cationic and mono-cationic produced a low reduction, ~1 log reduction and < 1 log reduction respectively. The anionic porphyrin showed negligible attachment to the bacterial cells and photoinactivation. From these results, they concluded that in addition to the number of positive charges on the PS, the presence of highly lipophilic trifluoromethyl groups increase the amphiphilic character of the PS and

interaction with the cell membrane as lipophilic molecules are able to pass through cell membranes.[54]

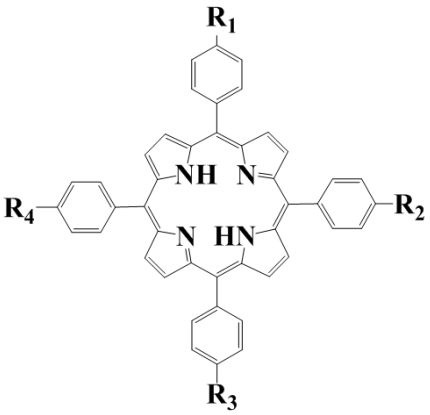

A_3B^+	R_1: $-O(CH_2)_3N^+(CH_3)_3I^-$	$R_2=R_3=R_4$: $-CF_3$
$ABAB^{2+}$	$R_1=R_3$: $-O(CH_2)_3N^+(CH_3)_3I^-$	$R_2= R_4$: $-CF_3$
A_3B^{3+}	$R_1=R_2= R_3$: $-O(CH_2)_3N^+(CH_3)_3I^-$	R_4: $-CF_3$
A_4^{4+}	$R_1=R_2=R_3=R_4$: $-O(CH_2)_3N^+(CH_3)_3I^-$	
$TTAP^{4+}$	$R_1=R_2=R_3=R_4$:	
TPP	$R_1=R_2=R_3=R_4$: H	
$TPPS_4^{4-}$	$R_1=R_2=R_3=R_4$: $SO_3^-Na^+$	

Figure 11. Series of porphyrins synthesized and tested against *E. coli*.[54]

Similarly, Alves *et al* compared the photodynamic inactivation efficiency of seven cationic porphyrins (Figure 12) that differ in *meso*-substituent groups, charge number and charge distribution against a Gram-positive bacterium, *E. faecalis*, and a Gram-negative bacterium, *E. coli*.[55] All the cationic porphyrins were effective PS against *E. faecalis* (~7 log reduction of 5 μM PS solutions) with the tricationic porphyrins being the most efficient. Against *E. coli*, the efficiency of PS followed the order: Tri-Py^+-Me-PF = Tri-Py^+-Me-CO_2Me > Tetra-Py^+-Me > Tri-Py^+-Me-CO_2H > Di-Py^+-Me-Di-CO_2H *adj.* > Di-Py^+-Me-Di-CO_2H *opp.* > Mono-Py^+-Me-Tri-CO_2H. The results show that the *meso*-substituent groups play a significant role in the photodynamic inactivation of *E. coli*. Like Caminos results, Alves *et al* showed that a high number of positive charges and an amphiphilic character increase the PDI efficiency. The distribution of the charges on

the PS is another factor that influences the efficiency of PDI. The *cis*-isomer showed a higher efficiency on the photoinactivation of *E. coli* and *E. faecalis* than the *trans*-isomer.[55]

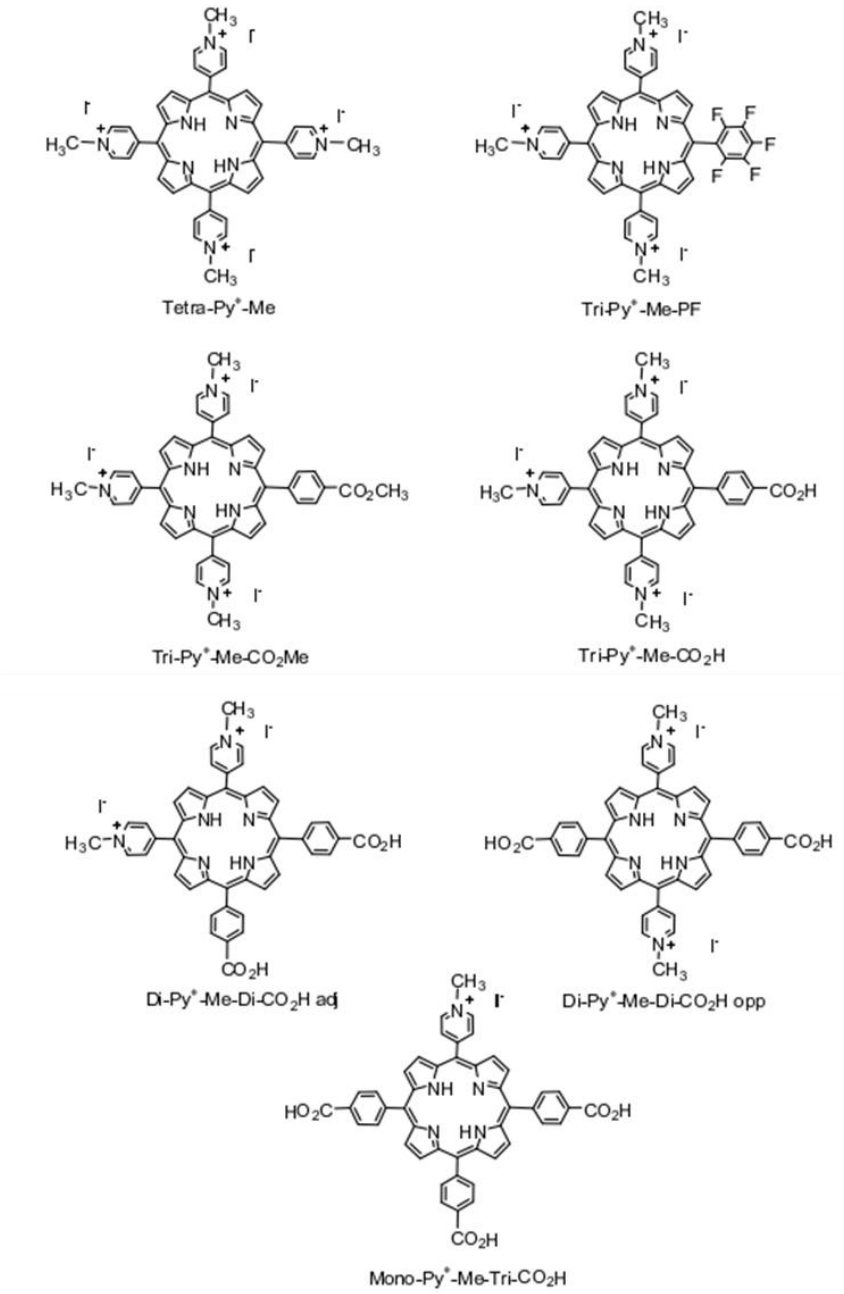

Figure 12. Series of porphyrins synthesized and tested against *E. faecalis* and *E. coli*.[55]

1.6.1.1 Mechanism of Internalization of Cationic Porphyrins

Thus far, not much is known about the internalization of cationic porphyrins and the location where the primary photodamage occurs. The uptake of cationic PSs through the outer membrane and into the periplasmic space and cytoplasm is thought to be mediated by electrostatic interactions and the "self-promoted" uptake pathway (Figure 13).[7,51,56] In the self-promoted uptake pathway, highly cationic molecules such as polycationic peptides, displace divalent cations that provide stability to neighboring LPS molecules. The large size of PS cause a distortion in the outer membrane, and facilitates the uptake of hydrophobic molecules.[56,57]

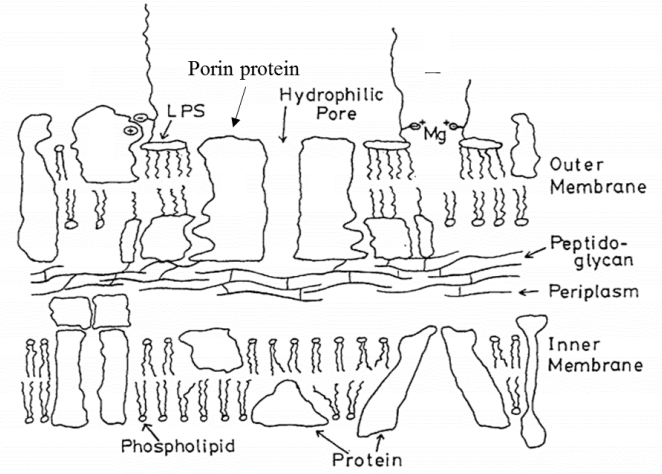

Figure 13. Illustration of a cross section of the cell envelope of Gram-negative bacteria.[56]

Minnock *et al* demonstrated that a tetracationic phthalocyanine interacted with bacterial cells through the self-promoted uptake pathway.[51] It was shown that the incubation of *E. coli* with the cationic phthalocyanine in the dark caused alterations in the outer membrane permeability to hydrophobic antibiotics and decreased the MICs of those antibiotics. In contrast, the MICs of hydrophilic molecules for *E. coli* were not affected. Additionally, in the presence of increasing concentrations of Mg^{+2}, the uptake of the

cationic phthalocyanine decreased and the photoinactivation effect against *E. coli* decreased. The results confirmed the hypothesis that the cationic phthalocyanine gained access across the outer membrane into the periplasmic space in Gram-negative bacteria.[51]

Ragas *et al*. used a combination of spectroscopic and time-resolved photophysical techniques to understand where a tetracationic porphyrin, 5,10,15,20-tetrakis(*N*-methylpyridinium)porphyrin ($TPy^{+}P$), localized in *E. coli* cells.[58] Their results found that a fraction of the tetracationic porphyrin was bound to the external structure of the cell wall while the remaining PS was internalized. Fluorescence lifetime changes indicated that the internalized PS was bound to the cytosolic nucleic acids, and exposure to visible light (7 nJ cm^{-1}) induced the formation of $^{1}O_2$ both inside and outside the cell.[58]

1.7 Research Objective

Many studies has been conducted to understand the localization and mechanism of internalization of tetracationic porphyrins in bacterial cells, [7,51,56,58,59] but they have not used microscopy to demonstrate the localization of PS with bacterial cells. Fluorescence microscopy has been a useful technique to assess the localization/uptake of PS in eukaryotic cells, however PDI research have not explored the uptake of cationic porphyrins in bacterial cells due to resolution limitations.[58]

The objectives of the current research project are to synthesize and characterize a series of cationic porphyrins bearing one to four trimethylammonium groups (Figure 14), evaluate their photodynamic inactivation efficacy, and investigate the extent of their interaction with *Escherichia coli* (*E. coli*), a model for Gram-negative bacteria, using fluorescence confocal microscopy and competitive binding.

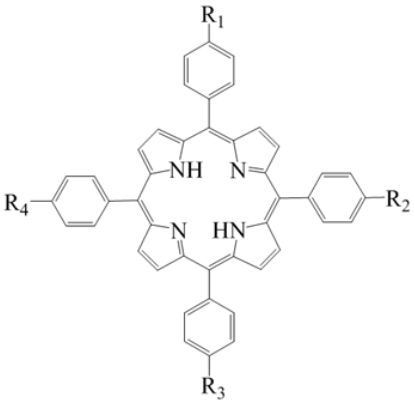

	Porphyrin	R_1	R_2	R_3	R_4
1a.	**A^+TPP**	$N^+(CH_3)_3I^-$	H	H	H
2a.	**cis-$TA^{2+}PP$**	$N^+(CH_3)_3I^-$	$N^+(CH_3)_3I^-$	H	H
	trans-$TA^{2+}PP$	$N^+(CH_3)_3I^-$	H	$N^+(CH_3)_3I^-$	H
3a.	**$TA^{3+}PP$**	$N^+(CH_3)_3I^-$	$N^+(CH_3)_3I^-$	$N^+(CH_3)_3I^-$	H
4a.	**$TA^{4+}PP$**	$N^+(CH_3)_3I^-$	$N^+(CH_3)_3I^-$	$N^+(CH_3)_3I^-$	$N^+(CH_3)_3I^-$

Porphyrin Substituent Abbreviations
A (amino) – NH_2
N (nitro) – NO_2
N^+ (*N, N, N*- trimethylammonium iodide) – $N^+(CH_3)_3I^-$

Figure 14. Cationic porphyrin derivatives.

1.7.1 Approach

To reach the goal of this work, the following specific aims were carried out: 1) To synthesize and characterize a series of cationic porphyrins containing one to four trimethylammonium groups; 2) To evaluate the charge effect of the cationic porphyrins in the photodynamic inactivation against *E. coli* cells; 3) To investigate the interaction of the cationic porphyrins towards *E. coli* cells using fluorescence confocal microscopy and competitive binding.

1.7.1.1 Syntheses and characterization of cationic porphyrins

The synthesis of the cationic porphyrin derivatives was performed using a multi-step synthetic approach. The porphyrin derivatives were characterized using ^{1}H NMR, FTIR, and mass spectroscopy. Absorbance and emission spectra were used to determine the fluorescence and singlet oxygen quantum yields.

1.7.1.2 Evaluation of dark and light toxicity of cationic porphyrins against *E. coli*

The photodynamic inactivation efficacy of the cationic porphyrins was tested against *E. coli* strain MG1655.

1.7.1.3 Investigate the interaction mechanism between cationic porphyrins and *E. coli*

The localization of cationic porphyrin derivatives with *E. coli* was investigated using fluorescence confocal microscopy and competitive binding.

CHAPTER 2: EXPERIMENTAL

2.1 Materials and Methods

All commercial chemicals and solvents were of reagent grade or higher and were used as received. All experiments with moisture/air-sensitivity were performed in anhydrous solvents under a nitrogen atmosphere. Column chromatography was performed using silica G60 (70-230 mesh). IR spectra were recorded on a Perkin-Elmer 100 IR spectrophotometer. ^{1}H NMR spectra were recorded on a 300 MHz or 500 MHz JEOL NMR spectrometer and are referenced with $CDCl_3$ and DMSO-d_6 solvents. Mass spectra were obtained using a Voyager Biospectrometry Laser MALDI-TOF spectrometer or Thermal Scientific MSQ Plus ESI spectrometer. UV-Vis spectra were recorded on a Cary 300 UV-visible spectrophotometer. Steady-state fluorescence emission was measured on a Jobin Yvon Fluorolog 3. Fluorescence microscopy z-stacking images were collected using a DeltaVision Elite Workstation based on an inverted microscope (1X-70; Olympus) equipped with a 100x, 1.4 NA oil immersion lens.

2.2 Syntheses and structural characterization of porphyrin derivatives

2.2.1 Synthesis of 5-(4'-*N*,*N*,*N*-trimethylammoniumphenyl)-10,15,20-triphenylporphyrin iodide (A^{+}TPP)

The synthesis of A^{+}TPP was accomplished by alkylating commercially available 5-(4'-aminophenyl)-10,15,20-triphenylporphyrin.[60] A mixture of 5-(4'-aminophenyl)-10,15,20-triphenylporphyrin (45 mg, 0.0714 mmol) and methyl iodide (CH_3I) (4 mL, 64.2 mmol) in anhydrous DMF (5 mL) was heated to 45 ºC and stirred for 24 h under

nitrogen gas. Dichloromethane (CH_2Cl_2) (50 mL) was added to the reaction mixture, and the solution was washed with water. The aqueous and organic layers were separated using a separatory funnel. The organic layer was collected. The solvent was removed using rotary evaporation to dryness. A minimal amount of CH_2Cl_2 was added followed by an excess of diethyl ether. The desired porphyrin precipitated down and was collected by vacuum filtration. Yield: 76% wt. ^{1}H NMR (300 MHz, $CDCl_3$, ppm): δ 8.88-8.90 (2H, d, β-pyrrole), 8.84 (4H, s, β-pyrrole), 8.79-8.81 (2H, d, β-pyrrole), 8.50-8.53 (2H, d, o-N^+Ph), 8.41-8.44 (2H, d, m-N^+Ph), 8.21-8.24 (6H, d, o-Por), 7.83-7.86 (9H, m, m/p-Por), 3.92 (9H, s, CH_3), -2.92 (2H, s, pyrrole-H). FTIR (solid, cm^{-1}): 3445 (N-H stretch), 2852-3135 (C-H stretch), 1595 (C=C bend). UV-vis (DMSO) λ_{max} (ε x 10^5 M^{-1} cm^{-1}): 417 (3.40), 514 (0.14), 548 (0.06), 589 (0.04), 645 (0.03) nm; ESI-MS (m/z): $[M - I]^+$ = 672.13; Calculated 672.31.

2.2.2 Synthesis of mixture cis-5,10-bis(4'-*N*,*N*,N-trimethylammoniumphenyl)-15,20-diphenylporphyrin iodide and trans-5,15-bis(4'-*N*,*N*,*N*-trimethylammoniumphenyl)-10,20-diphenylporphyrin iodide ($TA^{+2}PP$)

2.2.2.1 Synthesis of mixture cis-5,10-bis(4'-nitrophenyl)-15,20-diphenylporphyrin and trans-5,15-bis(4'-nitrophenyl)-10,20-diphenylporphyrin (TN_2PP)

Tetraphenylporphyrin (TPP) (127.6 mg, 0.207 mmol) was dissolved in dichloromethane (30 mL) and flushed with N_2 at room temperature. One aliquot of NO_2BF_4 (500 µL, 0.250 mmol; total 2.5 mL, 1.250 mmol) was added dropwise to the reaction mixture every 60 min totaling an addition of five aliquots. The reaction was stirred under N_2 for 24 h. Dichloromethane (50 mL) was added to the reaction mixture,

and the solution was washed with water. The aqueous and organic layers were separated using a separatory funnel. The organic layer was collected, and the solvent was removed using rotary evaporation to dryness. To remove sulfolane, a minimal amount of acetone (<5 mL) was added, followed by water (50 mL) which caused the porphyrins to precipitate down. The desired di-nitrated porphyrin was purified using silica chromatography, eluting with CH_2Cl_2: Hexanes (1:1). Yield: 67% wt. ^{1}H NMR (300 MHz, $CDCl_3$, ppm): δ 8.52-8.66 (8H, m, β-pyrrole), 8.34-8.37 (4H, d, J = 8.67 Hz, o-Ph-NO_2), 8.10-8.13 (4H, d, J = 8.64 Hz, m- Ph-NO_2), 7.93-7.95 (4H, d, o- Ph-H), 7.52-7.59 (6H, m, m/p-Ph-H), -3.07 (2H, s, pyrrole-NH). FTIR (solid, cm^{-1}): 3316 (N-H stretch), 2851-3102 (C-H stretch), 1594 (Aromatic), 1342,1513 (NO_2 stretch), 964 (C-N stretch). MALDI-TOF (m/z): $[M]^+$ = 704.5. Calculated for $[M]^+$ = 704.75.

2.2.2.2 Synthesis of mixture cis-5,10-bis(4'-aminophenyl)-15,20-diphenylporphyrin and trans-5,15-bis(4'-aminophenyl)-10,20-diphenylporphyrin (TA_2PP)

5,10-(4'-nitrophenyl)-15,20-triphenylporphyrin and 5,15-(4'-nitrophenyl)-10,20-triphenylporphyrin mixture (97.4 mg, 0.138 mmol) was dissolved in 37% HCl (42.5 mL) and sonicated to aid dissolution. $SnCl_2 \cdot H_2O$ (1.35g, 5.96 mmol) was added to this solution, and the reaction mixture was heated to 65 °C. The reaction was stirred for 24 h at 65 °C. Distilled H_2O (50 mL) was added to dilute the solution. Then 0.1 M NH_4OH was added until pH = 8 was reached. The solution was washed with chloroform (100 mL). The aqueous and organic layers were separated using a separatory funnel. The organic layer was collected, and the solvent was removed using rotary evaporation to dryness. Silica chromatography and chloroform were used to obtain the products. The

desired di-amine porphyrin mixture eluted as the second band. Yield: 87% wt. ^{1}H NMR (300 MHz, $CDCl_3$, ppm): δ 8.80-8.92 (8H, m, β-pyrrole), 8.19-8.22 (4H, d, o- Ph-H), 7.96-7.99 (4H, d, m- Ph-NH_2), 7.72-7.74 (6H, m, m/p-Ph-H), 7.01-7.04 (4H, d, o-Ph-NH_2), -2.74 (2H, s, pyrrole-NH). FTIR (solid, cm^{-1}): 3451, 3362, 3321 (N-H stretch), 2851-3026 (C-H stretch), 1616 (aromatic). MALDI-TOF (m/z): $[M]^+$ = 644.61; Calculated = 644.78.

2.2.2.3 Synthesis of mixture cis-5,10-bis(4'-*N*,*N*,*N*-trimethylammoniumphenyl)-15,20-diphenylporphyrin iodide and trans-5,15-bis(4'-*N*,*N*,*N*-trimethylammoniumphenyl)-10,20-diphenylporphyrin iodide ($TA^{+2}PP$)

5,10-(4'-aminophenyl)-15,20-triphenylporphyrin and 5,15-(4'-aminophenyl)-10,20-triphenylporphyrin mixture (26.5 mg, 0.0411 mmol) was dissolved in anhydrous DMF (5 mL) and flushed with N_2. CH_3I (4 mL, 64.25 mmol) was added and the reaction stirred for 24 h. Then dichloromethane (25 mL) and water (25 mL) were added to the reaction mixture. The aqueous and organic layers were separated using a separatory funnel. The desired porphyrin product and starting porphyrin resided in the organic layer. Therefore, the organic layer was collected, and the solvent was removed using rotary evaporation to dryness. CH_2Cl_2 (1 mL) was added back to the round bottom flask and an excess of diethyl ether was added which caused the alkylated porphyrin to precipitate down. The precipitate was collected by vacuum filtration. Yield: 75% wt. ^{1}H NMR (300 MHz, DMSO-d_6, ppm): δ 8.77-8.87 (8H, m, β-pyrrole), 8.47-8.50 (4H, d, J = 9.06 Hz, o-N^+Ph), 8.41-8.44 (4H, d, J = 9.09 Hz, m-N^+Ph), 8.19-8.22 (4H, d, o- Ph-H), 7.83-7.85 (6H, m, m/p-Ph-H), -2.95 (2H, s, pyrrole-NH), 3.91 (18H, s, CH_3). FTIR (solid, cm^{-1}):

3317, 3422 (N-H stretch), 2851-2988 (C-H stretch), 1596 (aromatic). MALDI-TOF (m/z): $[M - I^- - CH_3]^+$ = 715.97; Calculated = 715.93.

2.2.3 Synthesis of 5,10,15-tris(4'-*N*,*N*,*N*-trimethylammoniumphenyl)-20-phenylporphyrin iodide ($TA^{+3}PP$)

2.2.3.1 Synthesis of 5,10,15-tris(4'-nitrophenyl)-20-phenylporphyrin (TN_3PP)

Tetraphenylporphyrin (120.1 mg, 0.195 mmol) was dissolved in CH_2Cl_2 (30 mL) and flushed with N_2 at room temperature. One aliquot of NO_2BF_4 (500 µL, 0.250 mmol; total 5.3 mL, 2.5 mmol) was added dropwise to the reaction mixture every 60 minutes totaling an addition of four aliquots. The reaction was stirred under N_2 for 24 h. Dichloromethane (50 mL) was added to the reaction mixture, and the solution was washed with water. The aqueous and organic layers were separated using a separatory funnel. The organic layer was collected, and the solvent was removed using rotary evaporation to dryness. To remove sulfolane, a minimal amount of acetone (< 1 mL) was added, followed by water (25 mL) which caused the porphyrins to precipitate down. The porphyrin mixture was collected by vacuum filtration. The desired porphyrin was purified using silica chromatography, eluting with CH_2Cl_2: Hexanes (1:1). Yield: 44% wt. ^1H NMR (300 MHz, $CDCl_3$, ppm): δ 8.83-8.84 (2H, d, β-pyrrole), 8.73 (4H, s, β-pyrrole), 8.68-8.70 (2H, d, β-pyrrole), 8.56-8.59 (6H, d, J = 8.25 Hz, o-Ph-NO_2), 8.31-8.33 (6H, d, J = 8.67 Hz, m- Ph-NH_2), 8.10-8.12 (2H, d, o- Ph-H), 7.69-7.71 (3H, m, m/p-Ph-H), -2.91 (2H, s, pyrrole-NH). FTIR (solid, cm^{-1}): 3315 (N-H stretch), 2857-3046 (C-H stretch), 1593 (aromatic), 1341-1512 (NO_2). MALDI-TOF (m/z): $[M + 1]^+$ = 750.65; Calculated = 749.74.

2.2.3.2 Synthesis of 5,10,15-tris(4'-aminophenyl)-20-phenylporphyrin (TA_3PP)

5,10,15-tris(4'-nitrophenyl)-20-phenylporphyrin (34.1 mg, 0.0455 mmol) was dissolved in 37% HCl (25 mL) and sonicated to assist dissolution. $SnCl_2 \cdot H_2O$ (0.67g, 3.009 mmol) was added to this solution, and the reaction mixture was heated to 65 °C. The reaction was stirred for 24 h. Distilled H_2O (25 mL) was added to dilute the solution. Then 0.1 M NH_4OH to diluted solution until a pH = 8 was reached. The solution was washed with chloroform (50 mL). The aqueous and organic layers were separated using a separatory funnel. The organic layer was collected, and the solvent was removed using rotary evaporation to dryness. Silica chromatography was used to purify the product. The mixture was eluted with chloroform and methanol (1%) and the second band was collected giving the desired tri-amine porphyrin. Yield: 40% wt. ^1H NMR (300 MHz, $CDCl_3$, ppm): δ 8.92-8.93 (6H, m, β-pyrrole), 8.81-8.83 (2H, d, β-pyrrole), 8.20-8.24 (2H, d, o- Ph-H), 7.95-7.98 (6H, d, J = 8.25 Hz, m- Ph-NH_2), 7.72-7.76 (3H, m, m/p-Ph-H), 6.97-6.99 (6H, d, J = 8.25 Hz, o-Ph-NH_2), -2.68 (2H, s, pyrrole-NH). FTIR (solid, cm^{-1}): 3316 (N-H stretch), 2853-2922 (C-H stretch), 1598 (aromatic). MALDI-TOF (m/z): $[M - 1]^+$ = 658.51, $[M]^+$ = 659.58; Calculated $[M]^+$ = 659.80.

2.2.3.3 Synthesis of 5,10,15,20-tris(4'-*N*,*N*,*N*-trimethylammoniumphenyl)-20-phenylporphyrin iodide ($TA^{+3}PP$)

5,10,15-tris(4'-aminophenyl)-20-phenylporphyrin (39.1 mg, 0.059 mmol) was dissolved in anhydrous DMF (5 mL) and flushed with N_2. CH_3I (6 mL, 96.378 mmol) was added and the reaction stirred for 24 h at 45 °C. After 24 h, an excess of acetone (25 mL) was added which caused the alkylated porphyrin to precipitate down. The precipitate

was collected by vacuum filtration. Yield: 28% wt. ^{1}H NMR (300 MHz, DMSO-d_6, ppm): δ 8.85-8.91 (6H, m, β-pyrrole), 8.79-8.80 (2H, d, β-pyrrole), 8.49-8.52 (6H, d, J = 9.48 Hz, o-Ph-N^+), 8.42-8.45 (6H, d, J = 9.06 Hz, m- Ph-N^+), 8.20-8.23 (2H, d, o- Ph-H), 7.78-7.87 (3H, m, m/p-Ph-H), 3.93 (27H, s, CH_3), -2.96 (2H, s, pyrrole-NH). FTIR (solid, cm^{-1}): 3397, 3316 (N-H stretch), 2849-3005 (C-H stretch), 1597 (aromatic). MALDI-TOF (m/z): $[M - 3(I^-)]^+$ = 790.65; calculated $[M]^+$ = 1169.79.

2.2.4 Synthesis of mixture 5,10,15,20-tetrakis(4'-*N*,*N*,*N*-trimethylammoniumphenyl)phenylporphyrin iodide ($TA^{+4}PP$)

A mixture of 5,10,15,20-tetrakis(4'-aminophenyl) porphyrin (49.7 mg, 0.0737 mmol) and CH_3I (4 mL, 64.25 mmol) in anhydrous DMF (10 mL) was heated to 45 ºC and stirred for 24 h under N_2. After 24 h, excess acetone (25 mL) was added to precipitate down the product. The precipitate was collected by vacuum filtration. Yield 68% wt. ^{1}H NMR (500 MHz, DMSO-d_6, ppm): δ 8.89 (8H, s, β-pyrrole), 8.49-8.51 (8H, d, J = 9.60 Hz, m-N^+), 8.46-8.48 (8H, d, J = 9.65 Hz, o-N^+), 3.96 (36H, s, CH_3), -2.94 (2H, s, pyrrole-H). FTIR (solid, cm^{-1}): 3420 (N-H stretch), 2752-3019 (C-H stretch), 1577 (Aromatic). MALDI-MS (m/z): $[M - 3(I^-)]^+$ = 847.21; Calculated $[M]^+$ = 1354.81.

2.3 Stock solutions

Stock solutions (1 mM) of each porphyrin were prepared in DMSO and DMF. For biological assays, the stock solutions of photosensitizers prepared in DMSO were diluted to final concentrations in PBS, 1% DMSO solution (1x, pH 7.4).

2.4 Photophysical characterization of cationic porphyrins

2.4.1 Absorbance and emission studies

Absorption and emission measurements for the cationic porphyrins were collected on solutions prepared in DMSO. The fluorescence quantum yields for air-saturated solutions (Φ_F) in DMSO were determined using the comparative method, as shown in Eq (1). TPP with a quantum yield of 0.12 in benzene was used as the reference.[52] The porphyrin concentration ranged from 3 µM to 15 µM. The excitation wavelength was 520 nm and the excitation and emission slit width were 2 nm. The integrated area was measured using Origin (fluorescence software), and the slope of the best fit line was determined using linear regression analysis in GraphPad Prism version 7.03 for Windows, GraphPad Software, La Jolla California USA, www.graphpad.com.

2.4.2 Singlet oxygen quantum yield

The quantum yields of singlet oxygen were determined through the absorbance decay of DMA in DMF using the comparative method, as shown in Eq (2). Solutions containing DMA (50 µM) and the PS (~ 5 µM; OD = 0.1 at irradiation wavelength) were prepared in DMF, air saturated. After preparation, the solutions were protected from light. A volume of 2 mL of the solution was filled in a quartz cuvette (1 cm x 1 cm), set into a fluorometer (xenon lamp, Shimadzu RF5301 PC) and irradiated at 515 nm. The irradiation period, controlled by a shutter, was maintained for time intervals (0 – 600 s) which produced no photobleaching of DMA. The decay of DMA was monitored at 379 nm. A reference spectrum of the PS in DMF was taken before each experiment and subtracted from the final data. The experiments were performed three times for each

porphyrin derivative. The experimental design was confirmed by comparison with two references, TPP ($\Phi_\Delta = 0.62$)[54] and THPP ($\Phi_\Delta = 0.54$)[43] in DMF. The slope from the plot of DMA decay was determined using linear regression analysis in GraphPad Prism version 7.03 for Windows, GraphPad Software, La Jolla California USA, www.graphpad.com.

2.5 Bacterial growth conditions

E. coli (MG1655) was inoculated in liquid Luria-Bertani (LB) broth containing 50 µg /mL kanamycin and grew at 37 °C for 6-8 h until the optical density at 600 nm (OD_{600nm}) reached approximately 0.8 (a.u). Cell suspension solutions were prepared using PBS (1x, pH = 7.4). Bacterial cells were harvested through centrifuging (5×10^3 x g for 10 min, 4 °C) and washed with PBS. After discarding the supernatant, the remaining bacterial cell pellet was resuspended in PBS, 1% DMSO solution (1.0 mL) to an $OD_{600\ nm}$ ~ 0.6 – 0.8.

2.6 Irradiation conditions

The light toxicity of the cationic porphyrins was evaluated by exposing bacterial suspensions to white light (LumaCare, 400 – 700 nm) at an irradiance of 44 J cm^{-2}. The light power density was measured with an Ophir Vega power meter.

2.7 Photodynamic inactivation of *E. coli*

A bacterial suspension (OD_{600nm} ~0.6 – 0.8) in PBS, 1% DMSO solution (1.0 mL) was incubated at 37 °C for 30 min in the dark in the presence of each porphyrin (concentration = 1 nM to 10 µM). After 30 minutes, an aliquot of 100 µL representing the "dark toxicity" was removed for each experiment and stored in a 1.5 mL Eppendorf

centrifuge tube. The original cell suspension was centrifuged (5 x 10^3 x g, 10 min, 4 °C) to remove unbound PS. The obtained bacterial cell pellets were resuspended in PBS, 1% DMSO solution (900 µL) and exposed to white light (44 J/cm^2) for 20 min. After white light exposure, another aliquot of 100 µL representing the "light toxicity" sample was removed and stored in a new 1.5 mL Eppendorf centrifuge tube.

The survival percentage was determined by counting the colony-forming units (CFU). The control, dark toxicity and light toxicity solutions were serially diluted 10^6-fold with autoclaved distilled water. The drop-plate method was used to plate diluted samples onto agar plates. Four aliquots of 10 µL portions of the diluted bacterial suspensions were pipetted onto solid LB agar plates which contained 50 µg/mL kanamycin. After incubating for 24 h at 37 °C bacterial colonies were formed. The dilution containing 3-30 colonies was counted. The CFU per mL for each sample was determined by dividing the average CFU by the volume plated in mL (0.010 mL) and the dilution factor. The cell survival percentage of the dark and light samples were calculated as a percent of the control using Eq (3)

$$\text{Survival \%}_{\text{Dark/Light Toxicity}} = \frac{\text{CFU}_{\text{Dark/Light Toxicity}}}{\text{CFU}_{\text{Control}}} \text{ x } 100\% \qquad (3)$$

2.8 Fluorescence confocal laser scanning microscopy

To visualize the interaction between bacterial cells and porphyrins, fluorescence microscopy was used. Bacterial suspensions ($OD_{600\ nm}$ ~ 0.6 – 0.8) were incubated with each porphyrin (concentration = 1 µM) at 37 °C for 30 min in the dark. After discarding the unbound PS by centrifugation (5 x 10^3 x g, 10 min, 4 °C), the cell pellet and tightly-bound porphyrin was resuspended in PBS, 1% DMSO solution (1x, pH= 7.4, 500 µL).

Aliquots of 40 µL cell suspensions were pipetted to glass slides containing agarose pads (0.7%).

Samples were excited with 390 nm and emission captured at 679 nm. Z-stack images were collected at 0.5 µm z-increments on a DeltaVision Workstation (Applied Precision) based on an inverted microscope (1x-70; Olympus) using a 100x/ 1.4 NA oil immersion lens. Images were captured at room temperature with a 12-bit CCD camera (Cool Snap HQ; Photometric) and deconvolved using the interactive-constrained algorithm and the measured point spread function. All image analyses were performed using ImageJ v1.51n (National Institute of Health).

2.9 Photosensitizer binding with Mg^{+2}

The uptake mechanism of cationic porphyrins was studied by determining the effects that excess divalent cation, Mg^{+2}, have on the amount of PS associated with bacterial cells. A bacterial suspension (OD_{600nm} ~0.6 – 0.8) in PBS solution (1.0 mL) was incubated at 37 °C for 30 min in the presence of increasing concentrations of $MgCl_2$ (0, 10, 25, 50 mM). The cultures were centrifuged (5000 g for 10 min) and then resuspended with PS PBS solution ([PS] = 1 µM; 1 mL) at 37 °C in the dark for 30 min. After incubation, unbound PS was removed from the suspension by centrifuging (5000 g for 10 min). To extract the cell-bound PS, washed bacterial cells were treated with 2% sodium dodecyl sulfate (SDS) at room temperature for 14 h. The concentration of bound PS was analyzed by fluorescence. The samples were excited at 415 nm and the emission of the PS was monitored at the fluorescence maximum ($TA^{+3}PP$: 652 nm and $TA^{+4}PP$ 652 nm). The PS concentration was determined by interpolation with a calibration plot constructed

with known concentrations of each PS in 2% SDS. The concentration obtained for each sample were normalized by the total number of cells in the suspension to correct for variations between experiments. The number of PS molecules CFU^{-1} was calculated equation 4:

$$\text{PS molecules CFU}^{-1} = \frac{[\text{PS}] \times N_A}{\frac{\text{CFU}}{\text{mL}} \times 10^3} \quad (4)$$

where [PS] is the calculated PS concentration (mol/L), N_A represents Avogadro's number (6.022×10^{23} molecules mol^{-1}), and CFU mL^{-1} represents the concentration of cells. Aliquots of the control samples (without PS and $MgCl_2$) were serially diluted, and the drop-plate method was used to determine the CFU mL^{-1}. Three experiment replicates were performed.

2.10 Statistical analysis

Statistical analyses were performed by using GraphPad Prism (v7.03 for Windows, La Jolla California, CA, USA). Survival percentages are expressed as means ± standard deviation error of three independent experiments. Differences between the survival curve because of charge number and PS concentrations were assessed by two-way univariate analysis of variance (ANOVA) model with the Bonferroni post hoc test. A value of $p < 0.05$ was considered as statistically significant.

CHAPTER 3: RESULTS AND DISCUSSION

3.1 Syntheses and structural characterization of cationic porphyrins

In the present work, the cationic porphyrin derivatives were synthesized via methylation of amino phenyl-substituted porphyrins. The mono- and tetra- amino phenyl porphyrins derivatives are commercially available. However, the di-mixture and tris-amino phenyl-substituted porphyrins were obtained in a two-step synthetic approach. First, the nitration of the para phenyl position of TPP was carried out using NO_2BF_4 as a nitrating agent.[61] Then the nitro groups were reduced with $SnCl_2$ in acidic medium, as illustrated in Scheme 3.[62] In the final step, the amino phenyl porphyrin derivatives were alkylated using a large excess of methyl iodide.[60]

The successful synthesis of 5-(4'-*N*,*N*,*N*-trimethylammoniumphenyl)-10,15,20-triphenylporphyrin iodide (A^+TPP) was confirmed by FTIR, ^1H NMR and MALDI-TOF. The FTIR showed the characteristic stretching vibrations for N-H at 3445 cm^{-1}, C–H at 2852–2922 cm^{-1}, and C=C at 1595 cm^{-1} (Figure A1. 3). Additionally, the ^1H NMR spectra depicted the coupling pattern for the hydrogens associated to the β-pyrrole rings as two doublets and one singlet, and the chemical shifts for the hydrogens associated to the ammoniumphenyl group at δ 8.41 to 8.44 and δ 8.50 to 8.53 ppm (Figure A1.1). In addition, the chemical shift corresponding to the hydrogens of the methyl groups were found at δ 3.92 ppm. Finally, the molecular ion for A^+TPP was also identified in the MALDI-TOF at 672.20 m/z (Figure A1. 4).

The synthesis of mixture *cis*-5,10-bis(4'-*N*,*N*,*N*-trimethylammoniumphenyl)-15,20-diphenylporphyrin iodide and *trans*-5,15-bis(4'-*N*,*N*,*N*-

trimethylammoniumphenyl)-10,20-diphenylporphyrin iodide ($TA^{+2}PP$) was carried out through a three-step synthetic approach (Scheme 3). The first step of the synthesis involved the nitration of TPP to afford the nitrophenyl-substituted porphyrin. The nitration of TPP was confirmed through the appearance of the N-O stretching vibrations at 1342 and 1513 cm^{-1} (Figure A1. 7) and a molecular ion in the MALDI-TOF found at 703.44 m/z, which corresponds to the expected molecular ion. The molecule was further confirmed through the appearance of chemical shifts in the ^1H NMR (Figure A1. 5) at δ 8.10 to 8.13 and δ 8.34 to 8.37 ppm corresponding to the hydrogens on the nitrophenyl group. After the nitration reaction, a mixture of cis/trans isomers was obtained.

This compound was then reacted with $SnCl_2$ in concentrated HCl to reduce the nitro groups to amine groups. The successful synthesis of the aminophenylporphyrin was confirmed with MALDI-TOF (Figure A1. 12) with molecular ion of 644.81 m/z, corresponding to the expected molecular ion. Furthermore, the ^1H NMR (Figure A1. 9) confirmed this molecule due to the loss of the chemical shifts associated to the hydrogens from the nitrophenyl group and the appearance of the chemical shifts associated to the hydrogen corresponding to the aminophenyl groups at δ 7.02 to 7.04 ppm and δ 7.96 to 7.99 ppm.

In the last step, the porphyrin derivative was reacted with an excess of methyl iodide to alkylate the nitrogen, forming trimethylammonium. The synthesis was confirmed through the appearance of chemical shifts in the ^1H NMR (Figure A1. 13) at δ 8.42 to 8.45 ppm and δ 8.50 to 8.53 ppm corresponding to the hydrogens on the phenyl rings containing the trimethylammonium groups. In addition, the chemical shift

corresponding to the hydrogens of the methyl groups were found at δ 3.92 ppm. Analysis of MALDI-TOF (Figure A1. 16) did not agree with the expected molecular ion. Instead, the MALDI-TOF mass spectroscopy analysis showed the molecular ion of 713.93 m/z, corresponding to the molecular ion minus one methyl group, and an additional signal of 700.01 m/z, corresponding to the molecular ion minus two methyl groups.

The synthesis of mixture 5,10,15-tris(4'-*N*,*N*,*N*-trimethylammoniumphenyl)-20-phenylporphyrin ($TA^{+3}PP$) was carried out through a three-step synthetic approach (Scheme 3). In the first step TPP was nitrated to afford the nitrophenyl-substituted porphyrin. The successful synthesis of nitrophenyl porphyrin derivative was confirmed through the appearance of the N-O stretching vibrations at 1341 and 1512 cm^{-1} (Figure A1. 19) and the appearance of chemical shifts in the ^1H NMR (Figure A1. 18) at δ 8.31 to 8.33 and δ 8.56 to 8.59 ppm corresponding to the hydrogens on the nitrophenyl group. The molecule was further confirmed using MALDI-TOF (Figure A1. 20) with molecular ion found at 750.65 m/z.

In the second step, the nitro groups were reduced to amine groups using $SnCl_2$ in concentrated HCl. The successful synthesis of the aminophenyl porphyrin was confirmed with MALDI-TOF (Figure A1. 24) with molecular ion of 658.51 m/z, corresponding to the expected molecular ion. The ^1H NMR (Figure A1. 21) spectrum also confirmed the molecule due to the loss of the nitrophenyl hydrogens ppm signal and the addition of the aminophenyl hydrogens at δ 6.97 to 6.99 ppm and δ 7.95 to 7.98 ppm.

In the last step, the porphyrin derivative was reacted with an excess methyl iodide to alkylate the nitrogen, forming trimethylammonium. The synthesis was confirmed

through the appearance of chemical shifts in the ^{1}H NMR (Figure A1. 26) at 8.42 to 8.45 ppm and 8.49 to 8.52 ppm corresponding to the hydrogens on the phenyl rings containing the trimethylammonium groups. In addition, the chemical shift corresponding to the hydrogens of the methyl groups were found at δ 3.93 ppm. Analysis of MALDI-TOF (Figure A1. 28) did not agree with the expected molecular ion. Instead, the MALDI-TOF mass spectroscopy analysis showed the molecular ion of 790.65 m/z, corresponding to the molecular ion minus three iodide ions, and additional signals at 776.82 m/z, 756.74 m/z, and 742.85 m/z corresponding to the molecular ion minus one methyl groups, two methyl groups and three methyl groups, respectively.

The synthesis of 5,10,15,20-tetrakis(4'-*N*,*N*,*N*-trimethylammoniumphenyl)phenylporphyrin iodide ($TA^{+4}PP$) was confirmed by ^{1}H NMR, FTIR, and MALDI-TOF. The final product was confirmed through the appearance of chemical shifts in ^{1}H NMR at δ 8.46 to 8.48 ppm and δ 8.49 to 8.51 ppm (Figure A1. 30). In addition, the chemical shift corresponding to the hydrogens of the methyl groups were found at δ 3.96 ppm. Like the tricationic porphyrin derivative, analysis of the MALDI-TOF spectrum (Figure A1. 32) did not agree with the expected molecular ion. Instead, the MALDI-TOF mass spectroscopy analysis showed the molecular ion of 848.18 m/z, corresponding to the molecular ion minus four iodide ions, and additional signals at 799.41 m/z, 785.48 m/z, 771.48 m/z and 757.55 m/z corresponding to the molecular ion minus methyl groups.

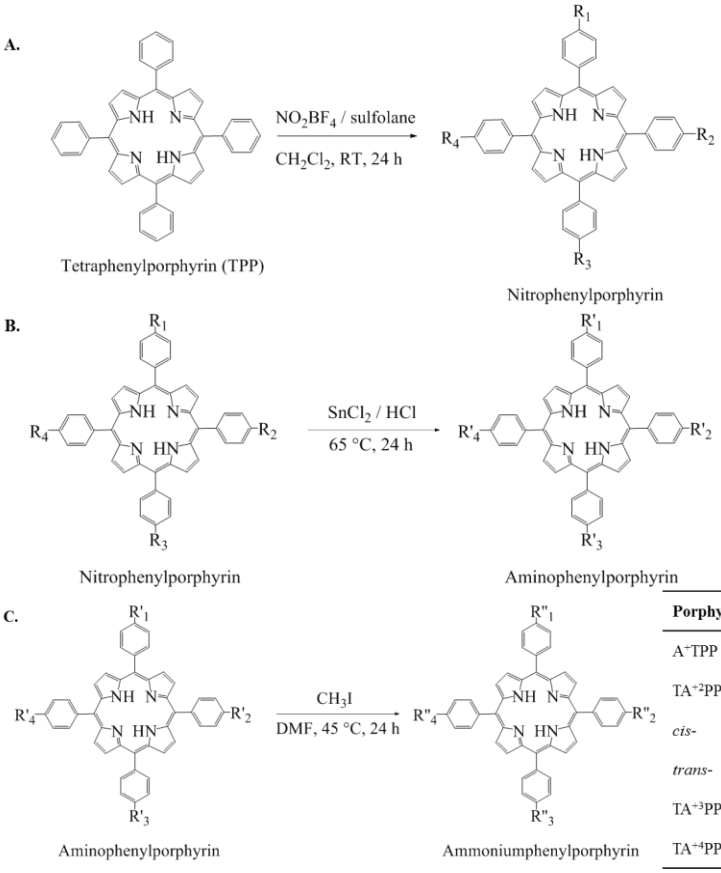

Porphyrin	R_1	R_2	R_3	R_4
TN_2PP				
cis-	NO_2	NO_2	H	H
trans-	NO_2	H	NO_2	H
TN_3PP	NO_2	NO_2	NO_2	H

Porphyrin	R'_1	R'_2	R'_3	R'_4
TA_2PP				
cis-	NH_2	NH_2	H	H
trans-	NH_2	H	NH_2	H
TA_3PP	NH_2	NH_2	NH_2	H

Porphyrin	R''_1	R''_2	R''_3	R''_4
A^-TPP	$^+N(CH_3)_3I^-$	H	H	H
$TA^{+2}PP$				
cis-	$^+N(CH_3)_3I^-$	$^+N(CH_3)_3I^-$	H	H
trans-	$^+N(CH_3)_3I^-$	H	$^+N(CH_3)_3I^-$	H
$TA^{+3}PP$	$^+N(CH_3)_3I^-$	$^+N(CH_3)_3I^-$	$^+N(CH_3)_3I^-$	H
$TA^{+4}PP$	$^+N(CH_3)_3I^-$	$^+N(CH_3)_3I^-$	$^+N(CH_3)_3I^-$	$^+N(CH_3)_3I^-$

Scheme 3. Multi-step synthetic route to the cationic porphyrin derivatives. (A) TPP nitration with NO_2BF_4 / sulfolane solution; (B) Nitro group reduction by $SnCl_2$, (C) alkylation of amine groups using excess CH_3I.

3.2 Spectroscopic characterization

The photophysical properties of the cationic porphyrins were characterized by spectroscopic techniques. Normalized absorption spectra of the cationic porphyrins solutions in DMSO are shown in Figure 15a. The Soret band wavelengths and the corresponding extinction coefficient values are presented in Table 2. The steady-state fluorescence emission spectra are shown with normalized intensities in Figure 15b and the emission wavelengths are provided in Table 2. The absorption spectra for the cationic porphyrins showed the typical Soret and Q-bands for porphyrins around 415 nm, 515 nm,

550 nm, 590 nm, and 650 nm. Similarly, the fluorescence showed two characteristic emission peaks for free-base porphyrins at 650 nm and 715 nm.

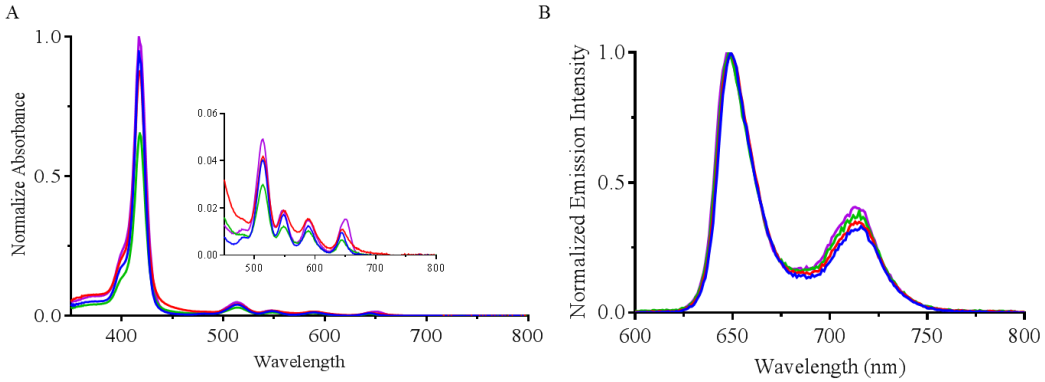

Figure 15. (A) Normalized absorption and (B) emission spectra for ~ 10 µM solutions of $A^{+}TPP$ (blue), $TA^{+2}PP$ (red), $TA^{+3}PP$ (green) and $TA^{+4}PP$ (purple) in DMSO. The four Q absorption bands are shown in the inset.

Table 2. Photophysical parameters for cationic porphyrins

Porphyrin	**λ_{Soret} (nm) [ε x 10^3 (M^{-1} cm^{-1})]**	**$\lambda_{Emission}$ (nm)[a]**	**Φ_F (520 nm)[b]**	**Φ_Δ[c]**
$A^{+}TPP$ (mono)	418 [355 ± 22]	649, 716	0.111 ± 0.005	0.65 ± 0.04
$TA^{+2}PP$ (di)	418 [285 ± 19]	649, 715	0.097 ± 0.013	0.61 ± 0.03
$TA^{+3}PP$ (tri)	418 [227 ± 0]	648, 715	0.116 ± 0.002	0.61 ± 0.06
$TA^{+4}PP$ (tetra)	418 [324 ± 38]	647, 713	0.106 ± 0.004	0.65 ± 0.04

[a] λ_{ex} = 520 nm. [b] Fluorescence quantum yields in DMSO were calculated based on the fluorescence spectra using TPP (Benzene) as a standard (Φ_F = 0.11)[52]; λ_{ex} = 520 nm. [c] $^1O_2$ quantum yields in DMF were calculated using TPP (DMF) as a standard (Φ_Δ = 0.62)[54]; $\lambda_{Irradiation}$ = 515 nm.

The fluorescence quantum yields were determined to indirectly characterize the efficiency with which the cationic porphyrin derivatives undergo ISC to the excited triplet state, an essential step in $^1O_2$ generation. Porphyrin derivatives typically generates low fluorescence quantum yields indicating that majority of photos absorbed by porphyrins undergo ISC to the excited triplet. Fluorescence quantum yields in DMSO were calculated relative to TPP in benzene. Results in Table 2 show the cationic porphyrin derivatives have similar fluorescence quantum yield values to the reference

TPP. These results demonstrate that the addition of trimethylammonium groups at the peripheral substituents does not alter the photophysical properties of the cationic porphyrins.

In PDI, the type II mechanism, which is associated to the generation of $^1O_2$, is the major pathway in cellular oxidative damage of Gram-negative bacteria.[34,45] Therefore, for PDI to kill bacteria, the PS should efficiently generate $^1O_2$. The $^1O_2$ quantum yields give an indication of the potential of the cationic porphyrin derivatives in PDI. The $^1O_2$ generation of the cationic porphyrin derivatives in DMF was detected using DMA. This probe reacts with $^1O_2$ irreversibly, undergoing a 1,4-cycloaddition that is detected as a decrease in the intensity of the DMA absorption band at 379 nm (Figure 9).[43] Additionally, DMA is photostable under the conditions of the experiment (Figure 16).

The $^1O_2$ quantum yield was calculated relative to the reference TPP ($\Phi_\Delta = 0.62$)[54] using the slope of the Stern-Volmer plot ($Ln(A_0/A)$ versus irradiation times) and Eq 2.[43,54] The experimental design was confirmed by comparing two porphyrins with known $^1O_2$ quantum yields in DMF, TPP ($\Phi_\Delta = 0.62$)[54] and THPP ($\Phi_\Delta = 0.54$).[43] The measured quantum yield values matched the literature values within ± 10% error ($\Phi_{\Delta,\,TPP} = 0.61$ and $\Phi_{\Delta,\,THPP} = 0.55$). The results, summarized in Figure 18 and Table 2, show that the DMA photodegradations in the presence of the cationic porphyrin derivatives were comparable to TPP. The $^1O_2$ quantum yields were calculated as 0.65 ± 0.04, 0.61 ± 0.03 and 0.65 ± 0.04 for A^+TPP, $TA^{+2}PP$ and $TA^{+4}PP$, respectively. Like the fluorescence quantum yield results, the $^1O_2$ quantum yields were not affected by the cationic substituents.

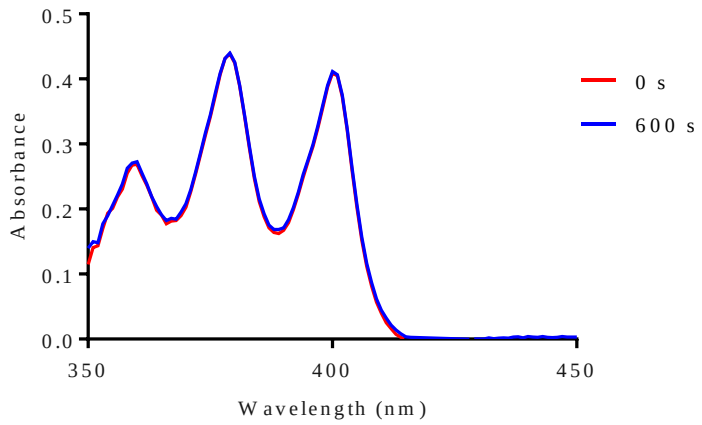

Figure 16. Absorbance spectra of DMA photobleaching experiments.

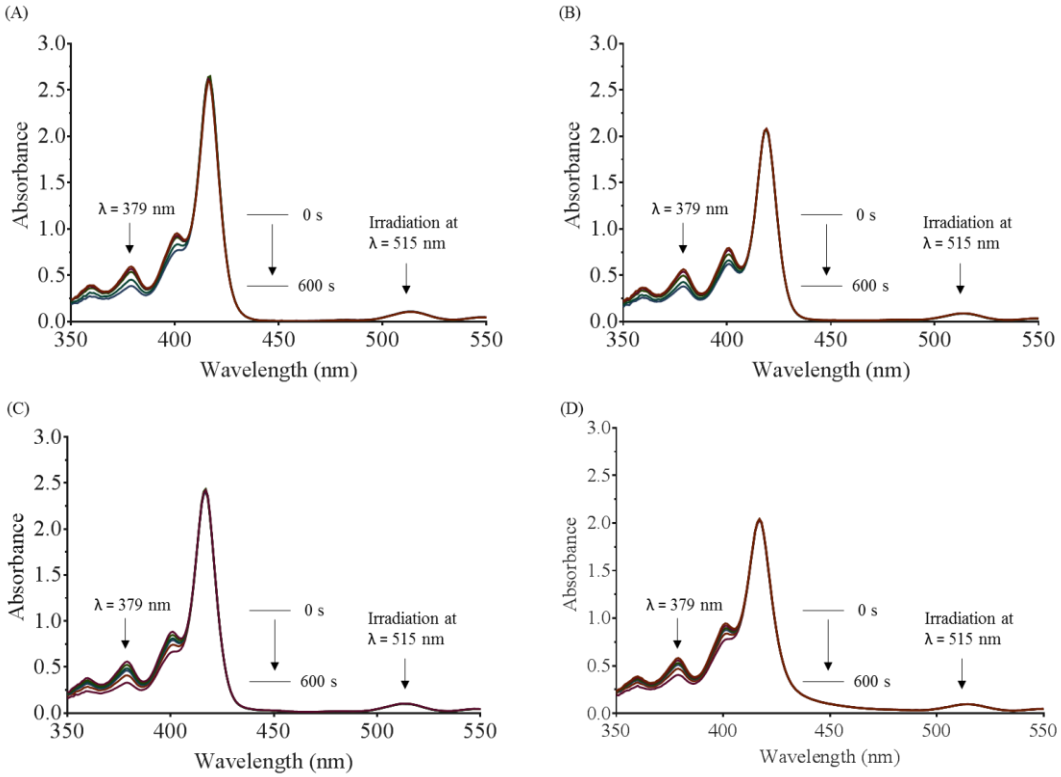

Figure 17. Absorbance spectra of (A) TPP, (B) THPP, (C) A+TPP, (D) TA+2PP, (E) TA+3PP and (F) TA+4PP in DMF using DMA as a 1O2 quencher and TPP as a reference (ΦΔ = 0.62).54 λex = 515 nm.

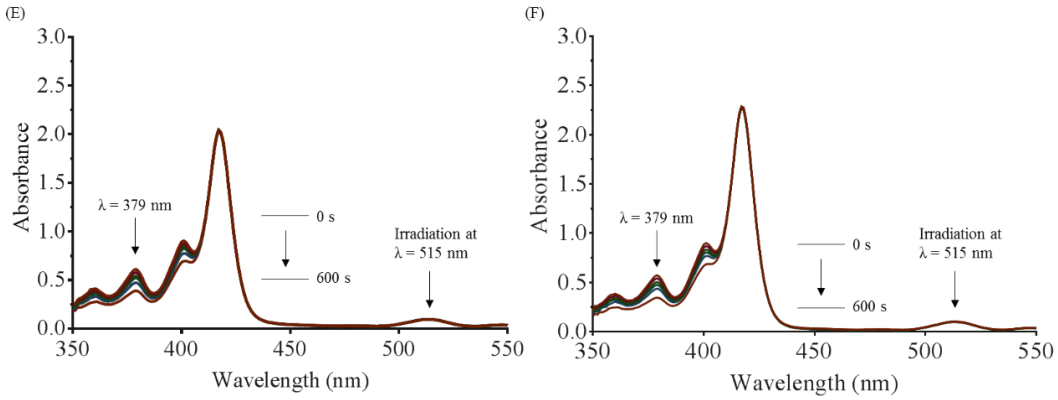

Figure 17, continue. Absorbance spectra of (A) TPP, (B) THPP, (C) $A^{+}TPP$, (D) $TA^{+2}PP$, (E) $TA^{+3}PP$ and (F) $TA^{+4}PP$ in DMF using DMA as a $^1O_2$ quencher and TPP as a reference ($\Phi_\Delta = 0.62$).[54] λ_{ex} = 515 nm.

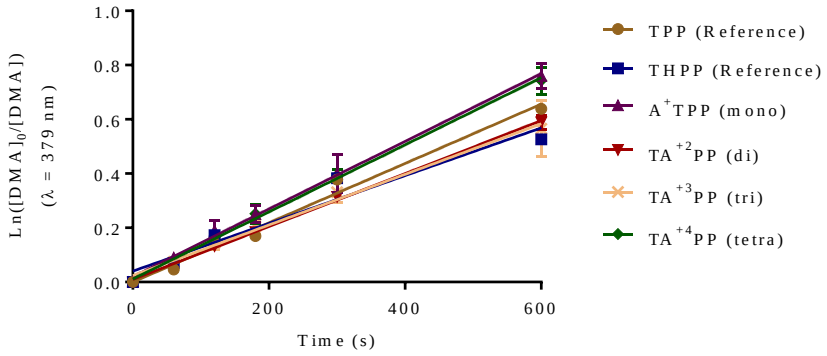

Figure 18. Stern-Volmer plots for the decay of DMA photosensitized by cationic porphyrins in DMF at irradiation wavelength of 515 nm. Values include standard deviation of three separate experiments.

3.3 Photodynamic inactivation of *E. coli*

The dark and light toxicity of the cationic porphyrin derivatives (Figure 20 and 21) were tested against *E. coli* under white light irradiation (400 – 700 nm, 44 J cm^{-2}) with concentrations between 0.001 and 10 μM. The efficiency of the PS was evaluated based on the number of viable CFU per mL in comparison to a control that was not incubated with a PS. The PDI effect of the synthesized cationic porphyrins was also compared to a commercially available tetracationic porphyrin derivative commonly used in PDI[55,59,63,64], 5,10,15,20-tetrakis(*N*-methylpyridinium)porphyrin ($TPy^{+}P$, tetra-

pyridinium, and a neutral porphyrin derivative, 5,10,15,20-tetrakis(3-hydroxyphenyl)porphyrin (THPP, neutral), Figure 19.

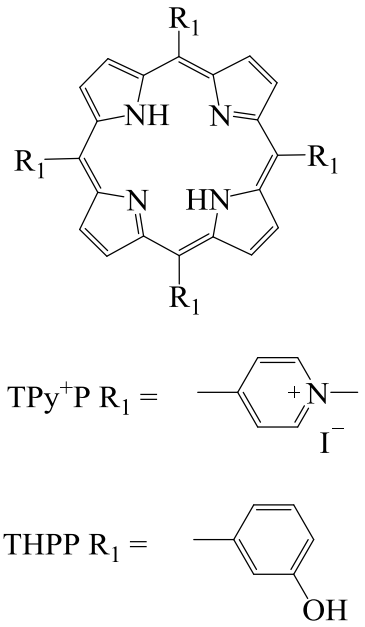

Figure 19. Structure of comparative PS for the photoinactivation of *E. coli*.

The cationic porphyrin derivatives showed minimum dark toxicity of *E. coli* at concentrations below 10 μM (Figure 20). At 10 μM the survival percentage was reduced to 29.0 ± 10.9%, 34.1 ± 1.8%, and 4.3 ± 0.6% for $TA^{+2}PP$, $TA^{+3}PP$ and $TA^{+4}PP$, respectively ($p < 0.0001$, ANOVA). The reason for the dark toxicity may be explained by the mechanism of interaction between the cationic PS and *E. coli*. The positive charges on the PS molecules promote electrostatic interactions with negatively-charged LPS molecules, displacing divalent cations and creating pores in the outer membrane via the self-promoted uptake pathway. Despite all the precautions taken during the performance of the dark experiments, we cannot completely rule out the effect of ambient light that may be partially responsible for the observed dark toxicity due to the formation of $^1O_2$ and ROS.

As shown by the results for the light toxicity (Figure 21 and Table 3), the photodynamic inactivation efficiency of the PS against *E. coli* followed the order: THPP (neutral) < A^{+}TPP (mono) < TA^{+2}PP (di) ≈ $TPy^{+}P$ (tetra-pyridinium) < TA^{+4}PP (tetra) < TA^{+3}PP (tri). The tricationic porphyrin derivative was the most effective PS against *E. coli* which is consistent with previous literature results for tricationic porphyrin derivatives against *E.coli*.[54,55] TA^{+3}PP caused a 96.733 ± 1.501% (0.01 μM), 99.996 ± 0.005% reduction (0.1 μM) and >99.999% reduction (1 μM). As expected, TA^{+4}PP was also a good PS against *E. coli*. In comparison to TA^{+3}PP at a lower concentration of PS, 0.01 μM, TA^{+4}PP only reduced cell survival by 9.3 ± 12.6% ($p < 0.05$, ANOVA). After incubation with higher concentrations of PS (0.1 and 1 μM), TA^{+4}PP showed comparable results as TA^{+3}PP, causing cell survival reductions of 99.991 ± 0.001 ($p > 0.05$, ANOVA) and >99.99999 ± 0.00002% ($p > 0.05$, ANOVA), respectively. Similarly, the dicationic porphyrin, TA^{+2}PP, showed significant reduction of cell survival at PS concentrations, 1 μM and 10 μM, causing 99.996 ± 0.006% and >99.999% reduction, respectively.

On the other hand, the photodynamic inactivation of *E. coli* cells by the monocationic porphyrin, A^{+}TPP, produced low reductions in cell survival. After incubation with 10 μM PS, cell reduction reached 99.977 ± 0.020%, and complete cellular survival reduction was achieved after incubating *E. coli* cells with 100 μM A^{+}TPP. The least effective PS against *E. coli* was the neutral porphyrin derivative, THPP, which failed to reduce cell survival even at highest concentration tested (10 μM). The lack of photodynamic inactivation is due to its low binding to *E. coli* cells. These results are consistent with previous literature reports of neutral porphyrin derivatives.[28,63]

Additionally, the IC_{50} values of the porphyrin derivatives were calculated from curves constructed by plotting cell survival (%) versus PS concentration (μM), shown in Figure 22. The efficiency of the cationic porphyrin derivatives according to IC_{50} values followed a similar trend as the $IC_{99.99}$ data: THPP (neutral) < $A^{+}TPP$ (mono) < $TA^{+2}PP$ (di) ≈ $TA^{+4}PP$ (tetra) < $TA^{+3}PP$ (tri).

According to the $^{1}O_2$ quantum yield results obtained (Table 2), all the cationic porphyrin derivatives are efficient $^{1}O_2$ generators. Nevertheless, the PDI data show that the photocytotoxic process against Gram-negative bacteria is dependent on the number of positive charges and the structure of the porphyrins. The positive charge on the peripheral of the PS molecule promote tight electrostatic interactions with negatively-charged LPS molecules at the surface of the outer membrane. Our experimental results demonstrated comparable results to previous studies, showing that the effect of number of positive charges did not follow the predicted trend that the phototoxicity would increase as the number of positive charges increased. These results suggest the involvement of another mechanism in the PDI process.

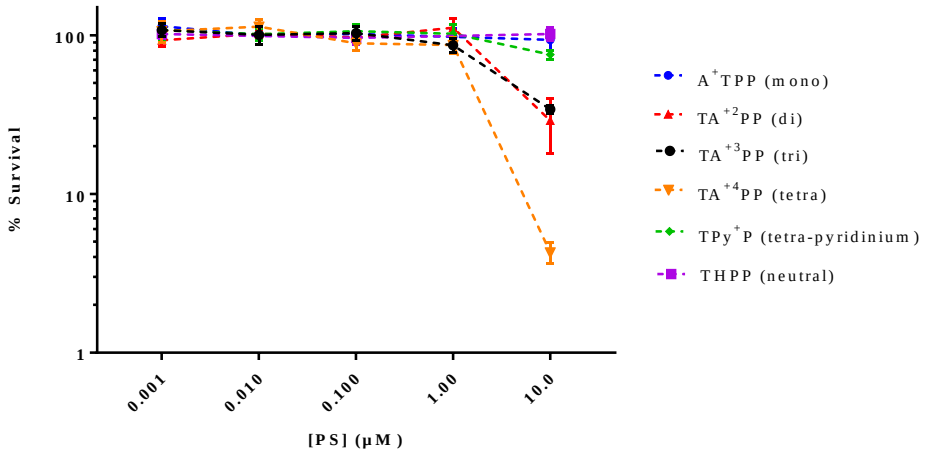

Figure 20. Dark toxicity of porphyrins against *E. coli.*

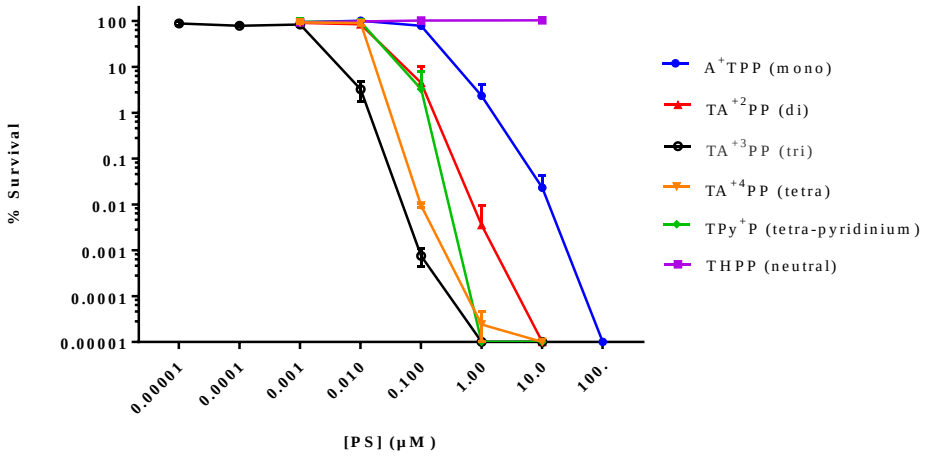

Figure 21. Light toxicity of porphyrins against *E. coli*.

Table 3. Cell survival reduction percentage of *E. coli* incubated with cationic porphyrin derivatives for 30 min and exposed to white light (400 - 700 nm, 44 J cm^{-2}). Values represent the mean of three independent experiments. A negative value indicates growth.

Porphyrin	0.001 µM	0.010 µM	0.100 µM	1.00 µM	10.0 µM
$TA^{+}PP$ (mono)	5.533 ± 9.693	-1.70 ± 7.62	21.067 ± 17.980	97.667 ± 1.716	99.977 ± 0.020
$TA^{+2}PP$ (di)	8.733 ± 8.784	15.600 ± 19.150	95.500 ± 5.629	99.996 ± 0.006	100.0 ± 0.0
$TA^{+3}PP$ (tri)	15.733 ± 7.720	96.733 ± 1.501	99.996 ± 0.005	100.0 ± 0.0	100.0 ± 0.0
$TA^{+4}PP$ (tetra)	7.090 ± 3.236	9.297 ± 12.600	99.991 ± 0.001	100.0 ± 0.0	100.0 ± 0.0
$TPy^{+}P$ (tetra-pyridinium)	3.533 ± 16.692	4.333 ± 14.333	96.733 ± 4.464	100.0 ± 0.0	100.0 ± 0.0

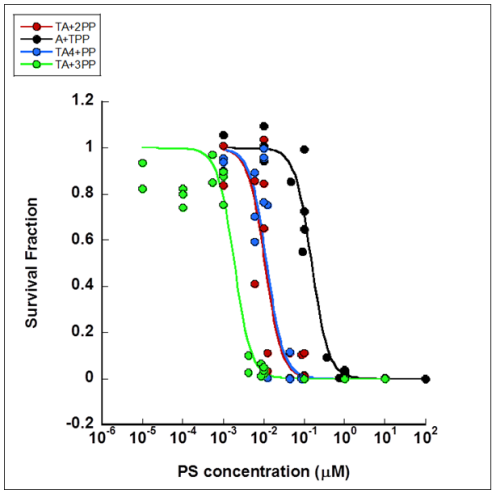

Porphyrin	IC_{50}	±	SD (μM)	R^2
A^{+}TPP (mono)	0.1537	±	0.0154	0.961
TA^{+2}PP (di)	0.0107	±	0.0016	0.764
TA^{+3}PP (tri)	0.0018	±	0.0002	0.948
TA^{+4}PP (tetra)	0.0119	±	0.0015	0.795

Figure 22. IC_{50} survival curve of cationic porphyrins against E. coli.

3.4 Photosensitizer binding

To further understand the results obtained from the photocytotoxicity of the cationic porphyrins, we investigated the interaction of PS with *E. coli* cells by using fluorescence confocal microscopy and competitive binding.

3.4.1 Fluorescence confocal laser scanning microscopy

The localization of the cationic porphyrin was investigated using fluorescence confocal microscopy to directly visualize the binding of PS to *E. coli*. Figure 23 shows the microscopy images of *E. coli* incubated with cationic porphyrin derivatives (1 μM) for 30 min in the dark. The cationic porphyrins were localized at the membrane of *E. coli* cells for the A^{+}TPP (mono), TA^{+2}PP (di) and TA^{+3}PP (tri). However, interestingly, the tetra-cationic porphyrin derivatives were localized intracellularly in the *E. coli* cells. These results demonstrate the uptake of highly cationic PS occurs likely through the self-promoted uptake pathway.[56]

The self-promoted uptake pathway involves the binding of the cationic molecules to LPS that results in displacement of divalent cations, resulting in pores and weakening

of the outer membrane.[56] The presence of large cationic PS widen the pores in the LPS layer allowing uptake of molecules inside the cell. The internalization of $TA^{+4}PP$ and $TPy^{+}P$ into the cytoplasm of the cell may explain why these porphyrins produced a PDI effect different than the expected trend.

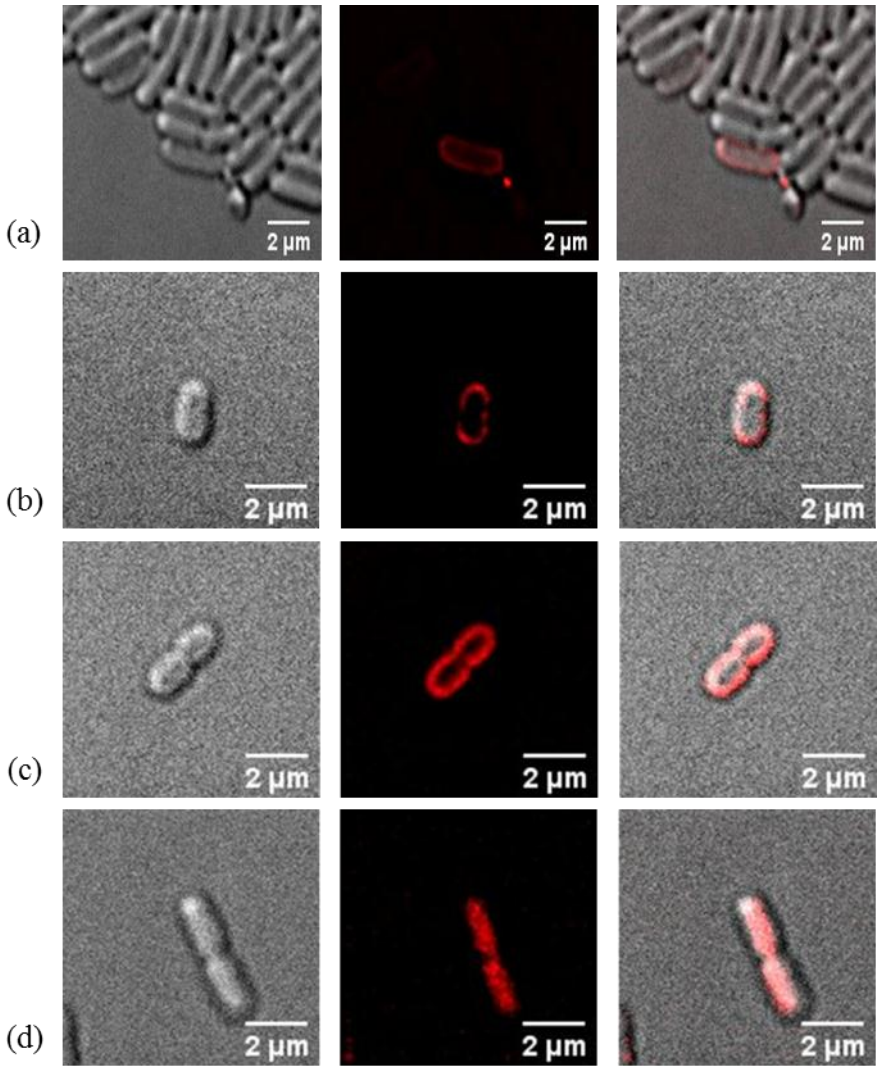

Figure 23. Microscopy images of cationic porphyrins. (a) $A^{+}TPP$ (mono); (b) $TA^{+2}PP$ (di); (c) $TA^{+3}PP$ (tri); (d) $TA^{+4}PP$ (tetra). Left: phase contrast bright-field image, middle: fluorescence image, and right: merge image. [PS] = 1 µM; Incubation time: 30 min.

To understand if the uptake of the tetracationic porphyrin was time dependent, additional microscopy experiments were conducted. *E. coli* was incubated in the dark

with the tetra-cationic porphyrin for the following times: 5 min; 10 min; 15 min; and 20 min (Figure 24). After 5 min and 10 min, $TA^{+4}PP$ was localized at the membrane of all *E. coli* cells. However, after 15 min, $TA^{+2}PP$ was found extracellularly and intracellularly, and after 20 min, the porphyrin was found localized inside the bacterial cells. These results demonstrate the time dependency of $TA^{+4}PP$ internalization and implied that the internalization of $TA^{+4}PP$ occurred as the concentration of PS interacting with the bacterial cell increased.

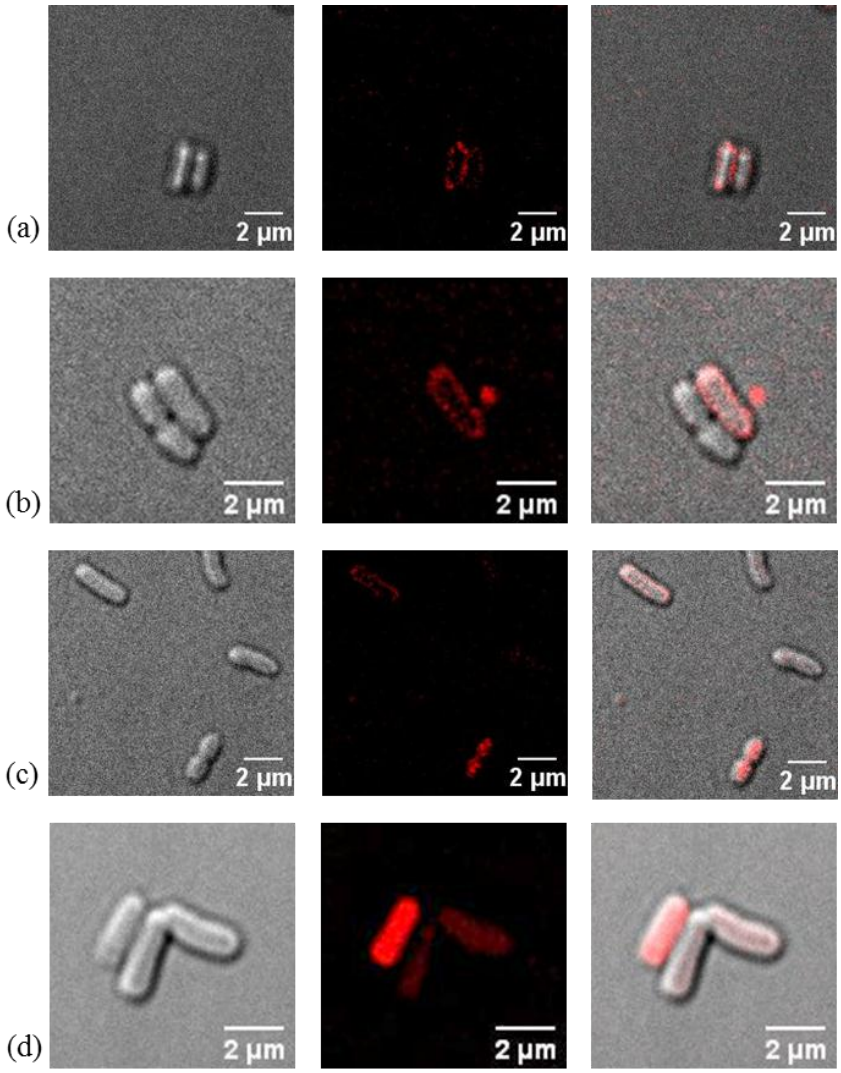

Figure 24. Microscopy images of $TA^{+4}PP$ at various irradiation times. (a) 5 min, (b) 10 min, (c) 15 min, and (d) 20 min. Left: phase contrast bright-field image, middle: fluorescence image, and right: merge image. [PS] = 1 µM.

3.4.2 Competitive binding with Mg^{+2}

Microscopy studies revealed the internalization of $TA^{+4}PP$ via the self-promoted uptake pathway. Since the self-promoted uptake pathway involves interaction of the compounds at divalent cations binding sites, the presence of excess divalent cations, such as Mg^{+2}, may cause a competitive inhibition of cationic compounds.[7,56] To confirm that the cellular internalization of $TA^{+4}PP$ in bacterial cells occurs via the self-promoted uptake pathway, the uptake of $TA^{+4}PP$ into *E. coli* cells was studied by incubating the tetracationic porphyrin in culture solutions pre-exposed to increasing concentrations of Mg^{+2}. The ability of Mg^{+2} to inhibit $TA^{+4}PP$ uptake was compared to $TA^{+2}PP$ (di) and $TA^{+3}PP$ (tri). The concentrations of Mg^{+2} was varied between 0 and 50 mM while the concentration of cationic porphyrin was kept constant. The amount of cationic porphyrin associated with *E. coli* cells was determined by measuring fluorescence of the PS in cell lysates obtained by treatment with 2% SDS. Calibration curves were constructed for each PS in 2% SDS (Figure 25).

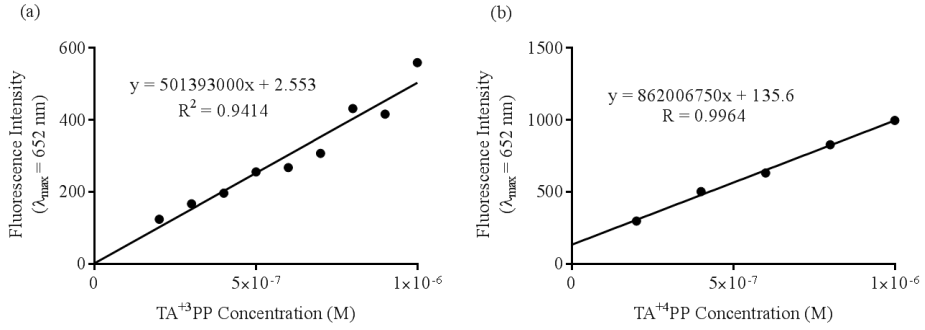

Figure 25. Calibration curves of fluorescence intensity at λ_{max} versus PS concentration (0.2 – 1.0 μM) in 2% SDS. (a) $TA^{+3}PP$ (tri); (b) $TA^{+4}PP$ (tetra).

As shown in Figure 26 and Table 4, increasing the concentrations of Mg^{+2} caused a reduction in the amount of $TA^{+4}PP$ associated to *E. coli*. Incubating cells with 50 mM Mg^{+2} reduced the uptake of $TA^{+4}PP$ by 74.5% ($p < 0.05$, ANOVA), implying that the

addition of excess Mg^{+2} prevents alterations in the outer membrane permeability functions of cells treated with $TA^{+4}PP$. On the other hand, incubating cells with 50 mM Mg^{+2} reduced the uptake of $TA^{+3}PP$ by only 47% ($p > 0.05$, ANOVA). The difference in performance may be due to differences in the interactions between the cationic porphyrins and *E. coli* as illustrated in microscopy images (Figure 23).

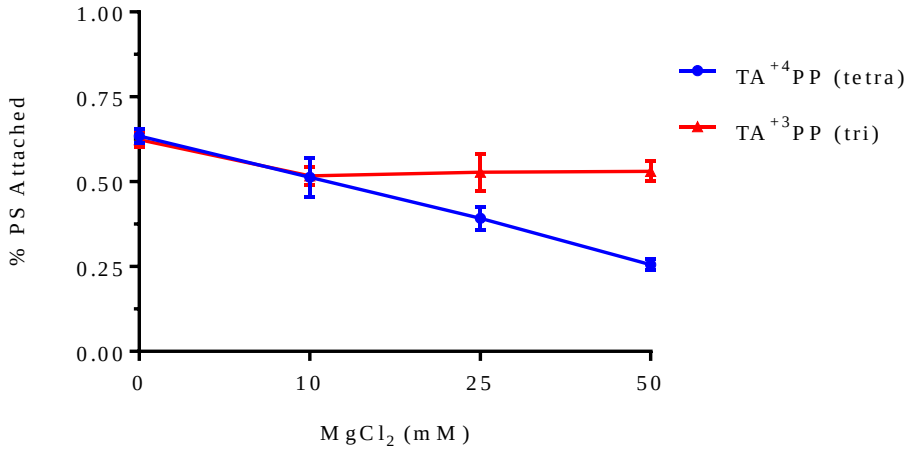

Figure 26. Effect of Mg^{+2} on the uptake of $TA^{+3}PP$ (tri) and $TA^{+4}PP$ (tetra) (1 µM) in *E. coli* cells with increasing concentrations of $MgCl_2$ (0, 10, 25, 50 mM).

Table 4. PS attachment percentages in the presence of $MgCl_2$.

$MgCl_2$ (mM)	$TA^{+3}PP$ (%)	$TA^{+4}PP$ (%)
0	62.4 ± 2.3	63.4 ± 2.0
10	51.7 ± 2.7	51.3 ± 5.7
25	52.8 ± 5.5	39.2 ± 3.4
50	53.0 ± 2.9	25.5 ± 1.7

CHAPTER 4: CONCLUSION AND FUTURE WORK

Alternative treatment options for infectious diseases is becoming increasingly important as antibiotic resistance continues to create clinical challenges throughout the world. PDI is a non-antibiotic treatment option that potentially eliminates the further development and spread of antibiotic resistant genes. The efficiency of PDI is directly related with the ability of the PS to generate $^1O_2$ and ROS during the photodynamic process. However, due to the short half-life and diffusion distances of the photogenerated species, the ability of $^1O_2$ and ROS to react with biomolecules and cause cell dead heavily depends on the interaction between the PS molecules and the bacterial cells. Although Gram-positive bacteria have been shown to be highly susceptible to PDI, the inactivation of Gram-negative bacteria has been more challenging due to the impermeability properties of the outer membrane.

To improve the efficacy of PDI against Gram-negative bacteria, researchers have investigated positively-charged porphyrins to promote electrostatic interactions with the outer membrane of the bacterium. Many of these studies have shown the tricationic porphyrin derivative to more efficient than the tetracationic porphyrin, and suggested the difference in efficacy to be due to the increased amphiphilic character of the tricationic porphyrin derivatives.[54,55] However, there is no current research using fluorescence confocal microscopy to investigate the mechanism of interaction of the PS to explain the differences observed. In the present study, a series of photosensitizers which contain one to four positively-charged groups, trimethylammonium iodide, were synthesized and characterized using spectroscopy techniques. Additionally, the ability of the cationic

porphyrins to generate $^1O_2$ were determined, and the effect of number of positive charges was evaluated during the PDI of *E. coli*. Finally, the mechanism of interaction between the cationic porphyrin and *E. coli* cells was demonstrated using fluorescence confocal microscopy and competitive binding. The project was divided into four specific goals: **1)** To synthesize and characterize a series of *meso*-substituted trimethylammonium porphyrin derivatives; **2)** To determine the photophysical and photochemical properties of the cationic porphyrins; **3)** To evaluate the dark and light toxicity of the cationic porphyrins against a Gram-negative bacterium, *E. coli*; and **4)** To investigate the mechanism of interaction between cationic porphyrin derivatives and *E. coli*.

The cationic porphyrin derivatives were successfully synthesized and characterized by ^{1}H NMR, FTIR and MALDI-TOF or ESI-MS. The photophysical properties of the cationic porphyrins were characterized by UV-VIS and fluorescence. The fluorescence quantum yield values were determined relative to TPP in benzene. This experiment was validated by comparing two porphyrins with known $^1O_2$ quantum yields in DMF, TPP ($\Phi_\Delta = 0.62$)[54] and THPP ($\Phi_\Delta = 0.54$).[43] The fluorescence quantum yields were found to be 0.11, 0.10, 0.12 and 0.11 for A^+TPP, TA^{+2}PP, TA^{+3}PP and TA^{+4}PP, respectively. The fluorescence quantum yields are comparable to TPP showing that the addition of cationic substituents did not affect the photophysical property. The $^1O_2$ quantum yields were determined by indirect detection of $^1O_2$ generation by monitoring the photodegradation of DMA. The $^1O_2$ quantum yields were calculated as 0.65 ± 0.04, 0.61 ± 0.03 and 0.65 ± 0.04 for A^+TPP, TA^{+2}PP and TA^{+4}PP, respectively. Like the

fluorescence quantum yield results, the $^1O_2$ quantum yields were not affected by the cationic substituents at the peripheral of the porphyrin.

The dark and light toxicity of the cationic porphyrin derivatives were tested against *E. coli* under white light irradiation (400 – 700 nm, 44 J cm^{-2}) with concentrations between 0.001 and 10 μM. The PDI effect of the synthesized cationic porphyrins was also compared to a commercially available tetracationic porphyrin derivative commonly used in PDI[55,59,63,64], 5,10,15,20-tetrakis(*N*-methylpyridinium)porphyrin (TPy^+P, tetra-pyridinium, and a neutral porphyrin derivative, 5,10,15,20-tetrakis(3-hydroxyphenyl)porphyrin (THPP, neutral).

$TA^{+3}PP$, tricationic porphyrin, was found to be the most efficient porphyrin against *E. coli* (IC_{50} 2 nM and $IC_{99.999}$ ~1 μM), followed by $TA^{+4}PP$ (IC_{50} 12 nM and $IC_{99.999}$ ~1 μM) and $TA^{+2}PP$ (IC_{50} 11 nM and $IC_{99.999}$ ~10 μM). A^+TPP was found to be the least efficient cationic porphyrin against *E. coli* (IC_{50} 153 nM and $IC_{99.999}$ ~100 μM) while THPP failed to cause any photoinactivation of *E. coli*.

The relationship of the number of positive charges and the extent of the interaction between the PS and the bacterial cells was visualized with fluorescence confocal microscopy. Z-stacking images show that the tetracationic porphyrin derivatives were the only cationic porphyrins to be localized inside the cells. Additionally, the uptake mechanism of $TA^{+4}PP$ was determined using competitive binding studies with Mg^{+2}. It was found that the presence of Mg^{+2} prior to the incubation of the cells with $TA^{+4}PP$ significantly decreased the uptake of $TA^{+4}PP$, providing more evidence that the uptake mechanism of $TA^{+4}PP$ may be mediated via the self-promoted uptake pathway.

Some of the requirements for ideal PS for PDI are to have a high efficiency at generating $^1O_2$ and ROS, to possess structural properties that enhance its interaction with bacterial cell membranes, and to be selective for microbial cells compared to host mammalian cells. One way to ensure the last feature is through active-targeting using antibody, peptides, or aptamers. However, although active-targeting PS can increase the selectivity for bacterial cells, targeting specific biomolecules could potentially promote the development of resistance against PDI.[65] It has been reported that in comparison to bacterial cells, the uptake process into host mammalian cells through endocytosis is slower, while the interaction with bacterial cells is relatively rapid.[66] Therefore, future studies can investigate the PDI selectivity of the cationic porphyrins synthesized in this work against Gram-negative bacteria compared with mammalian cells by tuning the conditions, incubation and irradiation times used for the PDI experiments.

Functionizing cationic porphyrins with secondary groups such as EDTA, which chelates divalent cations is another direction of interest. The removal of the divalent cations disrupts the stability and impermeability properties of the outer membrane,[28] and may lead to synergistic effects. Expanding the research to other types of bacteria such as Methicillin-resistant *Staphylococcus aureus* and *Pseudomonas aeruginosa* would increase the scope of PDI to inactivate even multidrug resistant bacteria.

REFERENCES

(1) Meroueh, S. O.; Bencze, K. Z.; Hesek, D.; Lee, M.; Fisher, J. F.; Stemmler, T. L.; Mobashery, S. Three-Dimensional Structure of the Bacterial Cell Wall Peptidoglycan. *Proc. Natl. Acad. Sci. U. S. A.* **2006**, *103* (12), 4404–4409.

(2) Nordqvist, C. What is Bacteria? What are Bacteria? http://www.medicalnewstoday.com/articles/157973.php (accessed Jun 18, 2017).

(3) Giri, D. Gram Staining: Principle, Procedure, Interpretation and Animation http://laboratoryinfo.com/gram-staining-principle-procedure-interpretation-and-animation/ (accessed May 14, 2017).

(4) Jori, G.; Fabris, C.; Soncin, M.; Ferro, S.; Coppellotti, O.; Dei, D.; Fantetti, L.; Chiti, G.; Roncucci, G. Photodynamic Therapy in the Treatment of Microbial Infections: Basic Principles and Perspective Applications. *Lasers Surg. Med.* **2006**, *38* (5), 468–481.

(5) Jiang, L.; Gan, C. R. R.; Gao, J.; Loh, X. J. A Perspective on the Trends and Challenges Facing Porphyrin-Based Anti-Microbial Materials. *Small* **2016**, *12* (27), 3609–3644.

(6) Alves, E.; Faustino, M. A. F.; Neves, M. G. P. M. S.; Cunha, Â.; Nadais, H.; Almeida, A. Potential Applications of Porphyrins in Photodynamic Inactivation beyond the Medical Scope. *J. Photochem. Photobiol. C Photochem. Rev.* **2014**, *22*, 34–57.

(7) George, S.; Hamblin, M. R.; Kishen, A. Uptake Pathways of Anionic and Cationic Photosensitizers into Bacteria. *Photochem. Photobiol. Sci.* **2009**, *8* (6), 788–795.

(8) Golkar, Z.; Bagasra, O.; Gene Pace, D. Bacteriophage Therapy: A Potential Solution for the Antibiotic Resistance Crisis. *J. Infect. Dev. Ctries.* **2014**, *8* (2), 129–136.

(9) Rossolini, G. M.; Arena, F.; Pecile, P.; Pollini, S. Update on the Antibiotic Resistance Crisis. *Curr. Opin. Pharmacol.* **2014**, *18*, 56–60.

(10) Fair, R. J.; Tor, Y. Perspectives in Medicinal Chemistry Antibiotics and Bacterial Resistance in the 21st Century. *Perspect. Medicin. Chem.* **2014**, 25–64.

(11) Von Nussbaum, F.; Brands, M.; Hinzen, B.; Weigand, S.; Hubich, D. Antibacterial Natural Products in Medicinal Chemistry - Exodus or Revival? *Angew. Chemie - Int. Ed.* **2006**, *45* (31), 5072–5129.

(12) Walsh, C. *Antibiotics: Actions, Origins, Resistance*; ASM Press, 2003.

(13) Discovery and Development of Penicillin http://www.acs.org/content/acs/en/education/whatischemistry/landmarks/flemingpenicillin.html (accessed Apr 23, 2017).

(14) Maffioli, S. I. A Chemist's Survey of Different Antibiotic Classes. In *Antibiotics*; Wiley-VCH Verlag GmbH & Co. KGaA, 2013; pp 1–22.

(15) Antimicrobial Resistance www.who.int (accessed May 1, 2017).

(16) General Background: About Antibiotic Resistance http://emeral.tufts.edu/med/apua/about_issue/about_antibiotics.html (accessed May 1, 2017).

(17) Spratt, B. G.; Spratt, B. G. Resistance to Antibiotics Mediated by Target Alterations Published by : American Association for the Advancement of Science Resistance to Antibiotics Mediated by Target Alterations. **2017**, *264* (5157), 388–393.
(18) Davies, J. Inactivation of Antibiotics and the Dissemination of Resistance Genes. *Science* **1994**, *264* (5157), 375–382.
(19) Davies, J.; Davies, D. Origins and Evolution of Antibiotic Resistance. *Microbiol. Mol. Biol. Rev.* **2010**, *74* (3), 417–433.
(20) Clatworthy, A. E.; Pierson, E.; Hung, D. T. Targeting Virulence: A New Paradigm for Antimicrobial Therapy. *Nat. Chem. Biol.* **2007**, *3* (9), 541–548.
(21) Merchat, M.; Bertolini, G.; Giacomini, P.; Villanueva, A.; Jori, G. Meso-Substituted Cationic Porphyrins as Efficient Photosensitizers of Gram-Positive and Gram-Negative Bacteria. *J. Photochem. Photobiol. B Biol.* **1996**, *32* (3), 153–157.
(22) Calin, M. A.; Parasca, S. V. Light Sources for Photodynamic Inactivation of Bacteria. *Lasers Med. Sci.* **2009**, *24* (3), 453–460.
(23) Wainwright, M. Photodynamic Antimicrobial Chemotherapy (PACT). *J. Antimicrob. Chemother.* **1998**, *42* (1), 13–28.
(24) Wainwright, M.; Phoenix, D. a; Nickson, P. B.; Morton, G. The Use of New Methylene Blue in Pseudomonas Aeruginosa Biofilm Destruction. *Biofouling* **2002**, *18* (4), 247–249.
(25) Wainwright, M.; Crossley, K. B. Photosensitising Agents - Circumventing Resistance and Breaking down Biofilms: A Review. *Int. Biodeterior. Biodegrad.* **2004**, *53* (2), 119–126.
(26) Berg, K.; Weyergang, A.; Prasmickaite, L.; Høgset, A.; Strand, M. R.; Wagner, E.; Selbo, P. K. Photodynamic Therapy. *Methods Mol. Biol.* **2010**, *635* (8), 133–145.
(27) Vecchio, D.; Gupta, A.; Huang, L.; Landi, G.; Avci, P.; Rodas, A.; Hamblina, M. R. Bacterial Photodynamic Inactivation Mediated by Methylene Blue and Red Light Is Enhanced by Synergistic Effect of Potassium Iodide. *Antimicrob. Agents Chemother.* **2015**, *59* (9), 5203–5212.
(28) Sperandio, F. F.; Huang, Y.-Y.; Hamblin, M. R. Antimicrobial Photodynamic Therapy to Kill Gram-Negative Bacteria. *Recent Pat Antiinfect Drug Discov* **2013**, *8* (2), 1–23.
(29) Hall, C. E. The Synthesis of Cationic Porphyrins for Use in Photodynamic Antimicrobial chemotherapy(PACT), 2008.
(30) DeRosa, M. C.; Crutchley, R. J. Photosensitized Singlet Oxygen and Its Applications. *Coord. Chem. Rev.* **2002**, *233–234*, 351–371.
(31) Dai, T.; Fuchs, B. B.; Coleman, J. J.; Prates, R. A.; Astrakas, C.; St. Denis, T. G.; Ribeiro, M. S.; Mylonakis, E.; Hamblin, M. R.; Tegos, G. P. Concepts and Principles of Photodynamic Therapy as an Alternative Antifungal Discovery Platform. *Front. Microbiol.* **2012**, *3* (APR), 1–16.
(32) Kim, S. Y.; Kwon, O. J.; Park, J. W. Inactivation of Catalase and Superoxide Dismutase by Singlet Oxygen Derived from Photoactivated Dye. *Biochimie* **2001**, *83* (5), 437–444.
(33) Ergaieg, K.; Chevanne, M.; Cillard, J.; Seux, R. Involvement of Both Type I and

Type II Mechanisms in Gram-Positive and Gram-Negative Bacteria Photosensitization by a Meso-Substituted Cationic Porphyrin. *Sol. Energy* **2008**, *82* (12), 1107–1117.

(34) Maisch, T.; Bosl, C.; Szeimies, R.; Lehn, N.; Abels, C. Photodynamic Effects of Novel XF Porphyrin Derivatives on Prokaryotic and Eukaryotic Cells. *Antimicrob. Agents Chemother.* **2005**, *49* (4), 1542–1552.

(35) Smith, K. M.; Cavaleiro, J. A. S. Porphyrin Synthesis 2. *Rev. Port. Quim* **1989**, *31*, 29–41.

(36) Giovannetti, R. The Use of Spectrophotometry UV-Vis for the Study of Porphyrins. In *The Use of Spectrophotometry UV-Vis for the Study of Porphyrins, Macro to Nano Spectroscopy*; 2012; pp 87–108.

(37) Quiroz-Segoviano, R. I. Y.; Serratos, I. N.; Rojas-Gonzalez, F.; Tello-Solis, S. R.; Sosa-Fonseca, R.; Medina-Juarez, O.; Menchaca-Campos, C.; Garcia-Sanchez, M. A. On Tuning the Fluorescence Emission of Porphyrin Free Bases Bonded to the Pore Walls of Organo-Modified Silica. *Molecules* **2014**, *19* (2), 2261–2285.

(38) Marin, D. M.; Payerpaj, S.; Collier, G. S.; Ortiz, A. L.; Singh, G.; Jones, M.; Walter, M. G. Efficient Intersystem Crossing Using Singly Halogenated Carbomethoxyphenyl Porphyrins Measured Using Delayed Fluorescence, Chemical Quenching, and Singlet Oxygen Emission. *Phys. Chem. Chem. Phys.* **2015**, *17* (43), 29090–29096.

(39) Luengas, S. L. P.; Marin, G. H.; Aviles, K.; Acuña, R. C.; Roque, G.; Nieto, F. R.; Sanchez, F.; Tarditi, A.; Rivera, L.; Mansilla, E. Enhanced Singlet Oxygen Production by Photodynamic Therapy and a Novel Method for Its Intracellular Measurement. *Cancer Biother. Radiopharm.* **2014**, *29* (10), 435–443.

(40) Wang, P.; Qin, F.; Zhang, Z.; Cao, W. Quantitative Monitoring of the Level of Singlet Oxygen Using Luminescence Spectra of Phosphorescent Photosensitizer. *Opt. Express* **2015**, *23* (18), 22991–23003.

(41) Fujii, M.; Usui, M.; Hayashi, S.; Gross, E.; Kovalev, D.; Künzner, N.; Diener, J.; Timoshenko, V. Y. Chemical Reaction Mediated by Excited States of Si Nanocrystals - Singlet Oxygen Formation in Solution. *J. Appl. Phys.* **2004**, *95* (7), 3689–3693.

(42) Spiller, W.; Kliesch, H.; Wöhrle, D.; Hackbarth, S.; Röder, B.; Schnurpfeil, G. Singlet Oxygen Quantum Yields of Different Photosensitizers in Polar Solvents and Micellar Solutions. *J. Porphyrins Phthalocyanines* **1998**, *2* (2), 145–158.

(43) Ormond, A. B.; Freeman, H. S. Effects of Substituents on the Photophysical Properties of Symmetrical Porphyrins. *Dye. Pigment.* **2013**, *96*, 440–448.

(44) Kuimova, M. K.; Yahioglu, G.; Ogilby, P. R. Singlet Oxygen in a Cell : Spatially Dependent Lifetimes and Quenching Rate Constants Singlet Oxygen in a Cell : Spatially Dependent Lifetimes and. **2009**, No. 13, 332–340.

(45) Maisch, T.; Baier, J.; Franz, B.; Maier, M.; Landthaler, M.; Szeimies, R.-M.; Baumler, W. The Role of Singlet Oxygen and Oxygen Concentration in Photodynamic Inactivation of Bacteria. *Proc. Natl. Acad. Sci.* **2007**, *104* (17), 7223–7228.

(46) Baier, J.; Maier, M.; Engl, R.; Landthaler, M.; Bäumler, W. Time-Resolved

Investigations of Singlet Oxygen Luminescence in Water, in Phosphatidylcholine, and in Aqueous Suspensions of Phosphatidylcholine or HT29 Cells. *J. Phys. Chem. B* **2005**, *109* (7), 3041–3046.

(47) Yoshikawa, T. T. Antimicrobial Resistance and Aging: Beginning of the End of the Antibiotic Era? *J. Am. Geriatr. Soc.* **2002**, *50* (7), 226–229.

(48) Nitzan, Y.; Gutterman, M.; Malik, Z.; Ehrenberg, B. Inactivation of Gram-Negative Bacteria by Photosensitized Porphyrins. *Photochem. Photobiol.* **1992**, *55* (1), 89–96.

(49) Denyer, S. .; Maillard, J.-Y. Cellular Impermeability and Uptake of Biocides and Antibiotics in Gram-Positive Bacteria and Mycobacteria. *J. Appl. Microbiol.* **2002**, *92*, 35S–45S.

(50) Malik, Z.; Ladan, H.; Nitzan, Y. Photodynamic Inactivation of Gram-Negative Bacteria: Problems and Possible Solutions. *J. Photochem. Photobiol. B Biol.* **1992**, *14* (3), 262–266.

(51) Minnock, A.; Vernon, D. I.; Schofield, J.; Parish, J. H.; Brown, S. B. Mechanism of Uptake of a Cationic Water-Soluble Pyridinium Zinc Phthalocyanine across the Outer Membrane of Escherichia Coli Mechanism of Uptake of a Cationic Water-Soluble Pyridinium Zinc Phthalocyanine across the Outer Membrane of Escherichia Coli. **2000**, *44* (3), 522–527.

(52) Angeli, N. G.; Lagorio, M. G.; San Román, E. A.; Dicelio, L. E. Meso-Substituted Cationic Porphyrins of Biological Interest. Photophysical and Physicochemical Properties in Solution and Bound to Liposomes. *Photochem. Photobiol.* **2000**, *72* (1), 49–56.

(53) Tim, M. Strategies to Optimize Photosensitizers for Photodynamic Inactivation of Bacteria. *J. Photochem. Photobiol. B Biol.* **2015**, *150*, 2–10.

(54) Caminos, D. A.; Spesia, M. B.; Durantini, E. N. Photodynamic Inactivation of Escherichia Coli by Novel Meso-Substituted Porphyrins by 4-(3-N,N,N-Trimethylammoniumpropoxy)phenyl and 4-(Trifluoromethyl)phenyl Groups. *Photochem. Photobiol. Sci.* **2006**, *5* (1), 56–65.

(55) Alves, E.; Costa, L.; Carvalho, C. M.; Tomé, J. P.; Faustino, M. A.; Neves, M. G.; Tomé, A. C.; Cavaleiro, J. A.; Cunha, Â.; Almeida, A. Charge Effect on the Photoinactivation of Gram-Negative and Gram-Positive Bacteria by Cationic Meso-Substituted Porphyrins. *BMC Microbiol.* **2009**, *9* (1), 70.

(56) Hancock, R. E. W.; Bell, A. Antibiotic Uptake into Gram-Negative Bacteria. *Eur. J. Clin. Microbiol. Infect. Dis.* **1988**, *7* (6), 713–720.

(57) Hancock, R. E. W. Alterations in Structure of the Cell Envelope. *Ann. Rev. Microbiol.* **1984**, *38*, 237–264.

(58) Ragas, X.; Agut, M.; Nonell, S. Free Radical Biology & Medicine Singlet Oxygen in Escherichia Coli : New Insights for Antimicrobial Photodynamic Therapy. *Free Radic. Biol. Med.* **2010**, *49* (5), 770–776.

(59) Costa, L.; Alves, E.; Carvalho, C. M. B.; Tomé, J. P. C.; Faustino, M. A. F.; Neves, M. G. P. M. S.; Tomé, A. C.; Cavaleiro, J. A. S.; Cunha, Â.; Almeida, A. Sewage Bacteriophage Photoinactivation by Cationic Porphyrins: A Study of Charge Effect. *Photochem. Photobiol. Sci.* **2008**, *7* (4), 415.

(60) Chen, B.; Wu, S.; Li, A.; Liang, F.; Zhou, X.; Cao, X.; He, Z. Synthesis of Some Multi-β-Substituted Cationic Porphyrins and Studies on Their Interaction with DNA. *Tetrahedron* **2006**, *62* (23), 5487–5497.

(61) Nicholas W. Smith, S. V. D. Efficient Nitration of Meso- Tetraphenylporphyrin with Nitronium Tetrafluoroborate. *Arkivoc* **2010**, *7* (2), 10–18.

(62) Walter, M. G.; Wamser, C. C.; Ruwitch, J.; Zhao, Y.; Stevens, M.; Denman, A.; Pi, R.; Rudine, A.; Peter, J. Syntheses and Optoelectronic Properties of Amino / Carboxyphenylporphyrins for Potential Use in Dye-Sensitized TiO 2 Solar Cells. *J. Porphyr. Phthalocyanines* **2007**, 601–612.

(63) Banfi, S.; Caruso, E.; Buccafurni, L.; Battini, V.; Zazzaron, S.; Barbieri, P.; Orlandi, V. Antibacterial Activity of Tetraaryl-Porphyrin Photosensitizers: An in Vitro Study on Gram Negative and Gram Positive Bacteria. *J. Photochem. Photobiol. B Biol.* **2006**, *85* (1), 28–38.

(64) Tavares, A.; Dias, S. R. S.; Carvalho, C. M. B.; Faustino, M. A. F.; Tomé, J. P. C.; Neves, M. G. P. M. S.; Tomé, A. C.; Cavaleiro, J. A. S.; Cunha, Â.; Gomes, N. C. M.; et al. Mechanisms of Photodynamic Inactivation of a Gram-Negative Recombinant Bioluminescent Bacterium by Cationic Porphyrins. *Photochem. Photobiol. Sci.* **2011**, *10* (10), 1659.

(65) Garland, M. J.; Cassidy, C. M.; Woolfson, D.; Donnelly, R. F. Designing Photosensitizers for Photodynamic Therapy: Strategies, Challenges and Promising Developments. *Future Med. Chem.* **2009**, *1* (4), 667–691.

(66) Demidova, T. N.; Hamblin, M. R. Photodynamic Therapy Targeted to Pathogens. *Int. J. Immunopathol. Pharmacol.* **2004**, *17* (3), 245–254.

APPENDIX: ADDITIONAL FIGURES

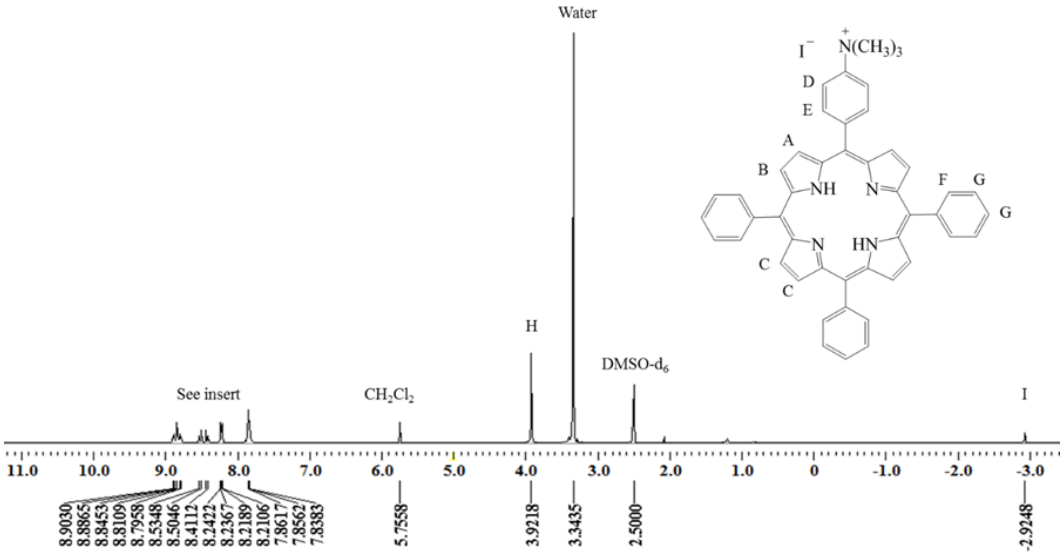

Figure A1.1. ^{1}H NMR of A^{+}TPP in DMSO-d$_6$.

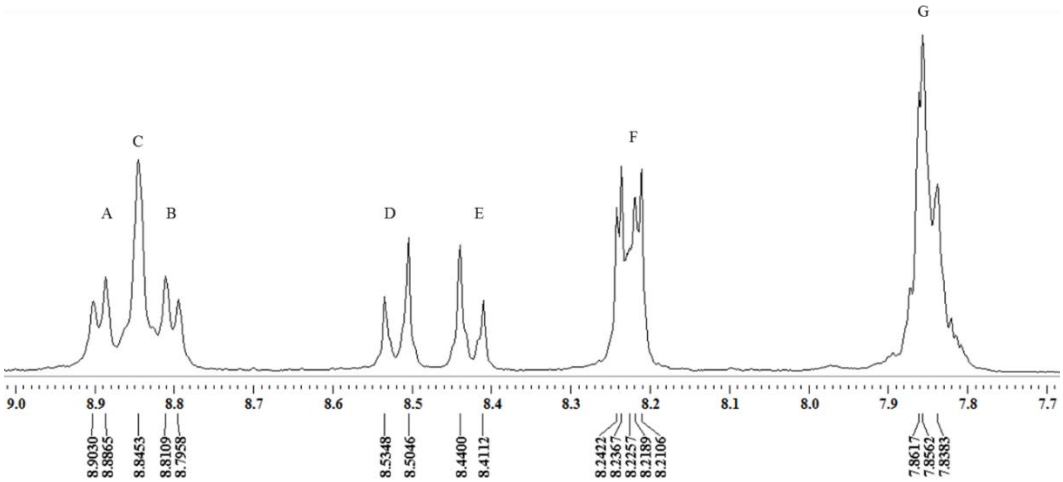

Figure A1. 2. ^{1}H NMR of aromatic region insert of A^{+}TPP in DMSO-d$_6$.

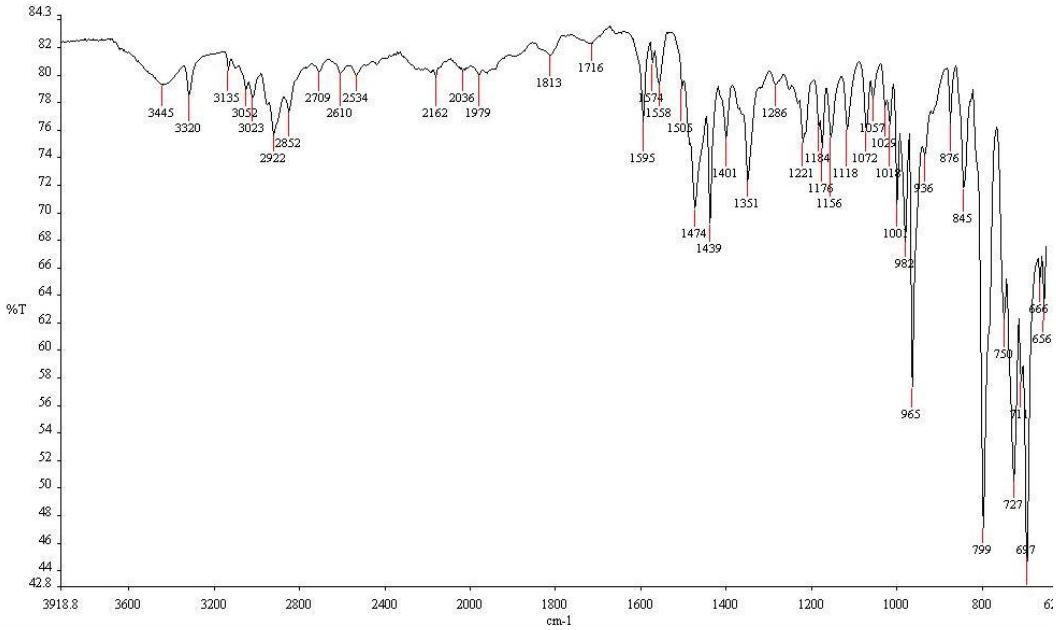

Figure A1. 3. FTIR of $A^{+}TPP$.

Wavenumber (cm^{-1})	Functional Group
3445	-N-H
2852-3135	-C-H
1595	-C=C

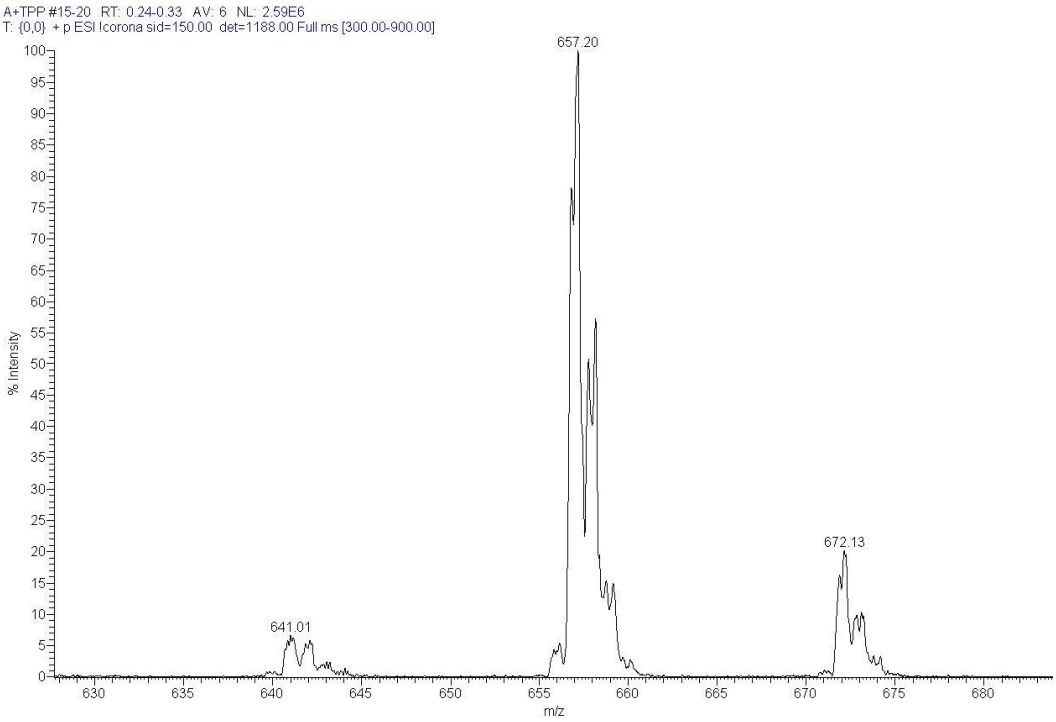

Figure A1. 4. ESI-MS spectrum of $A^{+}TPP\ [M - I^{-}]^{+} = 672.13$.

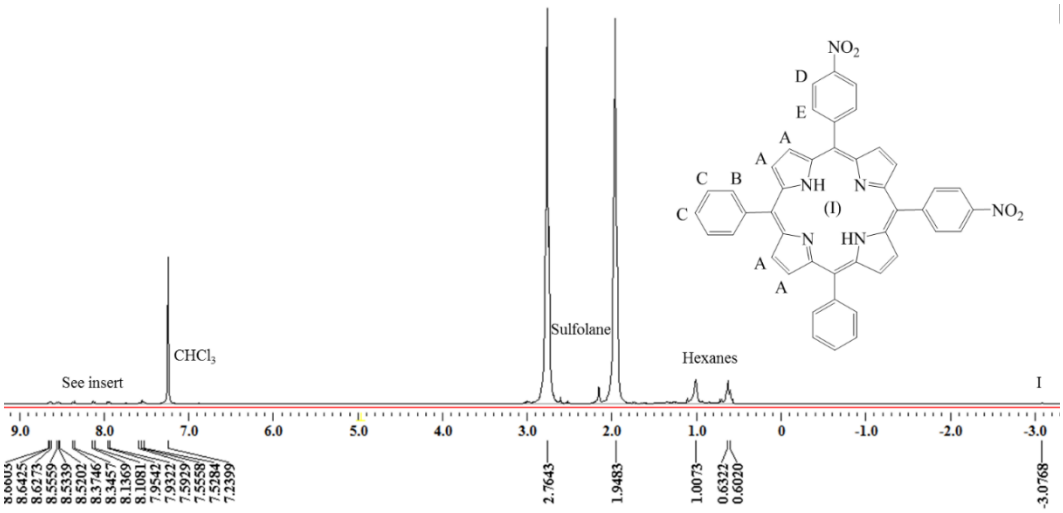

Figure A1. 5. ^{1}H NMR of TN_2PP in $CDCl_3$.

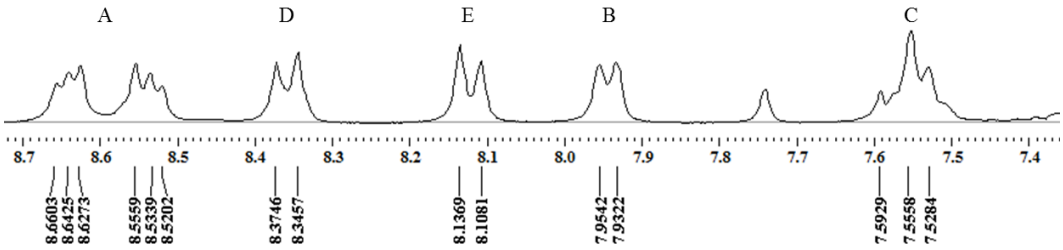

Figure A1. 6. ^{1}H NMR insert of aromatic region of TN_2PP in $CDCl_3$.

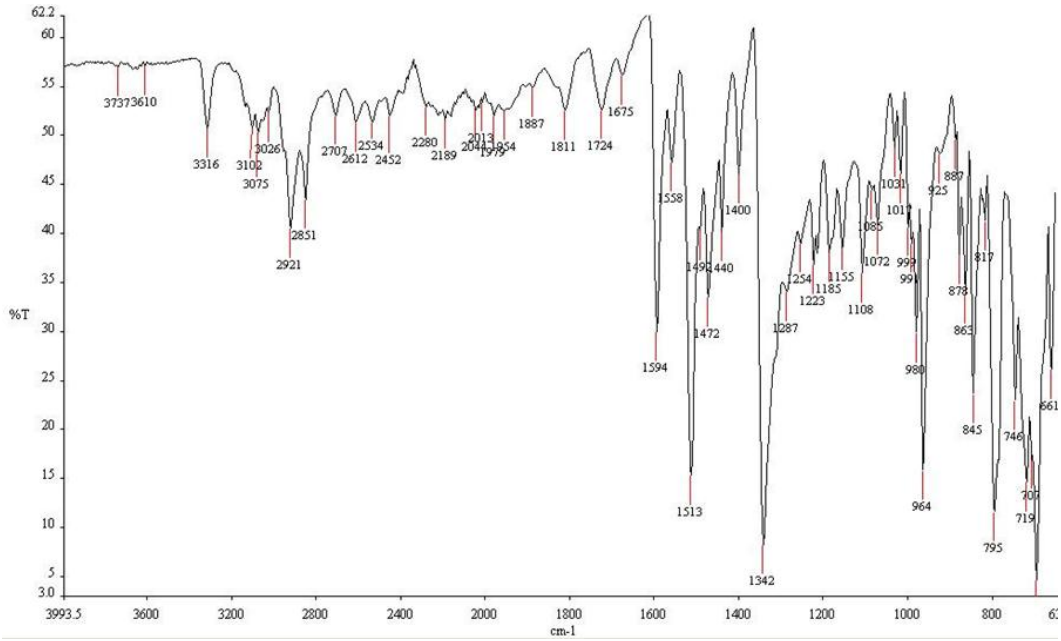

Figure A1. 7. FTIR of TN_2PP.

Wavenumber (cm^{-1})	Functional Group
3316	-N-H
2851-3102	-C-H
1594	-C=C
1342, 1513	-N-O
964	-C-N

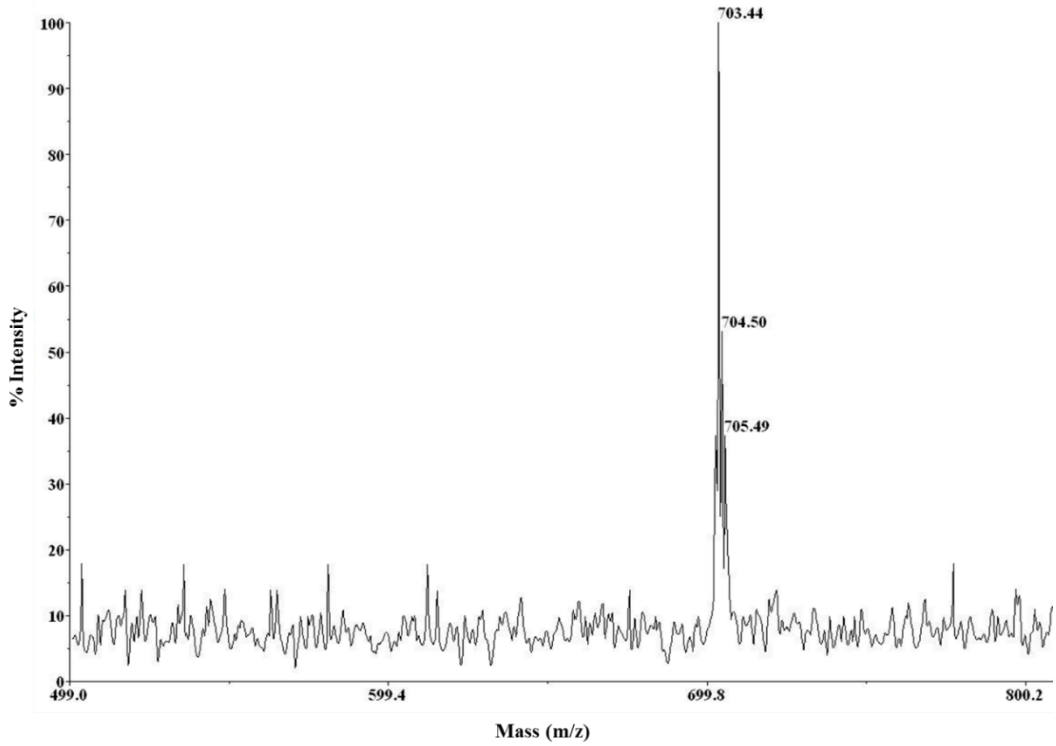

Figure A1. 8. MALDI-TOF spectrum of TN_2PP $[M]^+$ = 704.5.

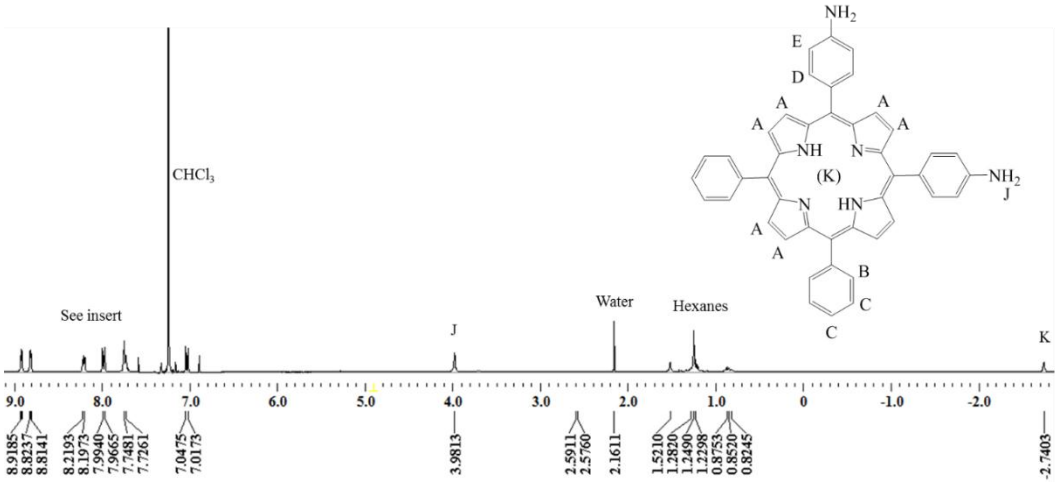

Figure A1. 9. ^{1}H NMR of TA_2PP in $CDCl_3$.

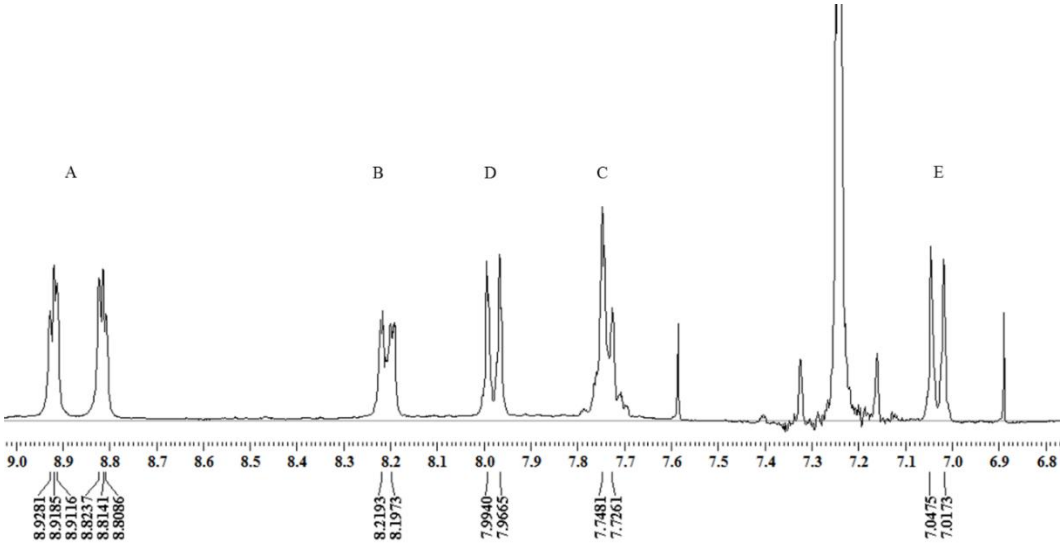

Figure A1. 10. ^{1}H NMR insert of aromatic region of TA_3PP in $CDCl_3$.

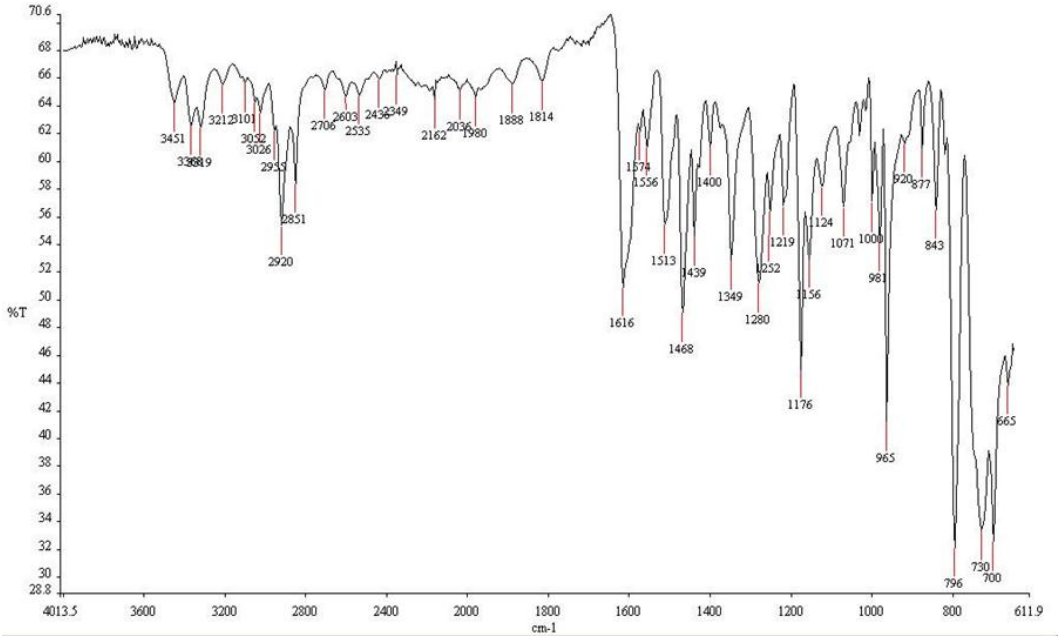

Figure A1. 11. FTIR of TA_2PP.

Wavenumber (cm^{-1})	Functional Group
3451, 3362, 3321	-N-H
2851-3026	-C-H
1616	-C=C

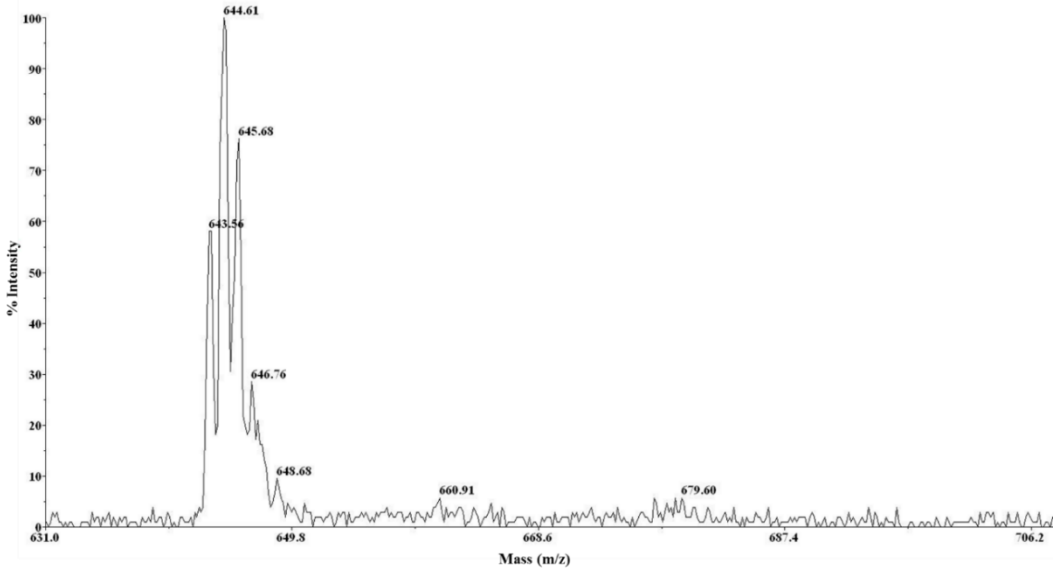

Figure A1. 12. MALDI-TOF spectrum of TA_2PP $[M]^+$ = 644.61.

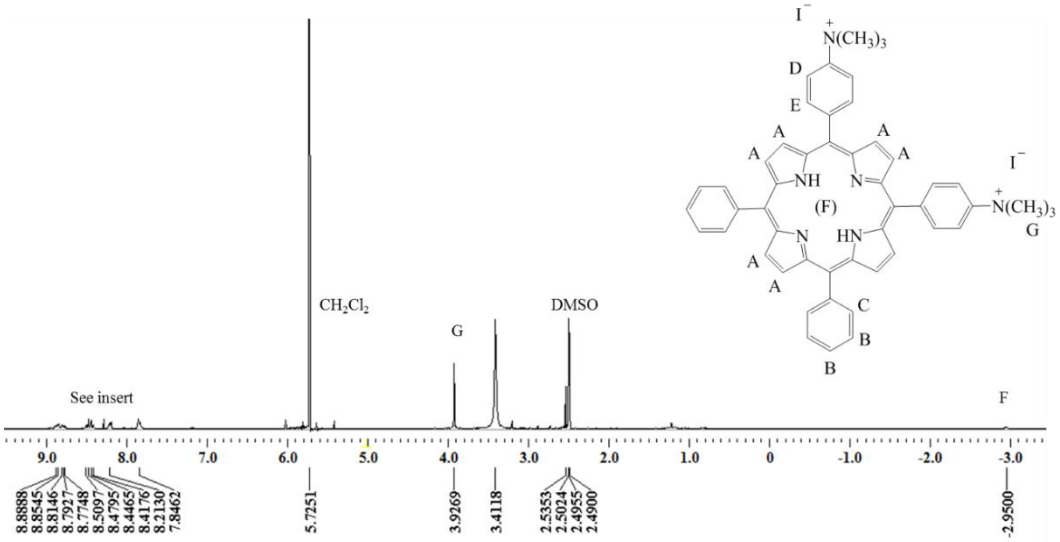

Figure A1. 13. ^{1}H NMR of TA^{+2}PP.

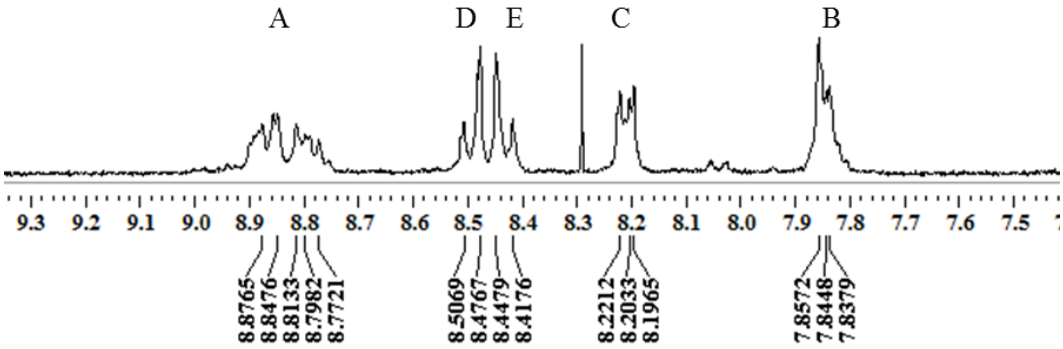

Figure A1. 14. ^{1}H NMR insert of aromatic region of TA^{+2}PP.

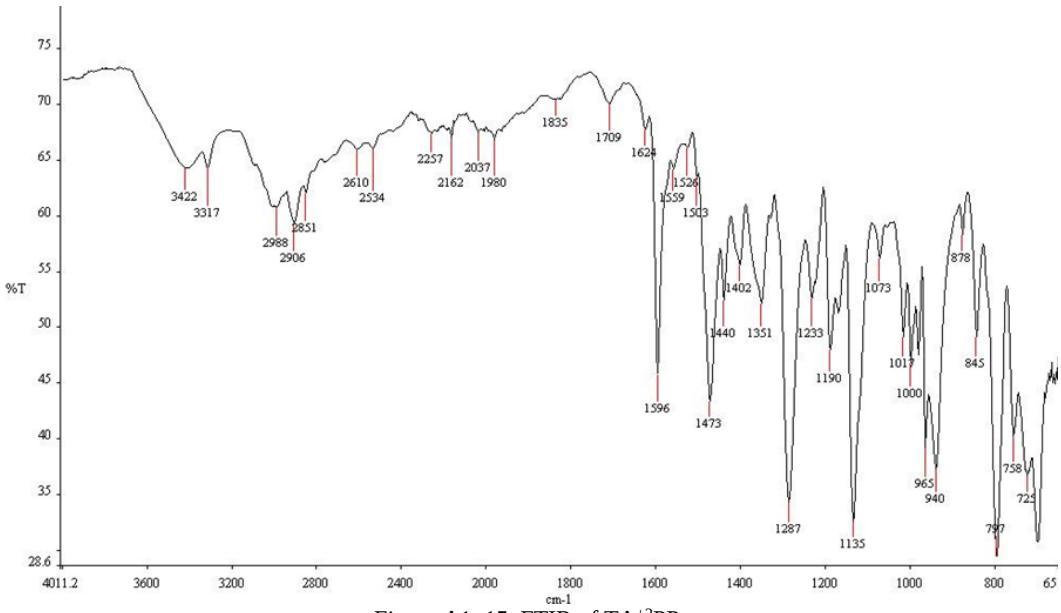

Figure A1. 15. FTIR of $TA^{+2}PP$.

Wavenumber (cm^{-1})	Functional Group
3317, 3422	-N-H
2851-2988	-C-H
1596	-C=C

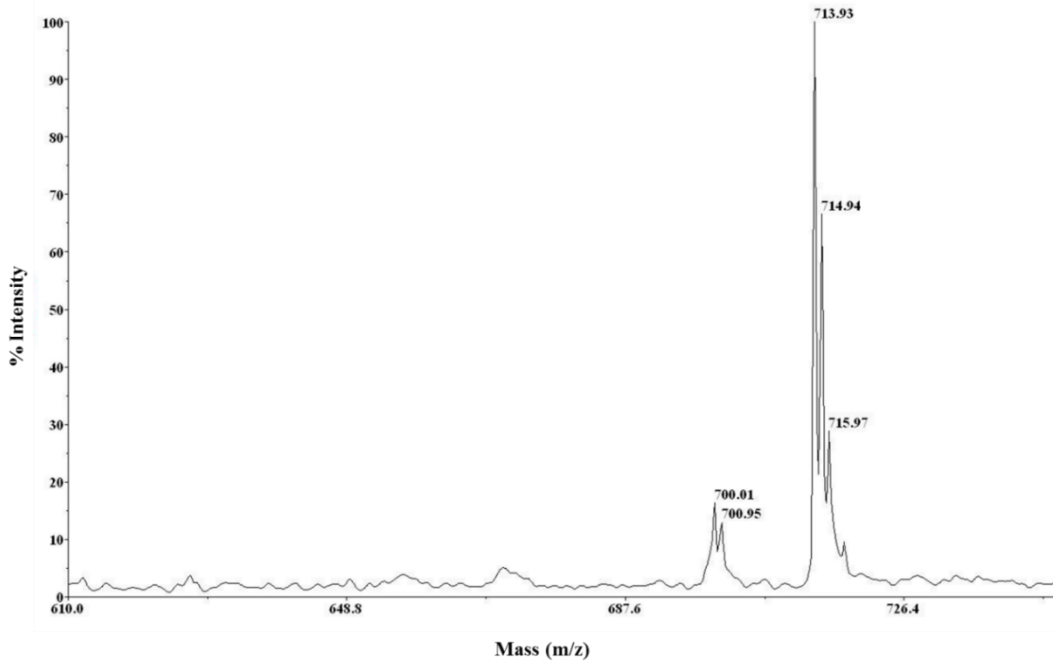

Figure A1. 16. MALDI-TOF spectrum of $TA^{+2}PP$ $[M - I - CH_3]^+ = 715.97$.

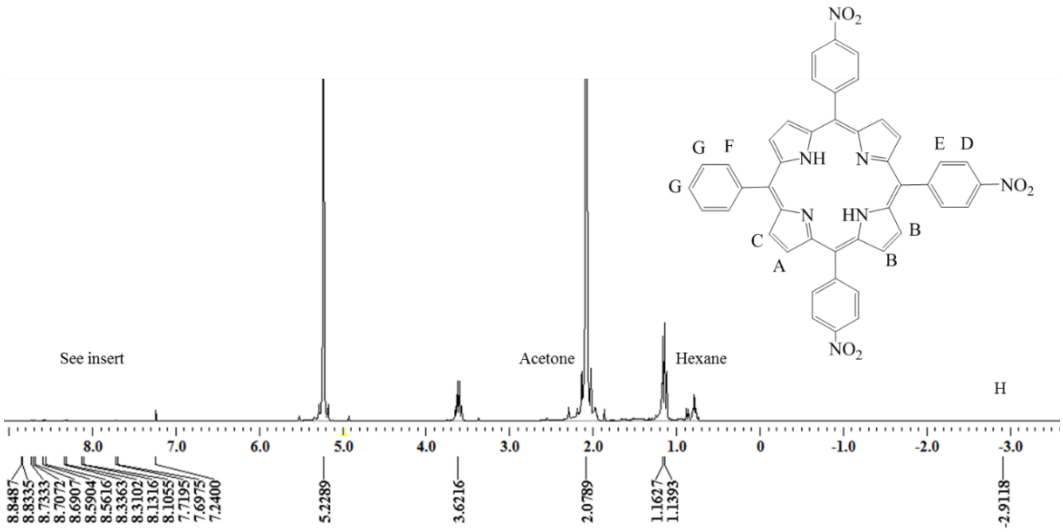

Figure A1. 17. ^{1}H NMR of TN_3PP.

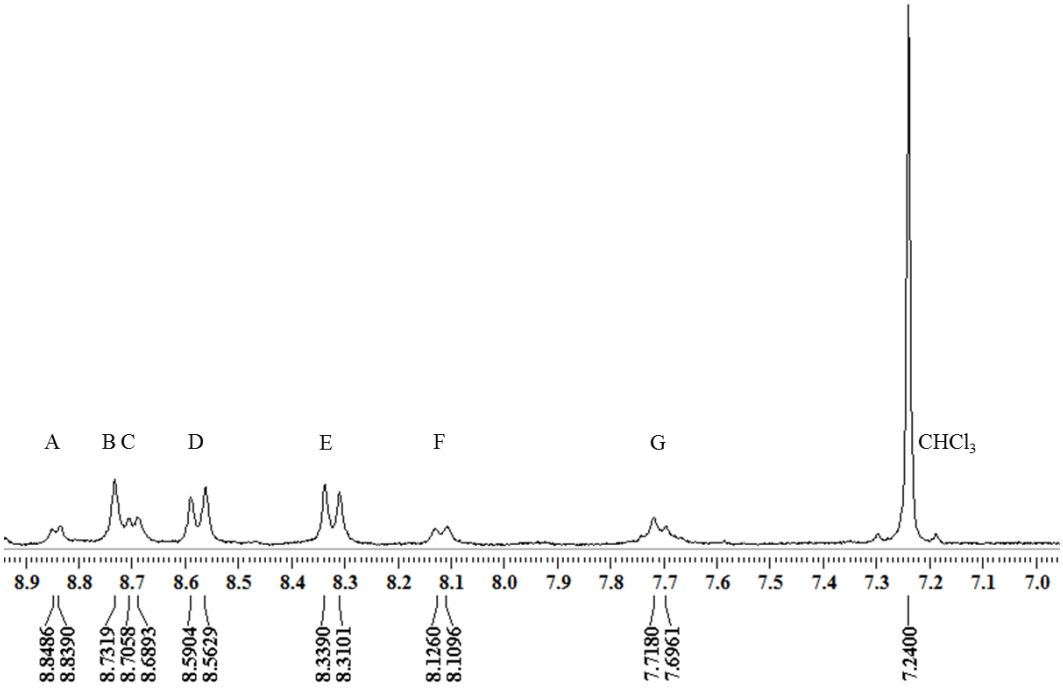

Figure A1. 18. Insert of ^{1}H NMR of TN_3PP.

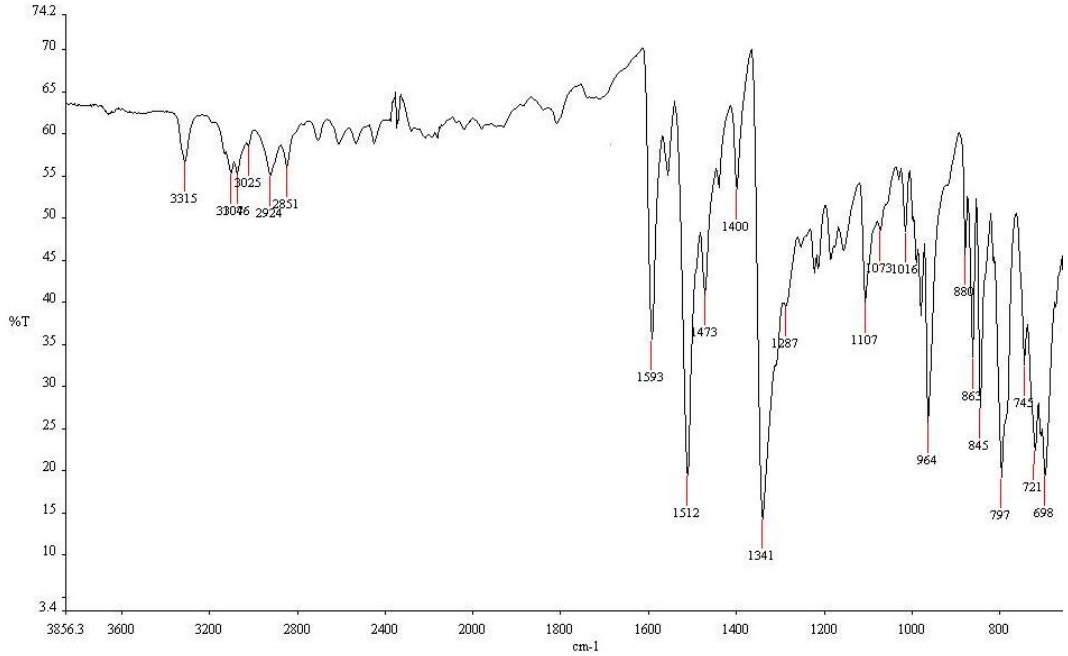

Figure A1. 19. FTIR of TN_3PP.

Wavenumber (cm^{-1})	Functional Group
3315	-N-H
2857-3046	-C-H
1593	-C=C
1341, 1512	-N-O

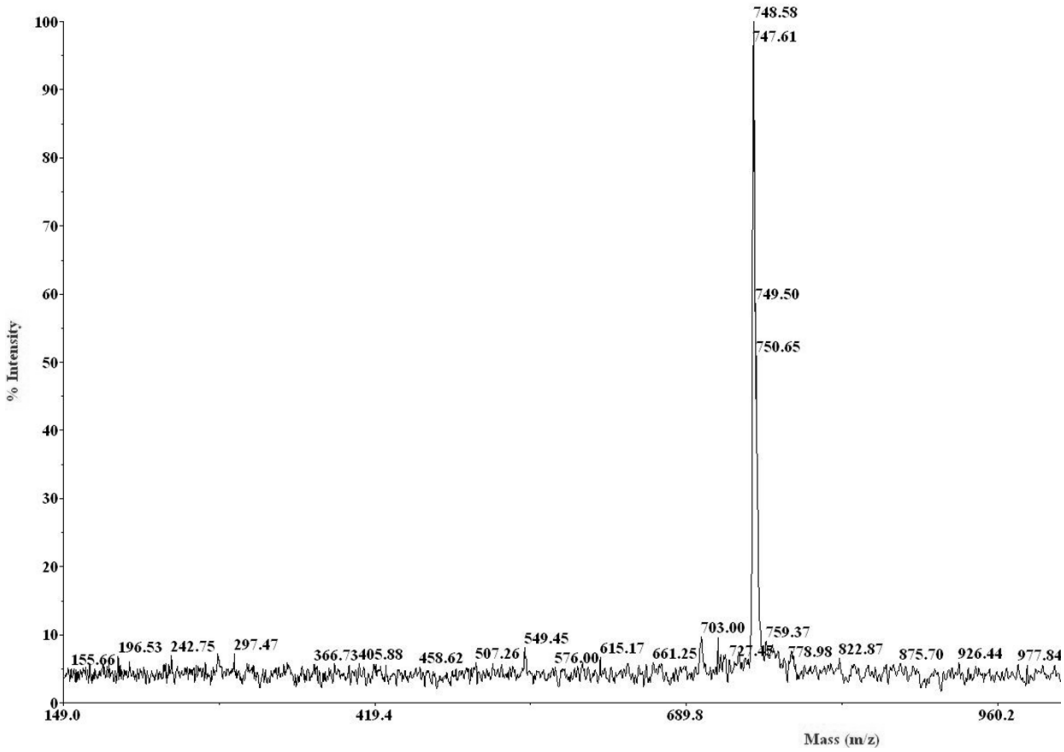

Figure A1. 20. MALDI-TOF spectrum of TN_3PP $[M + 1]^+ = 750.65$.

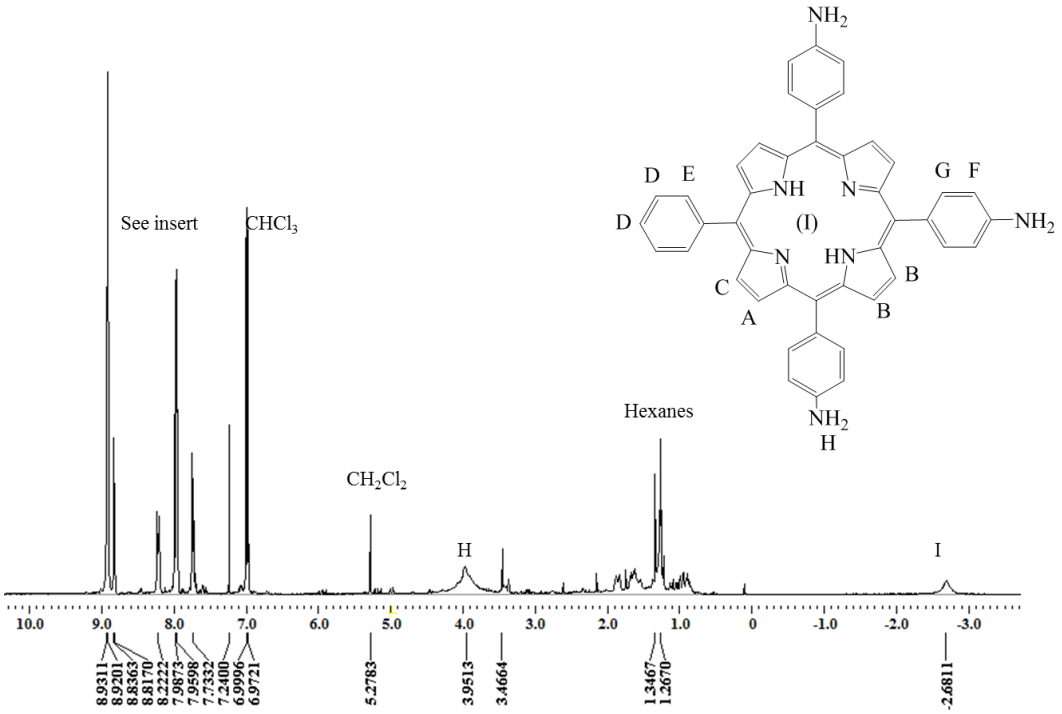

Figure A1. 21. ^{1}H NMR of TA_3PP in $CDCl_3$.

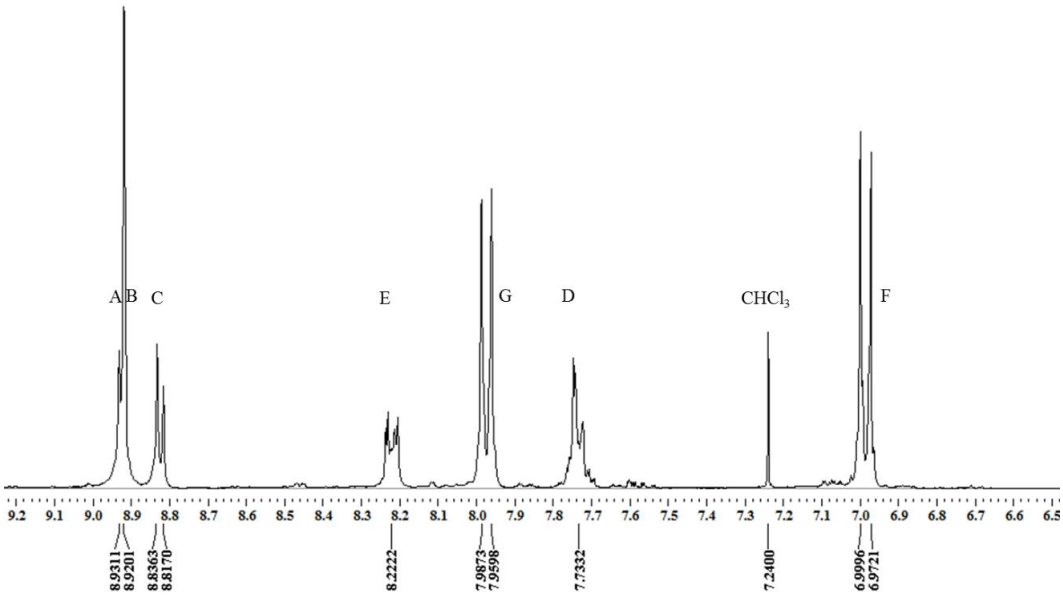

Figure A1. 22. ^{1}H NMR insert of aromatic region of TA_3PP.

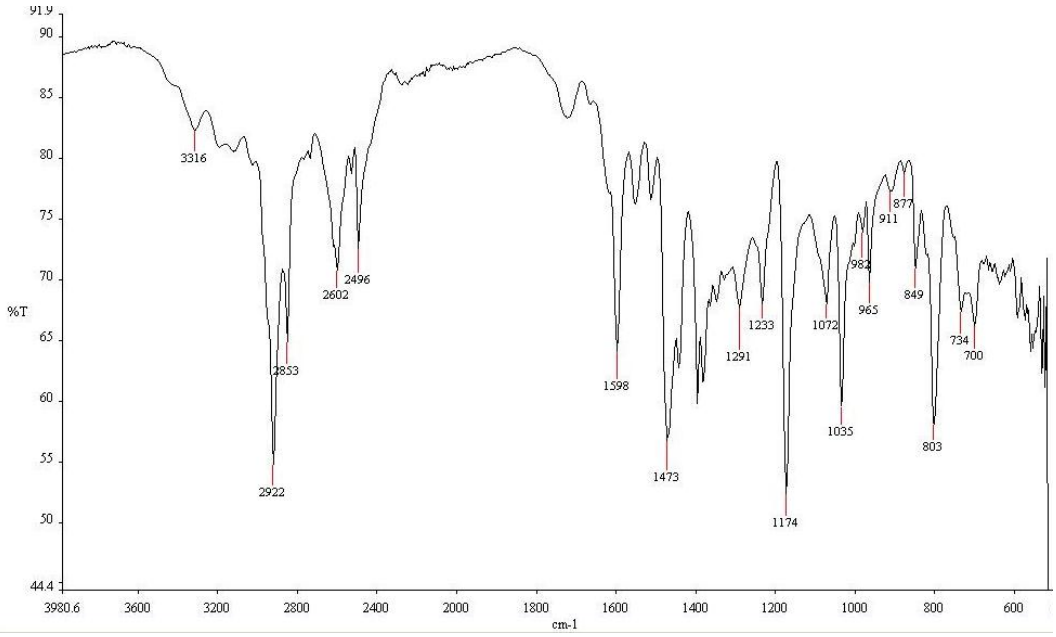

Figure A1. 23. FTIR of TA_3PP.

Wavenumber (cm^{-1})	Functional Group
3316	-N-H
2853-2922	-C-H
1598	-C=C

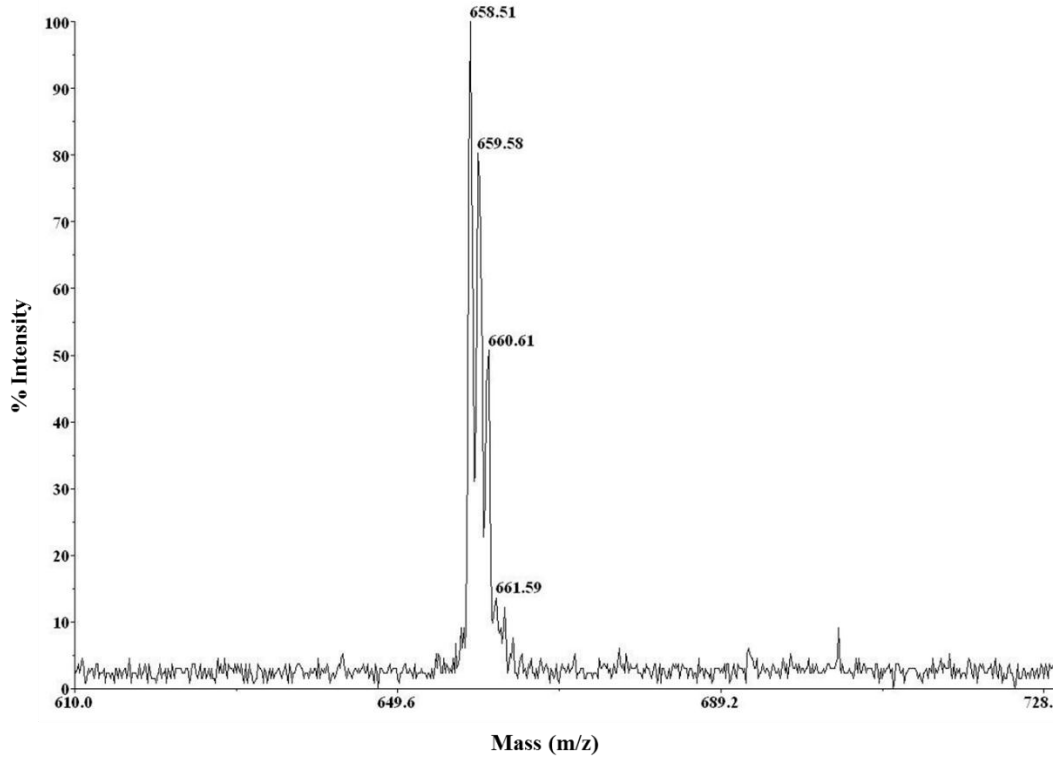

Figure A1. 24. MALDI-TOF spectrum of TA_3PP $[M]^+$ = 659.58.

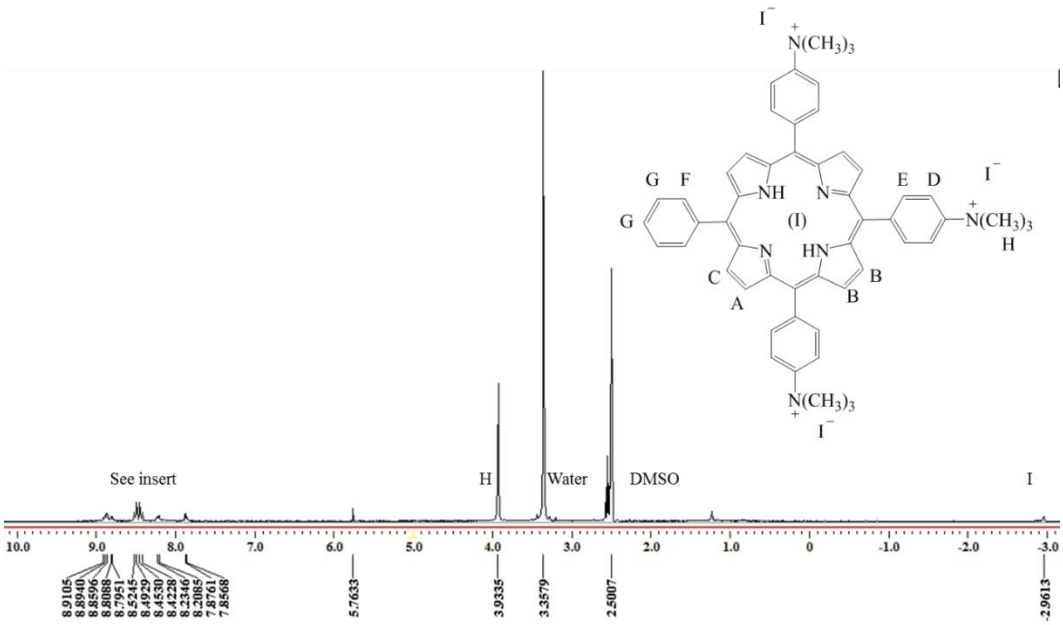

Figure A1. 25. ^{1}H NMR of TA^{+3}PP.

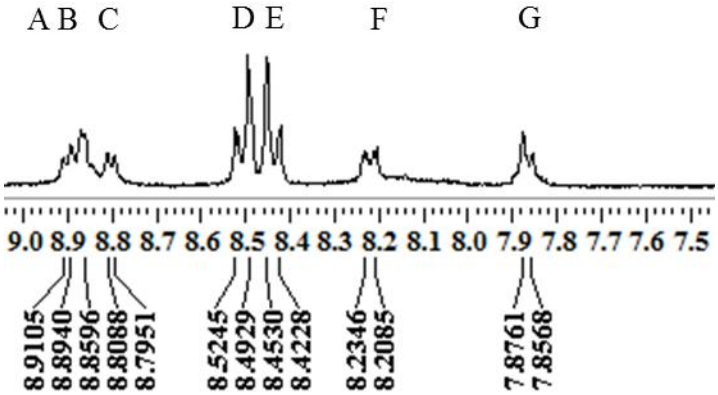

Figure A1. 26. Insert of ^{1}H NMR of TA^{+3}PP.

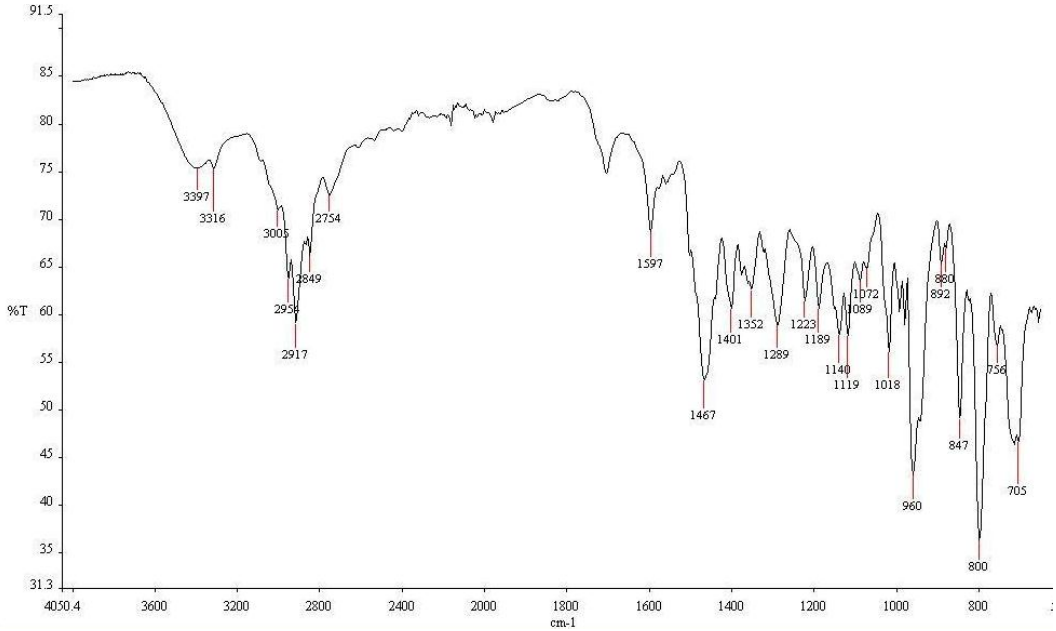

Figure A1. 27. FTIR of $TA^{+3}PP$.

Wavenumber (cm^{-1})	Functional Group
3397, 3316	-N-H
2849-3005	-C-H
1597	-C=C

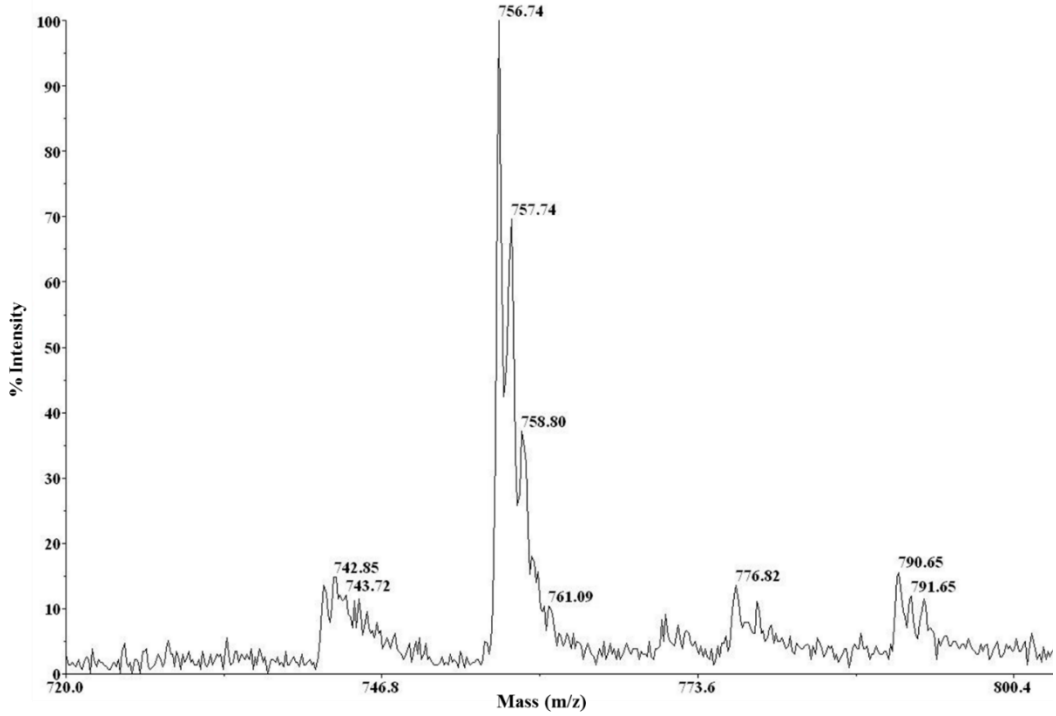

Figure A1. 28. MALDI-TOF spectrum of $TA^{+3}PP$ $[M - 3I^-]^+$ = 790.65.

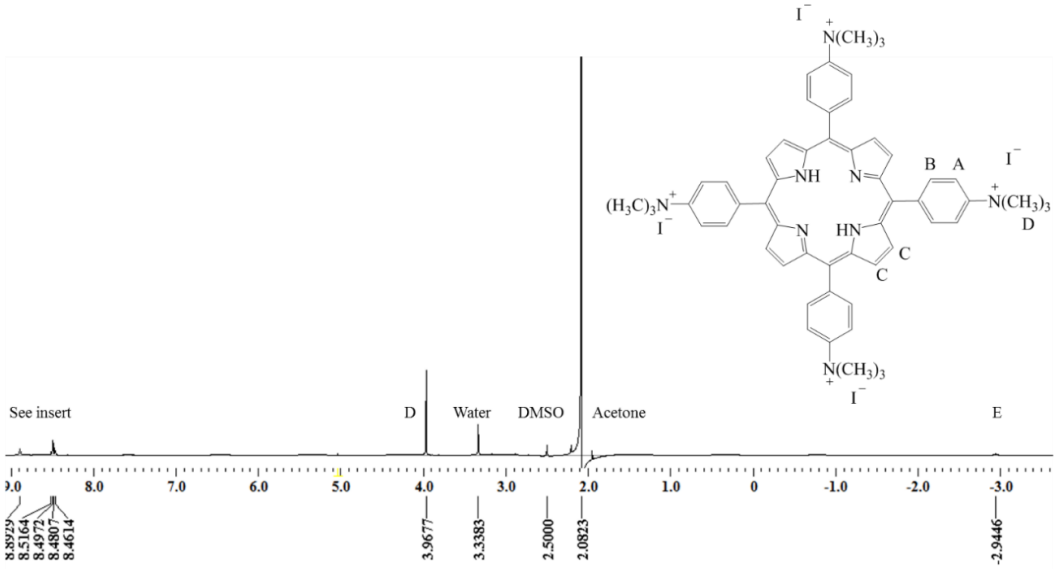

Figure A1. 29. ^{1}H NMR of TA^{+4}PP.

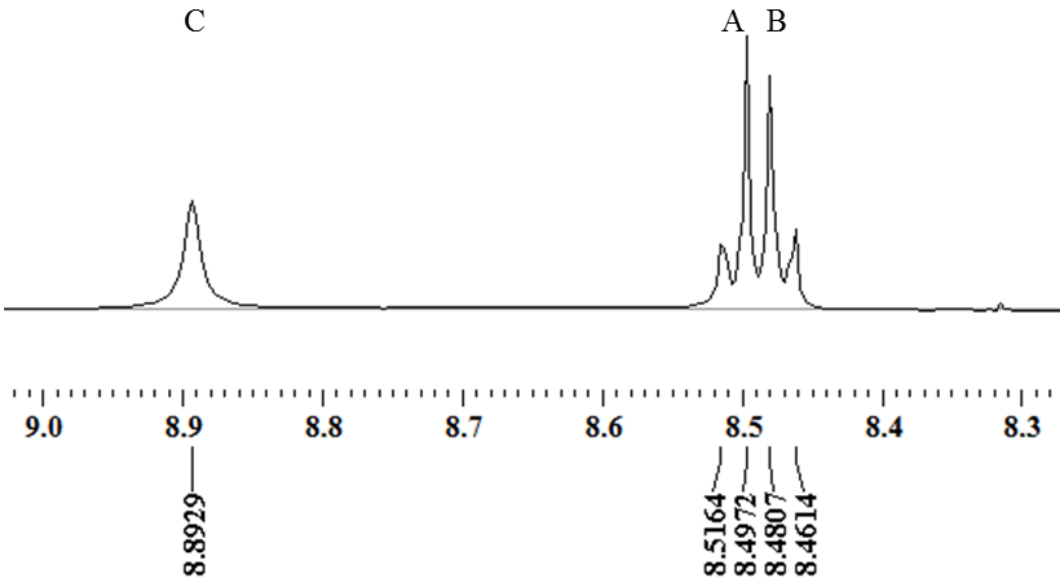

Figure A1. 30. Insert of ^{1}H NMR of TA^{+4}PP.

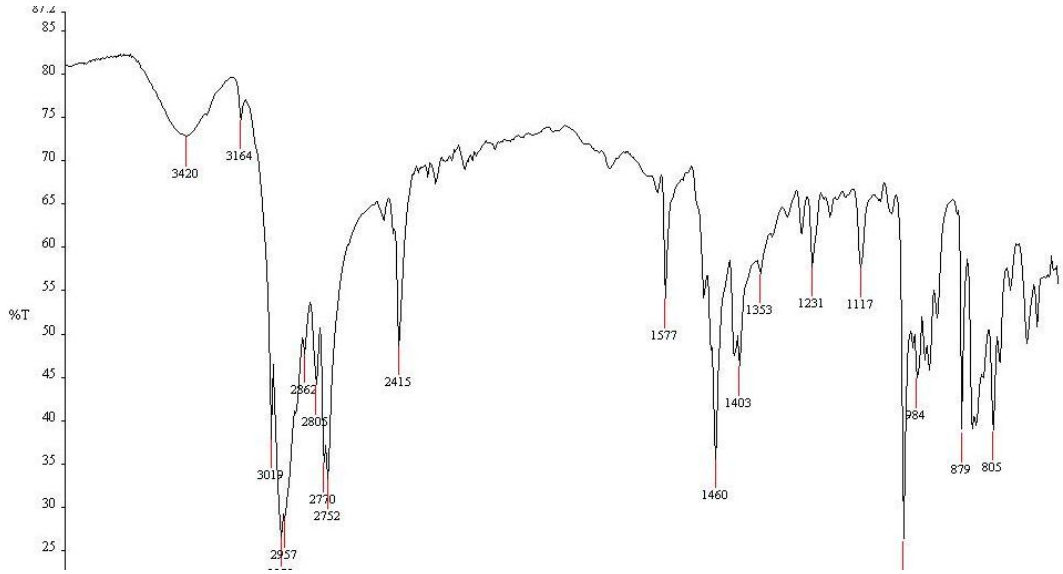

Figure A1. 31. FTIR of $TA^{+4}PP$.

Wavenumber (cm^{-1})	Functional Group
3420	-N-H
2752-3019	-C-H
1577	-C=C

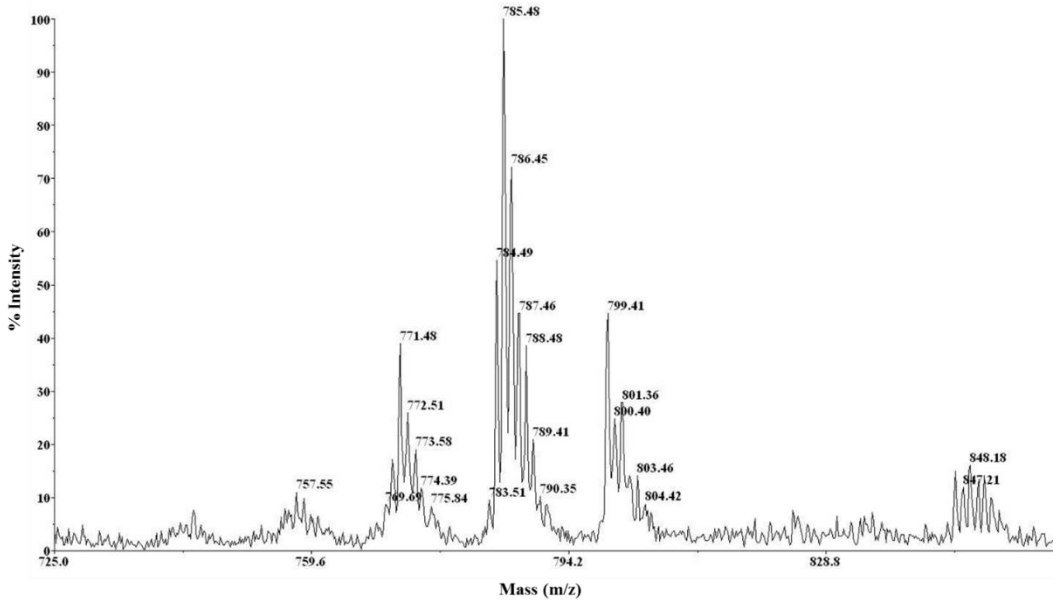

Figure A1. 32. MADLI-TOF spectrometry of $TA^{+4}PP$ $[M - 4I^-]^+ = 847.21$.